

AD

USAAVLABS TECHNICAL REPORT 67-80

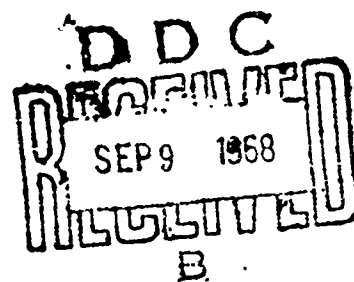
**EXPERIMENTAL INVESTIGATION OF LOW ASPECT
RATIO AND TIP CLEARANCE ON TURBINE
PERFORMANCE AND AERODYNAMIC DESIGN**

By

R. Marshall

C. Rogo

May 1968



**U. S. ARMY AVIATION MATERIEL LABORATORIES
FORT EUSTIS, VIRGINIA**

**CONTRACT DA 44-177-AMC-447(T)
CONTINENTAL AVIATION AND ENGINEERING CORPORATION
DETROIT, MICHIGAN**

*This document has been approved
for public release and sale; its
distribution is unlimited.*



Reproduced by the
CLEARINGHOUSE
for Federal Scientific & Technical
Information Springfield Va 22151



DEPARTMENT OF THE ARMY
U. S. ARMY AVIATION MATERIEL LABORATORIES
FORT EUSTIS, VIRGINIA 23604

Appropriate technical personnel have reviewed this report and concur with the conclusions contained herein.

The findings and recommendations outlined herein will be taken into consideration in the planning of future programs for turbines and turbine engines.

Disclaimers

The findings in this report are not to be construed as an official Department of the Army position unless so designated by other authorized documents.

When Government drawings, specifications, or other data are used for any purpose other than in connection with a definitely related Government procurement operation, the United States Government thereby incurs no responsibility nor any obligation whatsoever; and the fact that the Government may have formulated, furnished, or in any way supplied the said drawings, specifications, or other data is not to be regarded by implication or otherwise as in any manner licensing the holder or any other person or corporation, or conveying any rights or permission, to manufacture, use, or sell any patented invention that may in any way be related thereto.

Trade names cited in this report do not constitute an official endorsement or approval of the use of such commercial hardware or software.

Disposition Instructions

Destroy this report when no longer needed. Do not return it to the originator.

ACQUISITION 161		
CASTI	WHITE SECTION <input checked="" type="checkbox"/>	
CODE	BUFF SECTION <input type="checkbox"/>	
UNANNOUNCED	<input type="checkbox"/>	
JUSTIFICATION		
BY		
INTERVIEW/INTERVIEW		
DATE	TIME	DATE
2		

Task 1M125901A01409
Contract DA 44-177-AMC-447(T)
USAAVLABS Technical Report 67-80
May 1968

EXPERIMENTAL INVESTIGATION OF
LOW ASPECT RATIO AND TIP CLEARANCE ON
TURBINE PERFORMANCE AND AERODYNAMIC DESIGN

Summary Report
Continental Report No. 1043

By

R. Marshall
C. Rogo

Prepared By

CONTINENTAL AVIATION AND ENGINEERING CORPORATION
DETROIT, MICHIGAN

for

U.S. ARMY AVIATION MATERIEL LABORATORIES
FORT EUSTIS, VIRGINIA

This document has been approved
for public release and sale; its
distribution is unlimited.

SUMMARY

This report presents the aerothermodynamic design of three turbine flowpaths which were designed and cold-flow tested to evaluate the performance effects of span aspect ratio and tip clearance on turbine efficiency. The baseline configuration (called nominal) consisted of a turbine design which would satisfy the same aerothermodynamic conditions imposed on a fluid-cooled concept initiated under USAAVLABS Contract DA 44-177-AMC-184(T) (Reference 1). These conditions are representative of the problems inherent in small turbomachinery blading. Vane chords, blade chords, trailing edge thicknesses, and thickness-to-chord ratios were all maintained at values suitable for practical considerations.

An optimization study showed that high aspect ratio blading with low wheel speeds could produce the same or better performance than low aspect ratio blading with high rim speeds. As a result of the optimization study, a reduction in rim speed of 21 percent with respect to the fluid-cooled turbine was chosen as a limit to achieve reasonable performance. The two additional flowpaths consisted of 150 percent and 50 percent of nominal blading height.

Complete performance maps were generated for the three configurations, and tip clearance effects were evaluated at design speed over a range of pressure ratios. Inlet conditions to the turbine were maintained at 660°F and 29.9 inches of Mercury absolute. Nozzle vane and rotor blade test Reynolds numbers corresponded to 720,000 and 258,000 respectively.

FOREWORD

This report, prepared by Continental Aviation and Engineering Corporation, presents the aerodynamic design and testing of a set of turbine wheels and nozzles to determine the effects of low aspect ratio and tip clearance on turbine performance.

The program was sponsored by the U.S. Army Aviation Materiel Laboratories under Contract DA 44-177-AMC- 447(T). Experimental cold-flow tests were conducted to establish baseline data for evaluation of future axial turbine performance limits, to verify analytical methods, and to substantiate incremental efficiency improvement of the fluid-cooled concept conducted under Contract DA 44-177-AMC-184(T).

CONTENTS

	<u>Page</u>
SUMMARY	iii
FOREWORD	v
LIST OF ILLUSTRATIONS	viii
LIST OF TABLES	xii
LIST OF SYMBOLS	xiii
INTRODUCTION	1
DISCUSSION	1
CONCLUSIONS	75
RECOMMENDATIONS	77
REFERENCES	79
DISTRIBUTION	81

LIST OF ILLUSTRATIONS

<u>Figure</u>		<u>Page</u>
1	Fluid-Cooled Turbine - Test Stand Performance . .	2
2	Fluid-Cooled Turbine Flowpath	3
3	Turbine Blade Assembly	4
4	Turbine Rotor Assembly	5
5	Secondary Flow Formation in a Nozzle Cascade . . .	5
6	Influence of Blade Length Ratio h/c on Secondary Flow Losses of Turbine Cascade	6
7	Variation of Nozzle Loss Coefficient With Blade As- pect Ratio. Pitch Chord Ratio = 0.77 at M Exit = 0.8	7
8	Turbine Velocity Diagram Station and Sign Notations	10
9	Fluid-Cooled Turbine Velocity Diagrams	13
10	Effect of Meridional Constriction on Losses of a Nozzle	17
11	Nominal Aspect Ratio - Velocity Diagrams	19
12	Nominal Turbine Flowpath for Aspect Ratio Evaluation	20
13	Nominal Turbine Nozzle Geometry	20
14	Nominal Turbine Rotor Geometry	21
15	Nozzle Vane Velocity Distribution and Diffusion Factor Comparison; Hub Section, 12.5-Percent Blade Height	22
16	Rotor Blade Velocity Distribution and Diffusion Fac- tor Comparison; Hub Section, 12.5-Percent Blade Height	23
17	Rotor Blade Velocity Distribution and Diffusion Fac- tor Comparison; Tip Section, 87.5-Percent Blade Height	24

<u>Figure</u>		<u>Page</u>
18	Flowpath Comparison - Fluid-Cooled Turbine Design and Nominal Aspect Ratio Turbine	25
19	Profile Comparison of Nominal Aspect Ratio Nozzle Vane to Fluid-Cooled Turbine Design Vane - Mean Sections	26
20	Profile Comparison of Nominal Aspect Ratio Rotor to Fluid-Cooled Rotor	27
21	Aspect Ratio Evaluation - 150-Percent Nominal Turbine Flowpath	29
22	High Aspect Ratio - 150-Percent Nominal Flowpath Velocity Diagrams	30
23	Rotor Blade Velocity Distributions - High Aspect Ratio Design, Hub Section, 8-Percent Blade Height	31
24	Rotor Blade Velocity Distributions - High Aspect Ratio Design, Tip Section, 100-Percent Blade Height	31
25	Nozzle Vane Velocity Distributions - High Aspect Ratio Design, Tip Section, 100-Percent Height . . .	33
26	Machined Rotor - High Aspect Ratio Design	33
27	Low Aspect Ratio - 50-Percent Nominal Flowpath Velocity Diagrams	35
28	Rotor Blade Velocity Distributions - Low Aspect Ratio Design, Hub Section, 25-Percent Blade Height	36
29	Rotor Blade Velocity Distributions - Low Aspect Ratio Design, Tip Section, 100-Percent Blade Height	36
30	Aspect Ratio Evaluation - 50-Percent Nominal Turbine Flowpath	37

<u>Figure</u>		<u>Page</u>
31	High, Nominal, and Low Aspect Ratio Rotors	38
32	Front View of Turbine Test Stand	39
33	Rear View of Turbine Test Stand	39
34	Nozzle and Rotor Assembly in Test Rig	39
35	Aspect Ratio Evaluation Instrumentation Diagram, Axial Locations	43
36	Aspect Ratio Evaluation Instrumentation Diagram, Circumferential Locations	45
37	Recovery Calibration of Bare Wire Thermocouples .	47
38	Standard Cobra-Type Probe, Front View	49
39	Standard Cobra-Type Probes, Side View	49
40	Discharge Survey Cobra Probe Recovery Calibration	49
41	High Aspect Ratio Overall Performance - Clearance at 1.5-Percent Blade Height	50
42	Nominal Aspect Ratio Overall Performance - Clear- ance at 1.5-Percent Blade Height	51
43	Low Aspect Ratio Overall Performance - Clearance at 1.5-Percent Blade Height	52
44	High Aspect Ratio Performance - Efficiency Versus Ratio of Mean Wheel Speed to Isentropic Velocity Ratio	53
45	Nominal Aspect Ratio Performance - Efficiency Versus Ratio of Mean Wheel Speed to Isentropic Velocity Ratio	54

<u>Figure</u>		<u>Page</u>
46	Low Aspect Ratio Performance - Efficiency Versus Ratio of Mean Wheel Speed to Isentropic Velocity Ratio	55
47	Effect of Aspect Ratio on Efficiency - Clearance at 1.5-Percent Blade Height	57
48	High Aspect Ratio Performance - Torque Characteristics	58
49	Nominal Aspect Ratio Performance - Torque Characteristics	59
50	Low Aspect Ratio Performance - Torque Characteristics	60
51	Effect of Aspect Ratio on Limit Load Work Capability - Clearance at 1.5-Percent Blade Height	61
52	Nozzle Wall Velocity Distributions for Low, Nominal, and High Aspect Ratio Blading	64
53	Rotor Discharge Pressure and Angle Survey Data for Low, Nominal, and High Aspect Ratio Turbines . . .	65
54	Nozzle Efficiency Versus Exit Total-to-Static Pressure Ratio for Nominal and Low Aspect Ratio Vanes	66
55	Nominal Aspect Ratio - Rotor Clearance Effect on Performance at Rated Design Equivalent Speed . . .	68
56	High Aspect Ratio - Rotor Clearance Effects on Performance at Rated Design Equivalent Speed	69
57	Turbine Efficiency Versus Rotor Blade Height at 1.5, 3.5, and 5.0-Percent Blade Height Clearance	70
58	Comparison of Test Data to Theoretical Prediction of Turbine Efficiency as a Function of Clearance and Blade Height	71
59	Test Rig - Turbine Aspect Ratio	73

LIST OF TABLES

<u>Table</u>		<u>Page</u>
I	Fluid-Cooled Turbine Design Point Criteria	14
II	Blade Loss Breakdown of the Nominal Aspect Ratio Design and Fluid-Cooled Turbine	16
III	Geometric Design Parameter Comparison of Nominal Aspect Ratio to Fluid-Cooled Turbine	28
IV	Velocity Triangle and Diffusion Parameter Compari- son of Nominal Aspect Ratio to Fluid-Cooled Turbine	29
V	Blade Loss Breakdown of Three Aspect Ratio Turbines	32
VI	Test Plan for Turbine Aspect Ratio and Tip Clear- ance Evaluation	41
VII	Test Schedule	41
VIII	Overall Effects of Span Aspect Ratio on Performance - Clearance at 1.5 -Percent Blade Height	62
IX	Comparison of Performance and Exit Swirl for High, Nominal, and Low Aspect Ratio Turbines at Two Speeds	63

LIST OF SYMBOLS

A	area, in. ²
C	curvature, ft ⁻¹
C ₀	isentropic velocity corresponding to total head, fps
c _p	specific heat at constant pressure
c	actual chord, in.
D	diffusion parameter, dimensionless
g	gravitational constant, 32.17 ft/sec ²
ΔH	turbine work, Btu/lb
h	blade height, in.
K _B	blockage factor dimensionless
i	incidence angle, deg
J	mechanical equivalent of heat, 778.2 ft - lb/Btu
l	blade surface length, ft
l ₀	orthogonal length, ft
M	Mach number
N	rotational speed, rpm
σ	throat dimension, in.
P	stagnation pressure, psia
R	radius, in.
S	entropy
s	pitch spacing, in.

T	stagnation temperature, °R
t	trailing edge thickness, in.
t	static temperature, °R
U	blade velocity, fps
ϕ_n	nozzle Zweifel coefficient
ϕ_r	rotor Zweifel coefficient
V	absolute gas velocity, fps
W_a	airflow, lbs/sec
W	relative gas velocity, fps
Y_T	Loss coefficient, $\frac{\text{Loss of total head pressure}}{\text{Total pressure at blade outlet} - \text{Static pressure at blade outlet}}$
w	gas weight flow, lbs/sec
z	number of blades
α	relative gas flow angle measured from axial direction, deg
β	absolute gas flow angle measured from axial direction, deg
γ	ratio of specific heats
δ	ratio of inlet stagnation pressure to sea level standard

$$\epsilon = \frac{\gamma_{sl}}{\gamma} \left[\frac{\left(\frac{\gamma + 1}{2} \right)^{\frac{\gamma}{\gamma - 1}}}{\left(\frac{\gamma_{sl} + 1}{2} \right)^{\frac{\gamma_{sl}}{\gamma_{sl} - 1}}} \right]$$

η_t total-to-total adiabatic efficiency, %

$$\theta_{cr} = \frac{T}{T_{sl}} \left(\frac{\gamma}{\gamma + 1} \right)^{\frac{(\gamma_{sl} + 1)}{(\gamma_{sl})}}$$

$\zeta (s)$ local loss coefficient, $\frac{\text{Loss of total head pressure}}{\text{Inlet dynamic head}}$

η efficiency, $\frac{\text{Actual velocity}}{\text{Isentropic velocity}}$, corresponding to total-to-static pressure ratio

ρ density, slugs/ft³

Subscripts:

av average

cr conditions at Mach number of 1.0

h hub

m	mean condition
p	pressure surface
r	radial direction
s	suction surface
sl	standard sea level conditions
T	total condition
t	tip
x	axial direction
θ	tangential direction

INTRODUCTION

Under a previous USAAVLABS Contract, DA 44-177-AMC-184(T), a 5-pound-per-second, fluid-cooled turbine was designed with the objective of demonstrating high temperature technology for small, lightweight, high performance turboshaft engines. The gas generator turbine had been tested to show a design point efficiency of 81 percent (peak island of 82 percent) (Figure 1). Conventional blading would be expected to yield a total-to-total adiabatic efficiency of over 85 percent. Deterioration of performance was attributed to high secondary losses arising from short, thick blading and low aspect ratios. The small blade heights evolved from a combination of high compressor pressure ratio and low mass flows, whereas long, thick chords were necessary because of mechanical considerations, fabrication techniques, and cooling requirements. Figures 2 through 4 describe the turbine geometry tested.

The aerodynamic design objectives of this machine reflect the aspect ratio and short blade problems associated with small, high pressure ratio turbomachinery. A redesign of this turbine, was, therefore, chosen as a nominal version to evaluate the effects of span aspect ratio and tip clearance on efficiency. Two additional flow passages (150 percent of nominal and 50 percent of nominal) were also designed for the subject study contract. Hardware was procured and the three turbine versions were tested for performance on a cold-flow rig. Rotor tip clearance was varied from 1.5 to 5.0 percent of the blade span for end loss performance effects.

DISCUSSION

The aerodynamics of any cooled turbine are necessarily compromised by mechanical design, fabrication techniques, heat transfer, and cooling requirements. A further stipulation of a "small" gas turbine will uniquely define the maximum blade heights of the machine. For a given cycle, any practical limitation on minimum axial chords simply results in lower blade aspect ratios as the size of the machine is decreased. This type of blading characteristically has high secondary flow losses (References 2 through 8). Figure 5 describes how these secondary flows are formed in a nozzle cascade with plane walls. A circulatory flow is generated from the pressure to the suction side of the blading near the walls that interacts with the main and corner flows. These losses are mainly confined to the ends of the blades. Figure 6 (from Reference 5) shows the influence of blade-length ratio on secondary flow losses of several turbine cascades. These data, correlated

into one curve, show secondary losses extending one chord length from the wall. The curve suggests that losses on blading with an aspect ratio* of $h/c \leq 2.0$ will be comprised mainly of secondary losses. As shown in Figure 2, the original blading was designed for h/c values in the 0.5 to 0.7 region.

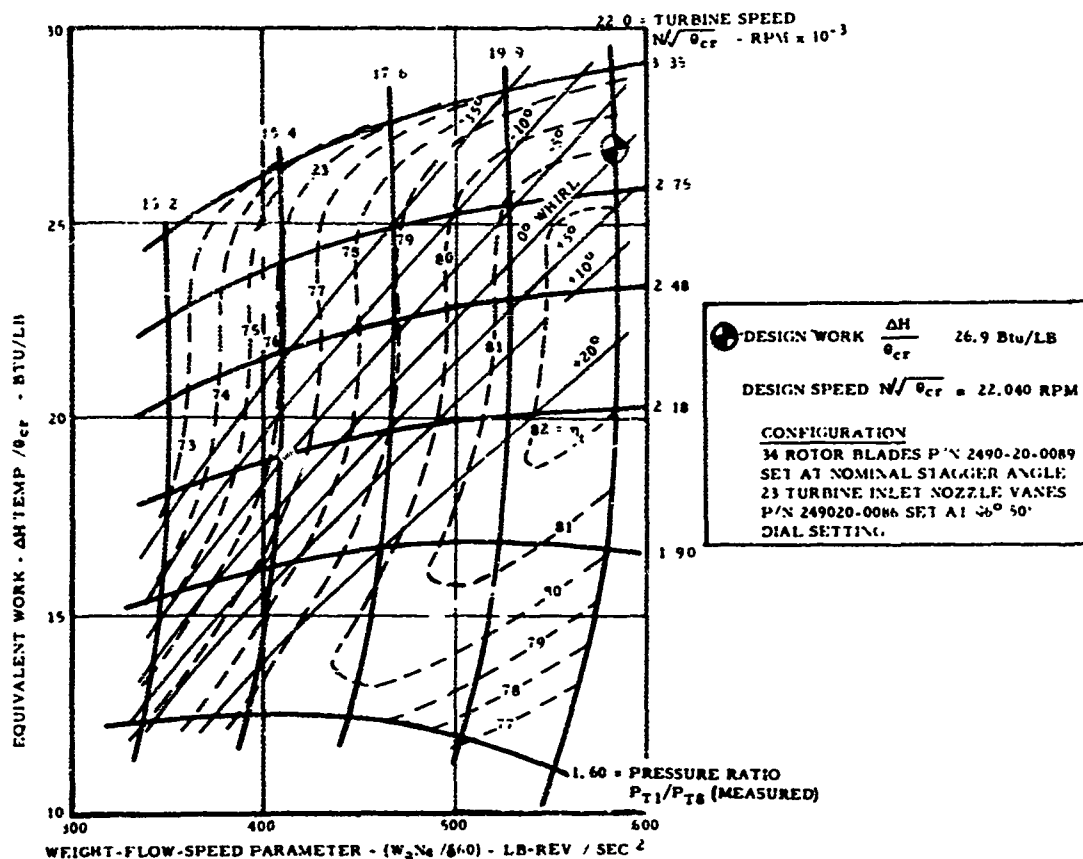


Figure 1. Fluid-Cooled Turbine - Test Stand Performance.

* To define aspect ratio as a ratio of annulus height to mean throat width of the cascade is not considered representative. For example, one-half the blades in a given cascade of fixed height could be removed and efficiency would change drastically. This change would be due to increased blade loading and not to any blading aspect ratio effects.

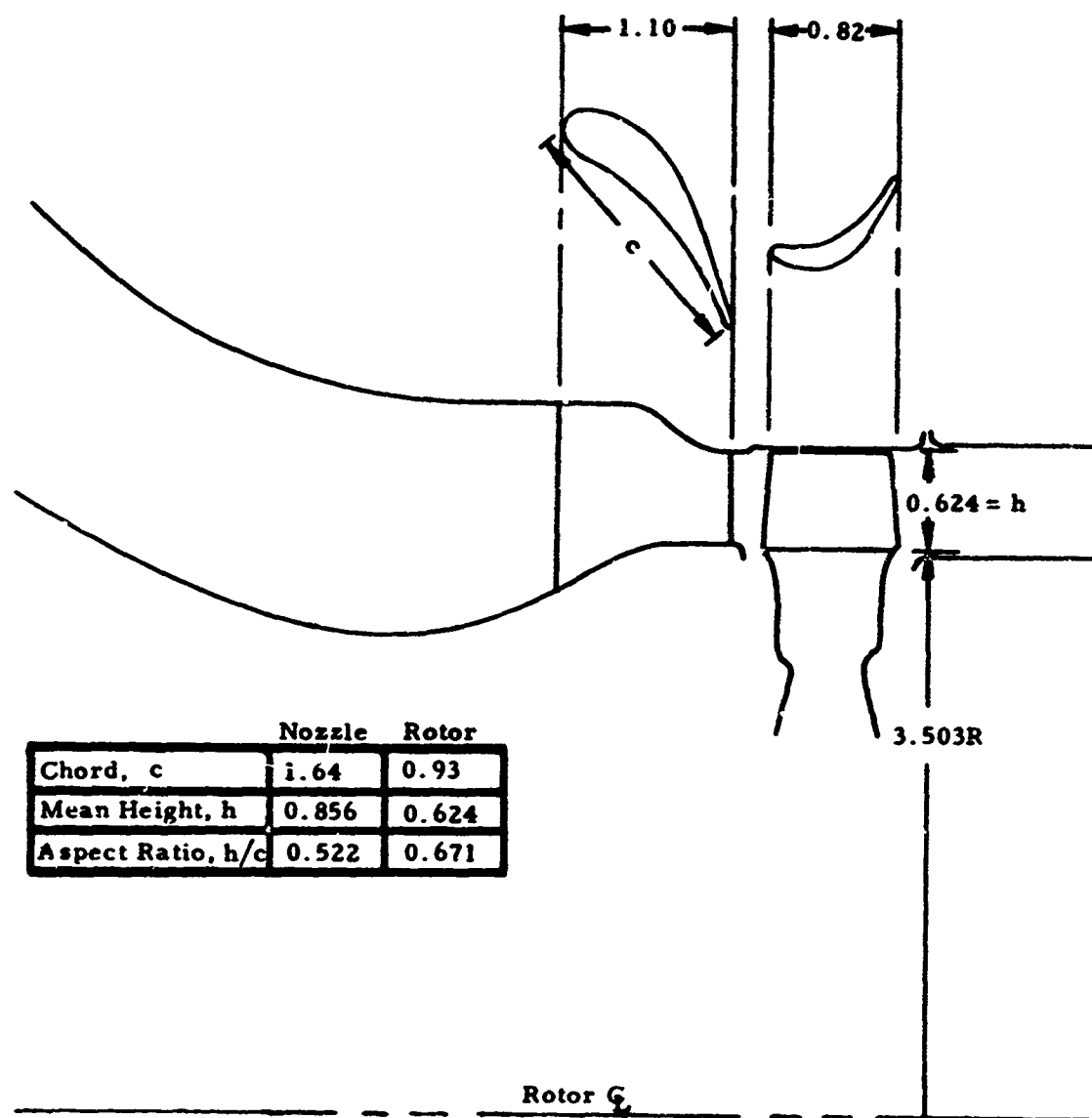


Figure 2. Fluid-Cooled Turbine Flowpath.

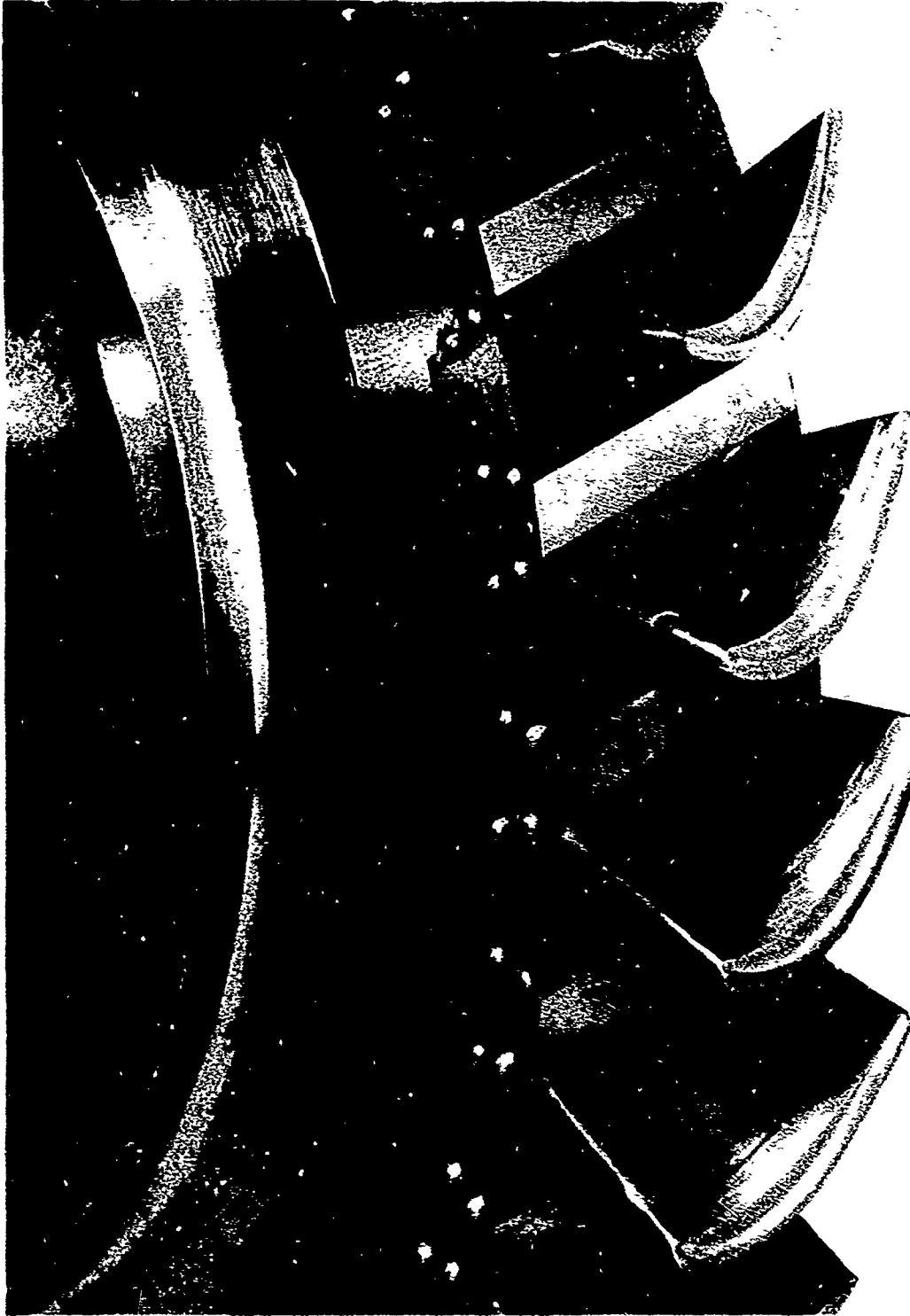


Figure 3. Turbine Blade Assembly.

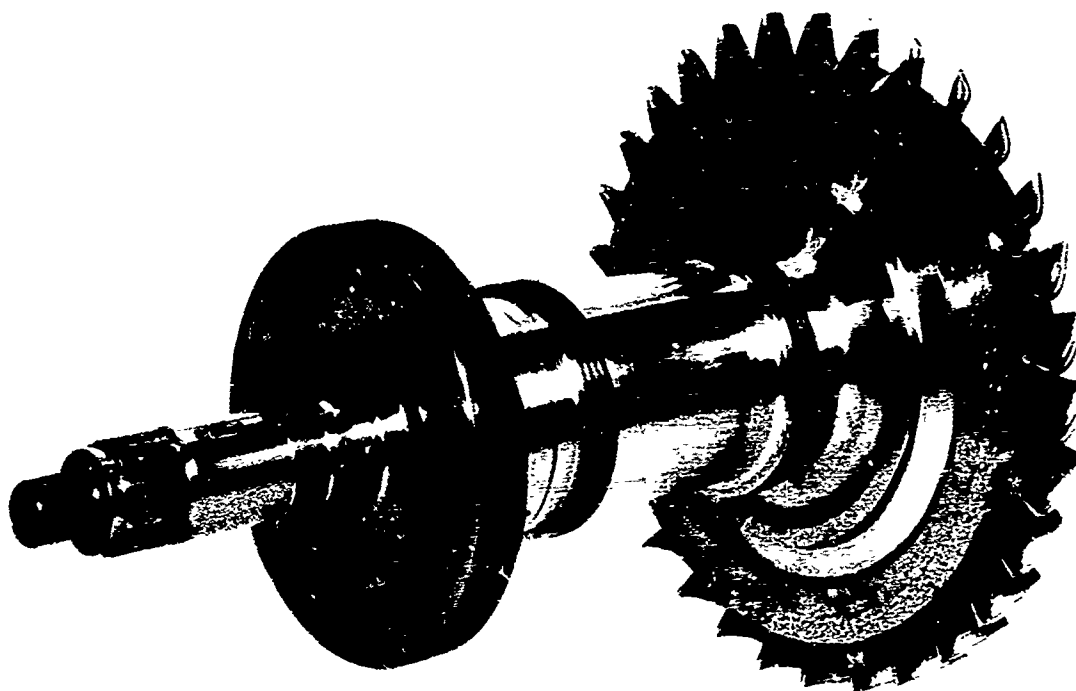


Figure 4. Turbine Rotor Assembly.

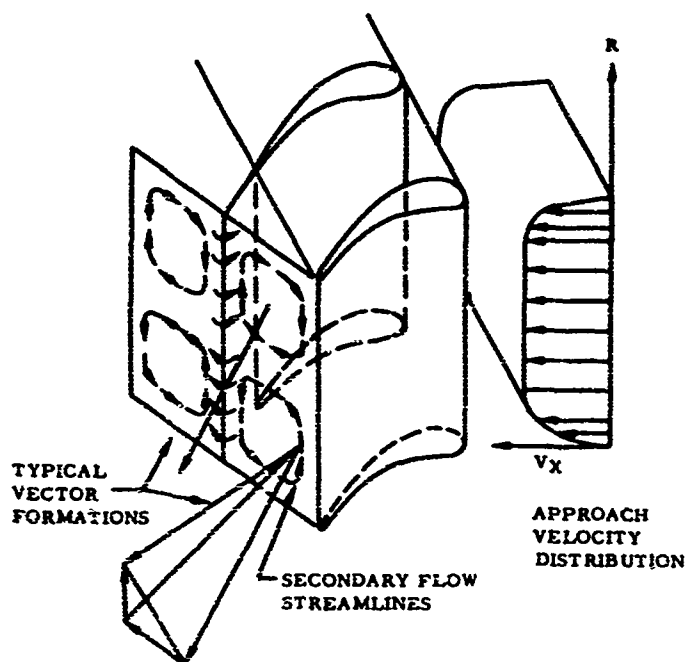


Figure 5. Secondary Flow Formation in a Nozzle Cascade.

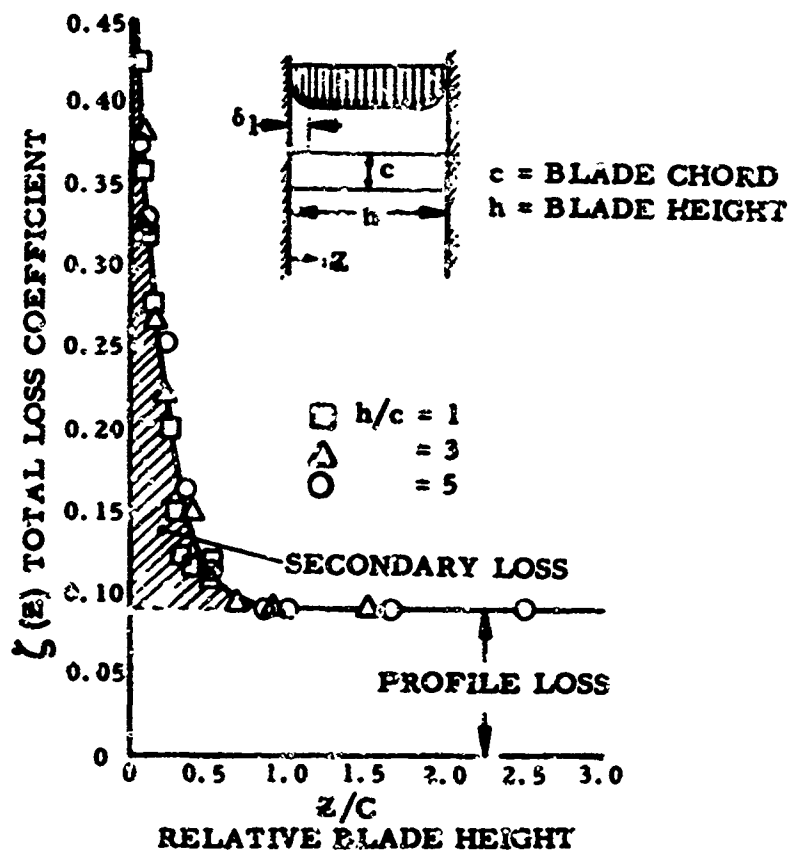


Figure 5. Influence of Blade Length Ratio h/c on Secondary Flow Losses of Turbine Cascade.

An illustration of span aspect ratio effect is shown in Figure 7 as derived from Reference 4. Lines of constant blade height have also been superposed onto Figure 7. This set of curves shows that once the blade height is fixed, the loss is comparatively independent of the aspect ratio. This characteristic may exist when the boundary layers remain fixed in size as the chord is varied for a given span. The three-dimensional flow through the nozzle and rotor is further complicated by the blade shape, clearance velocity distributions, inlet boundary layers, and vorticity. The general solution to this problem is a highly complex one requiring vast amounts of experimentation. However, the required amount of testing can be reduced when a given geometry is selected for investigation. In this case, a specific evaluation was made on a variation of the fluid-cooled turbine.

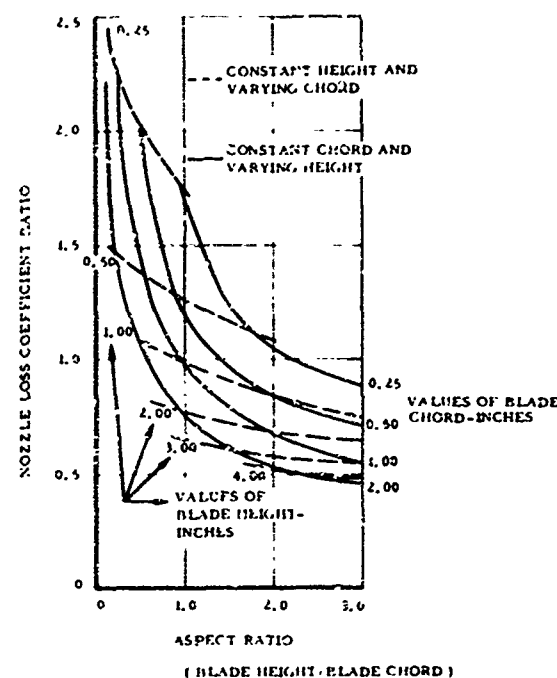


Figure 7. Variation of Nozzle Loss Coefficient With Blade Aspect Ratio.
Pitch Chord Ratio = 0.77 at M Exit = 0.8.

Aerodynamic Design

The aerodynamic design of a turbine consists of (1) selection of wheel speed and flowpath to achieve a desired level of efficiency, (2) determination of velocity triangles, and (3) selection of airfoil section geometry to match the velocity diagrams. Each of these items is inter-related and further restricted by heat transfer and mechanical design requirements. A lengthy trial and error process was used for a suitable compromise of all the parameters involved.

Flowpath and Velocity Diagrams. The triangles were calculated from the basic compressible relations for axisymmetric flow, which may be stated as:

$$gJc_p \frac{\partial T}{\partial r} = gJt \frac{\partial S}{\partial r} + \frac{V_\theta \partial V_\theta}{\partial r} + \frac{V_\theta^2}{r} + \frac{V_x \partial V_x}{\partial r} - \frac{V_x \partial V_r}{\partial x}$$

(Radial Equilibrium Equation) (1)

$$W = 2 \pi g K_B \int_{r_h}^{r_t} \rho V_x r dr = \text{Constant} \quad \text{(Continuity Equation)} \quad (2)$$

$$gJ \Delta H = \Delta(UV_\theta) = gJc_p \Delta T \quad \text{(Energy Equation along a Streamtube)} \quad (3)$$

Simultaneous solution of the above equations requires definition of a flowpath which is interrelated with efficiency and practical blade dimensions. Blade element performance was estimated from a combination of published loss data and a semiempirical correlation used in a Continental computer program. Efficiency penalties were broken down into:

1. Clearance Effects
2. Profile Losses
3. Secondary Losses
4. Trailing Edge Losses
5. Reynolds Number and Disc Friction Effects
6. Incidence Losses

Initially, a free vortex solution was obtained to estimate radial variations in the loss coefficients. Relaxation procedures were then used to solve the nonisentropic radial equilibrium equation. Radial variations in loss and flow conditions were then calculated in eight annular sectors for any given set of axial stations.

Airfoil Section Geometry

Having satisfied the reaction, annulus geometry, and cycle conditions in terms of velocity diagrams, the blade shapes must be defined. This is inherently a lengthy iterative process balancing the aerodynamic blade loadings against practical size and shape. Typical analysis for a rotor blade at a given radial station is as follows:

An initial estimate of a pitch/chord value is made by the use of a Zweifel coefficient, (ϕ) (Reference 7), defined by:

$$\phi = \frac{4 \pi r_{m9} h_r V_{x9}}{z S' (W_9)^2} \quad (r_{m9} V_{\theta 9} - r_{m5} V_{\theta 5})$$

where:

z = number of blades

S' = meridional blade surface area x radius to center of gravity

h_r = rotor blade height

r_{m9} = rotor outlet mean radius

r_{m5} = rotor inlet mean radius

V_θ, W, V_x = rotor velocity components as obtained from velocity diagrams

(See Figure 8 for notations.)

Specification of the hub-tip ratio, tip diameter, and aspect ratio, along with the Zwiefel coefficient, gives a first approximation of the required number of blades. The local throat area required is calculated from the equation of continuity and the requirements imposed by the velocity diagrams evolved from the general radial equilibrium equations. For subsonic discharge, the local throat dimension σ_g is obtained from the relation $\sigma_g = (S_g - t_g) \cos \alpha_g$. For supersonic discharge, the local throat dimension is obtained from the relation

$$\sigma_g = (S_g - t_g) (\cos \alpha_g) \left(\frac{A_{cr}}{A} \right) \text{ where } \left(\frac{A_{cr}}{A} \right) \text{ corresponds}$$

to the supersonic critical velocity ratio. A thickness/chord ratio is selected (consistent with current practice) to achieve low mechanical stress levels.

Incidence and deviation considerations fix the inlet and outlet blade angles. Additional conditions specified during the initial phases of the design are:

1. A parabolic or hyperbolic mean line is used.
2. One of the following blade thickness distributions, or a combination thereof, is selected:
 - a. British T-6.
 - b. NACA 65 series.
 - c. NACA 63 series.

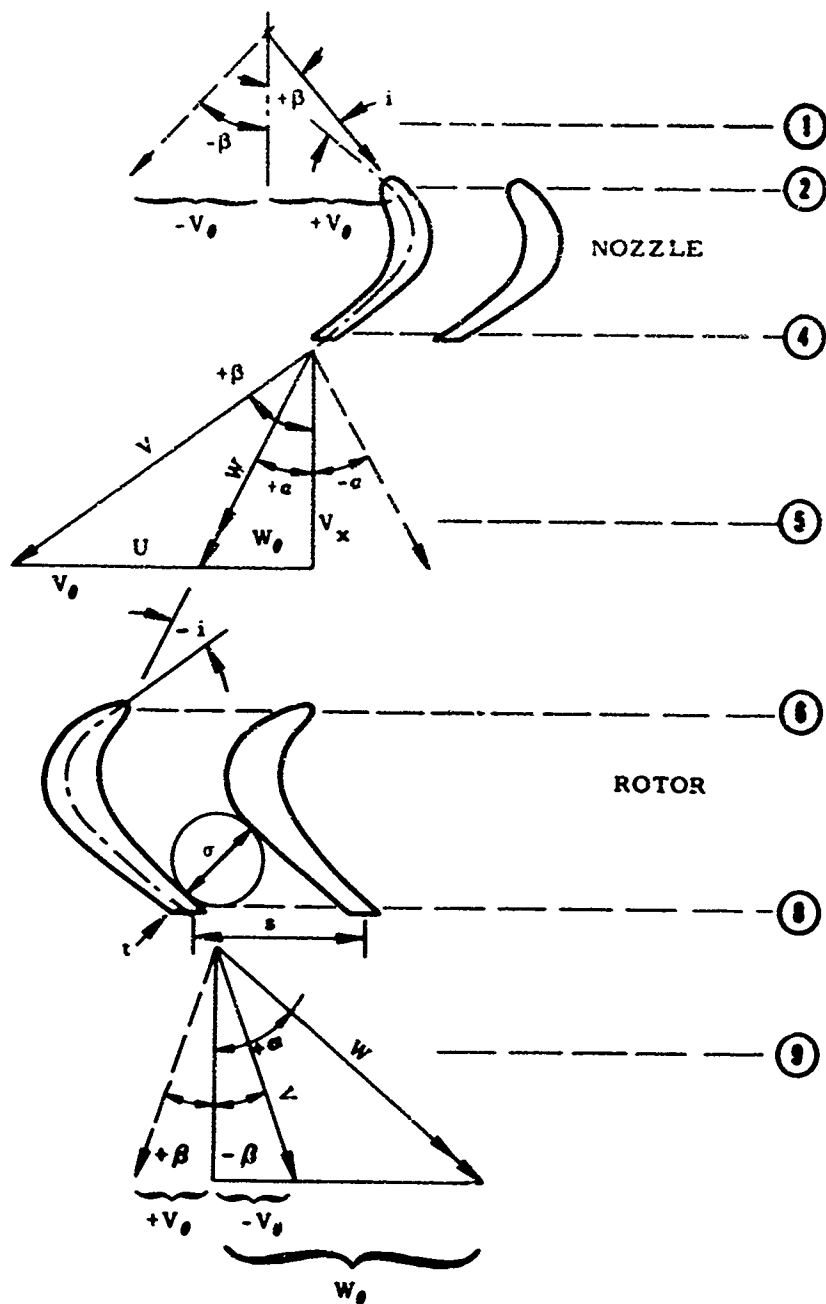


Figure 8. Turbine Velocity Diagram Station and Sign Notations.

d. NACA Primary series.

e. NACA Secondary series.

A computer program is used to wrap the thickness distribution about the mean line and is repeated until throat requirements are met. Initially a primary series was selected for the nozzle and a T-6 series for the rotor blade nominal design. The blade coordinates thus given were then refined to satisfy diffusion loading requirements.

Velocity distributions around the blading are obtained using simplified NACA stream filament techniques (Reference 9). A linear variation of total pressure is assumed through the channel and mean line flow conditions established from the equation of continuity. Suction and pressure surface local velocities V_s and V_p are then obtained from the local mean line value V_m from

$$\frac{V_s}{V_m} = e^{m_1} \quad \text{and} \quad \frac{V_p}{V_m} = e^{m_2}$$

where:

$$m_1 = \left[\frac{C_s l_o}{2} \left(1 + \frac{C_p - C_s}{4 C_s} \right) \right]$$

$$m_2 = \left[\frac{-C_s l_o}{2} \left(1 + 3 \frac{\{C_p - C_s\}}{4 C_s} \right) \right]$$

The local suction and pressure surface curvatures C_s and C_p are calculated from the blade coordinates. The blade surface velocities thus calculated are examined to find if they fall within the prescribed limits. Modifications are made to the blade shape, and the velocities are recalculated. If warranted, solidity and incidence changes are made. The iterative procedure is continued until aerodynamic loading requirements are satisfied. Similar procedures are used for the nozzle design.

Blade loading limits were estimated by the use of diffusion factors defined as:

D_p = Pressure surface diffusion parameter

$$= \frac{\text{Blade Inlet Relative Velocity} - \text{Minimum Blade Surface Relative Velocity}}{\text{Blade Inlet Relative Velocity}}$$

D_s = Suction surface diffusion parameter

$$= \frac{\text{Maximum Blade Surface Relative Velocity} - \text{Blade Outlet Relative Velocity}}{\text{Maximum Blade Surface Relative Velocity}}$$

D_{tot} = Total diffusion parameter

$$= D_p + D_s$$

In the past NACA has generally recommended that a high efficiency turbine be designed for:

1. $D_s \leq 0.10$

2. $D_{tot} \leq 0.50$

Nominal Aspect Ratio Design

This turbine is essentially a redesign of the fluid-cooled turbine. Its function is that of a single-stage gas generator turbine driving a 9.2 pressure ratio compressor with 5 pound per second airflow. Table I summarizes the design point requirements. Figure 9 gives the design velocity triangles.

Cold-flow testing of the fluid-cooled turbine showed an efficiency of 81 percent at this design condition (Figure 1). Conventional efficiency calculation techniques predict at least an 85 percent potential. The degradation of performance is assumed to be attributable to high secondary losses due to short, thick blading and low aspect ratio effects. The two most important factors leading to more desirable aerodynamic blade shapes over the fluid-cooled turbine are:

- a. The required nozzle crossflow area through the vanes for combustor primary air was reduced from 4.5 to 1.5 square inches.

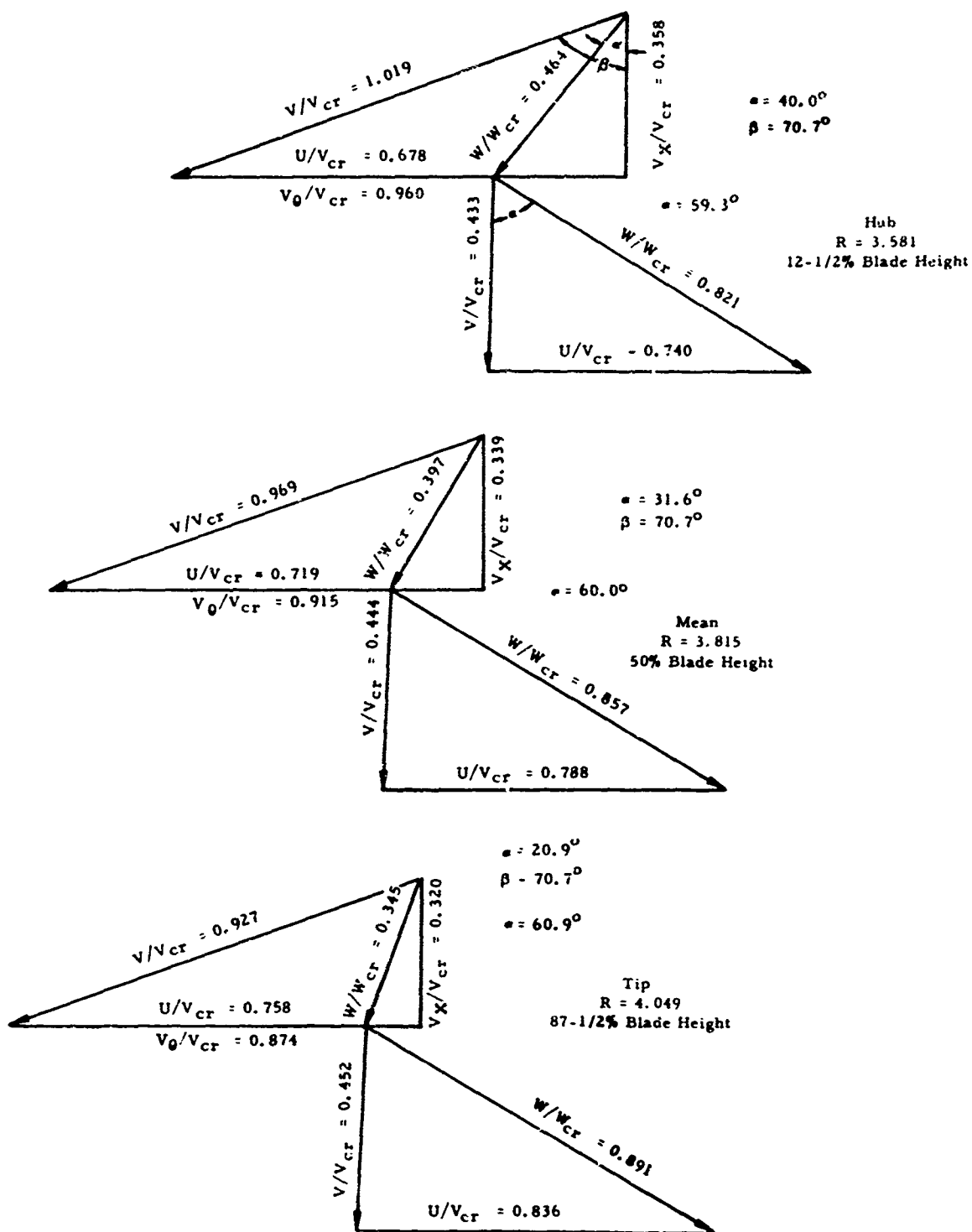


Figure 9. Fluid-Cooled Turbine Velocity Diagrams.

TABLE I
FLUID-COOLED TURBINE DESIGN POINT CRITERIA

	Nonregenerated Version
Airflow, pounds per second	5.0
Compressor Pressure Ratio	9.2:1
Turbine Inlet Temperature, °F	2,300
Rotative Speed, rpm	50,000
Referred Speed, $\frac{N}{\sqrt{\theta_{cr}}}$, rpm	22,060
Referred Flow, $\frac{W_a N}{60} \epsilon \frac{\text{Lb} \cdot \text{Rev}}{\text{Sec}^2}$	513
Turbine Work, ΔH , Btu per pound	138.4
Specific Work, $\frac{\Delta H}{\theta_{cr}}$, Btu per pound	26.94

- b. Recent data were obtained showing that the upper limit on fuel cooling temperatures is 500°F rather than the 330°F limit imposed on the original design.

The nozzle performs the dual function of accelerating the gases to produce turbine work and of providing a flowpath for combustor primary air. Reduction of cross-flow area, item a, allows the use of shorter axial chords, lower thickness-chord ratios, and higher aspect ratio blading. Item b alleviates heat transfer limitations on the rotor and permits more and longer blades to be used. This allows a trade-off between reaction and blade height with constant parameters of flow, work, rotational speed, and exit Mach number. With secondary losses a predominant efficiency factor, a judicial reduction of reaction for aspect ratio may be expected to produce better performance.

Most of the practical size limitations on blade manufacture were established under the fluid-cooled contract and, in general, were adhered to in this design. A significant departure was made in a thinning of the nozzle trailing edge thickness from 0.050 to 0.025 inch. Heat transfer analysis showed that this change could be made by the use of several film cooling holes on the pressure surface, as opposed to trailing edge convection cooling applied in the fluid-cooled turbine. All other chordal geometrical parameters, such as thickness chord ratios, maximum thicknesses, minimum trailing edge thicknesses, and so forth, were maintained fixed within limits of manufacturability. The flow, work, and rotational speed are fixed by the compressor, and the exit critical velocity ratio is fixed by stress and life considerations at 0.43 (same as fluid-cooled turbine). Within these limitations, a parametric study was made to optimize the vane and rotor span aspect ratios.

A reduction of rim speed at a given flow and rotative speed results in longer blading when the meridional Mach numbers are invariant. This means higher aspect ratios, lower end wall loss effects, and lower disc friction losses. At the same time, the overall turning angles, rotor trailing edge to pitch ratios, profile losses, tip clearance, and wake losses are all increasing. Overall performance was obtained by an iterative procedure on the individual blade losses and the equations of motion and energy to satisfy equilibrium. This was done on a computer program that is essentially an outgrowth and modification of the Ainley blade loss treatment (Reference 4). Numerous additions and changes were made to reflect the most recent turbine performance data, particularly in the treatment of secondary losses. Analytical studies showed that rim speed could be reduced while maintaining essentially the same efficiency.

As a result of optimization studies, a reduction of rim speed of 21 percent with respect to the fluid-cooled turbine was chosen as a limit to achieve reasonable performance. Table II shows a comparison of the blade loss breakdown of the two turbines.

Nozzle profiling on the shrouds was also used to minimize the effect of secondary losses. Figure 10 (taken from Reference 8) shows the improvements that can be made with various wall shapes. The best performance gains are obtained from unsymmetrical constriction on the outer wall near the nozzle throat. This type of meridional constriction was introduced in the design, and blade shapes were varied until satisfactory velocity distributions were attained.

TABLE II
BLADE LOSS BREAKDOWN OF THE NOMINAL
ASPECT RATIO DESIGN AND FLUID-COOLED TURBINE

Parameter	Nominal Aspect Ratio Design	Fluid-Cooled Turbine Design
<u>Nozzle Vane</u>		
Profile Loss, Y_p	0.0490	0.043
Trailing Edge Loss, Y_{te}	0.0142	0.047
Incidence Loss, Y_i	0	0
Secondary Loss, Y_s	0.0806	0.084
Clearance Loss, Y_{cl}	0	0
Total Loss, Y_{tot}	0.1438	0.174
Mean Exit Angle	70.76°	69.4°
Mean Camber Angle	70.76°	69.4°
Average Vane Height	0.772	0.858
<u>Rotor Blade</u>		
Profile Loss, Y_p	0.0620	0.040
Trailing Edge Loss, Y_{te}	0.0760	0.061
Incidence Loss, Y_i	0	0
Secondary Loss, Y_s	0.1994	0.266
Clearance Loss, Y_{cl}	0.0488	0.038
Total Loss, Y_{tot}	0.3862	0.410
Mean Exit Angle	55.7°	54.8°
Mean Camber Angle	104.2	85.2
Blade Height	0.724	0.624

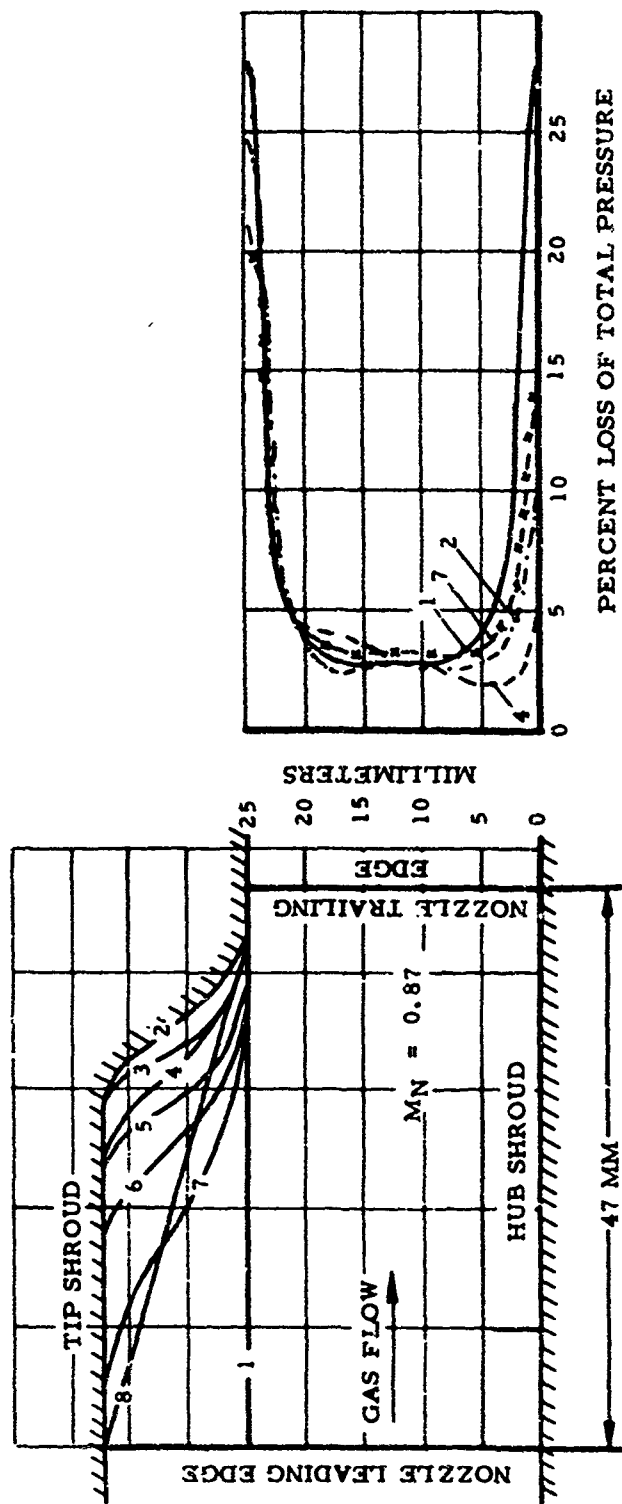


Figure 10. Effect of Meridional Constriction on Losses of a Nozzle.

The nominal design velocity triangles and geometry description are presented in Figures 11 through 14. As a basis of comparison, the velocity distributions and diffusion factors of the turbine are superimposed and a comparison of the two design flowpaths is given in Figures 15 through 18. The improvements are evidenced by a lowering of average rotor diffusion factors from 0.79 to 0.63 and a reduction of nozzle total diffusion factor from 0.75 to 0.10 at the hub section. Other aerodynamic benefits are an increase of rotor and nozzle blade aspect ratios of 16 and 30 percent, respectively; 33 percent reduction of disc friction losses; and a generally smaller, lighter turbine. Vane and rotor blade geometries are compared in Figures 19 and 20, and some of the more important design parameters are summarized in Tables III and IV.

The design analysis predicted an efficiency of 82.5 percent. A similar analysis applied to the fluid-cooled turbine was found to be conservative by approximately 2 percent. The performance capability is, therefore, predicted as 84.7 percent in a finely tuned version.

High Aspect Ratio - 150 Percent of Nominal Design

One of the objectives of the test program was to separate experimentally the singular effect of span aspect ratio on turbine performance. The upper end of the performance regime can be established from tests on a turbine with blading 50 percent longer than the nominal design. Identical airfoils (and, therefore, identical reaction and loading) were maintained over that blade span common to both turbine flowpaths. The extended portion of the blading is loaded so that both the nominal and the high aspect ratio blading have similar average total diffusion factors. The overall design procedure was the same as that used for the nominal flowpath.

Figure 21 describes the evolved flowpath, and Figure 22 presents the design velocity triangles. Extended blading was matched to the velocity diagrams so that total aerodynamic loading was preserved. Velocity distributions and diffusion factors at the hub and tip of the rotor are given in Figures 23 and 24, and for the nozzle vane in Figure 25. Meridional constriction was used on the outer wall of the nozzle so that the ratio of local flow area to inlet flow area was the same at all points as for the nominal flowpath design. Aerodynamic similarity was preserved wherever possible so that the effects of span aspect ratio could be isolated. Table V gives a detailed blade loss breakdown and comparison to the nominal design. The design analysis predicts an

uncompensated total-to-total adiabatic efficiency of 85 percent. A photograph of the finish-machined rotor is presented in Figure 26.

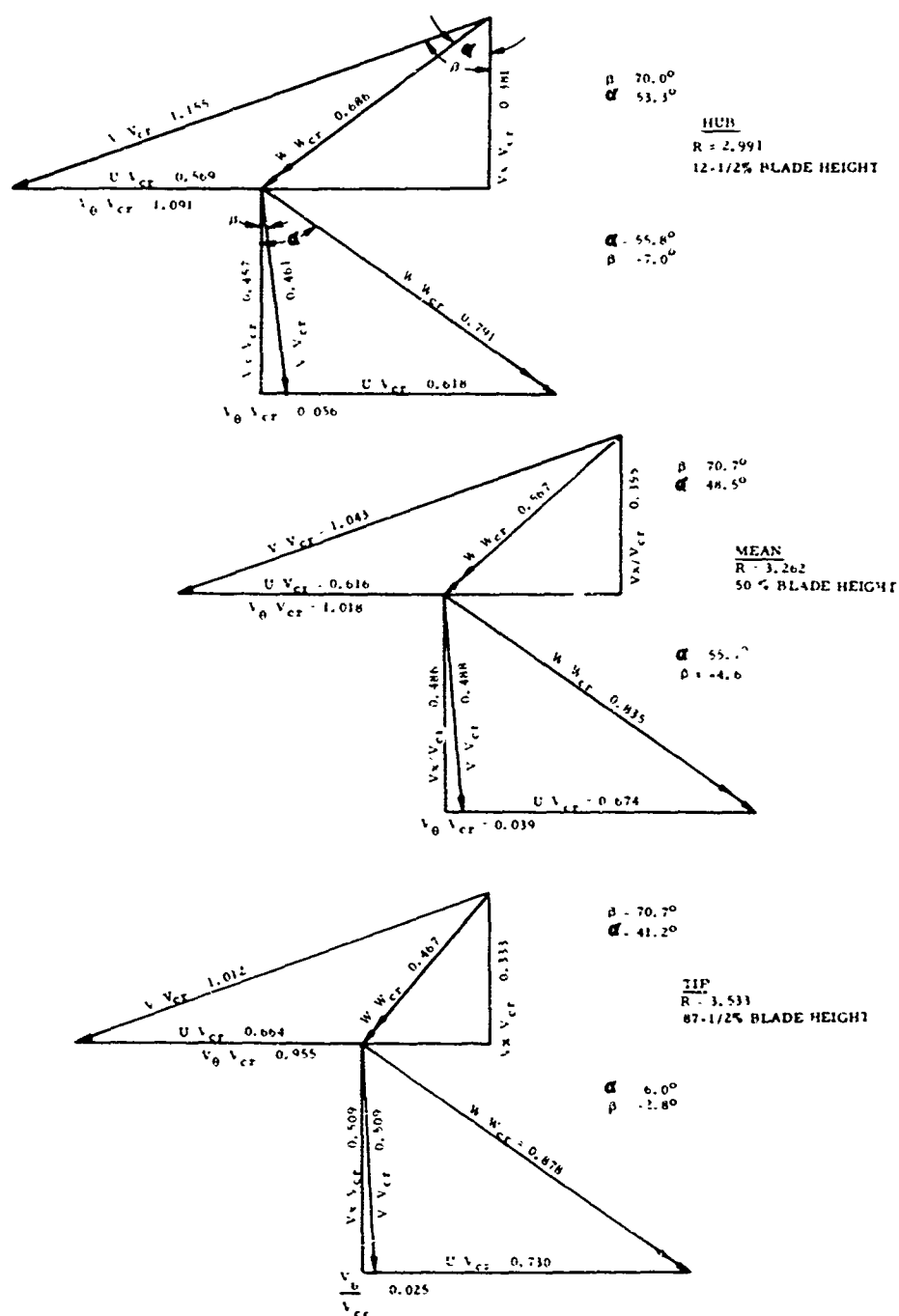


Figure 11. Nominal Aspect Ratio - Velocity Diagrams.

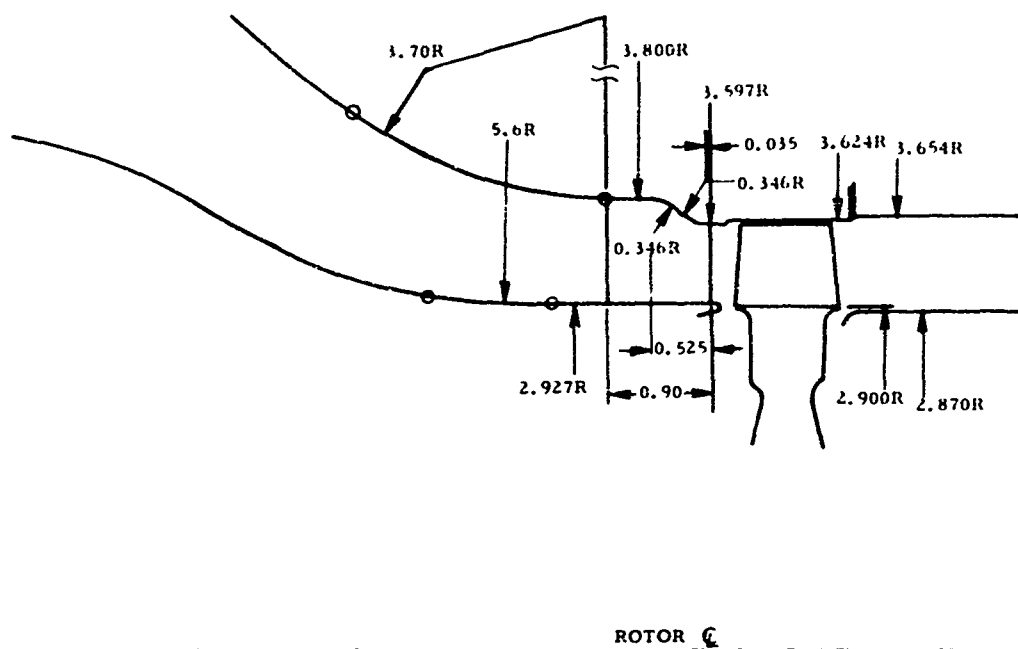


Figure 12. Nominal Turbine Flowpath for Aspect Ratio Evaluation.

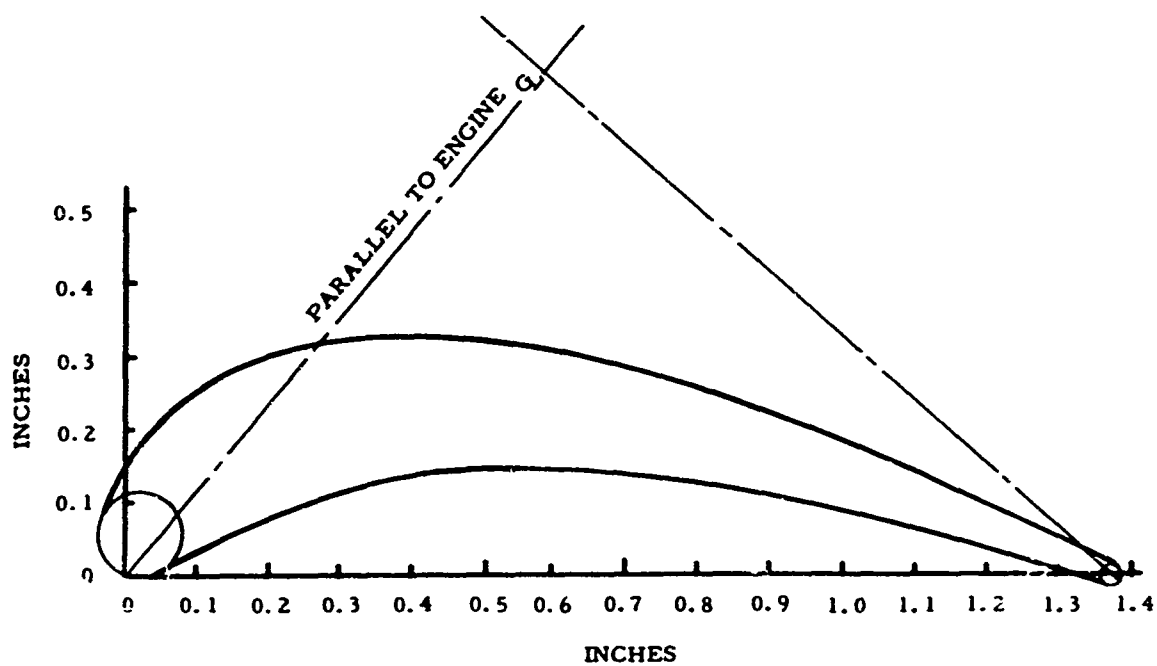


Figure 13. Nominal Turbine Nozzle Geometry.

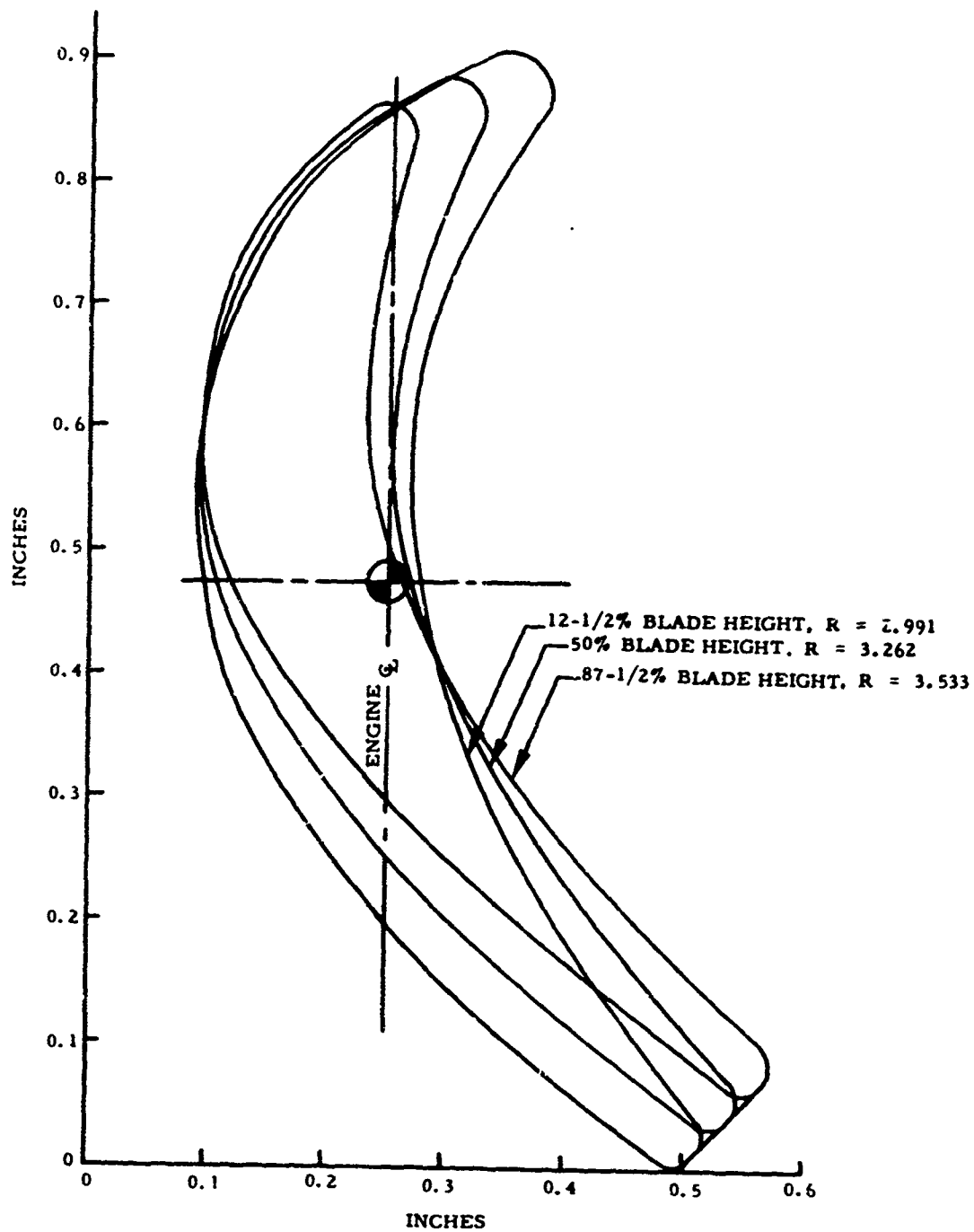


Figure 14. Nominal Turbine Rotor Geometry.

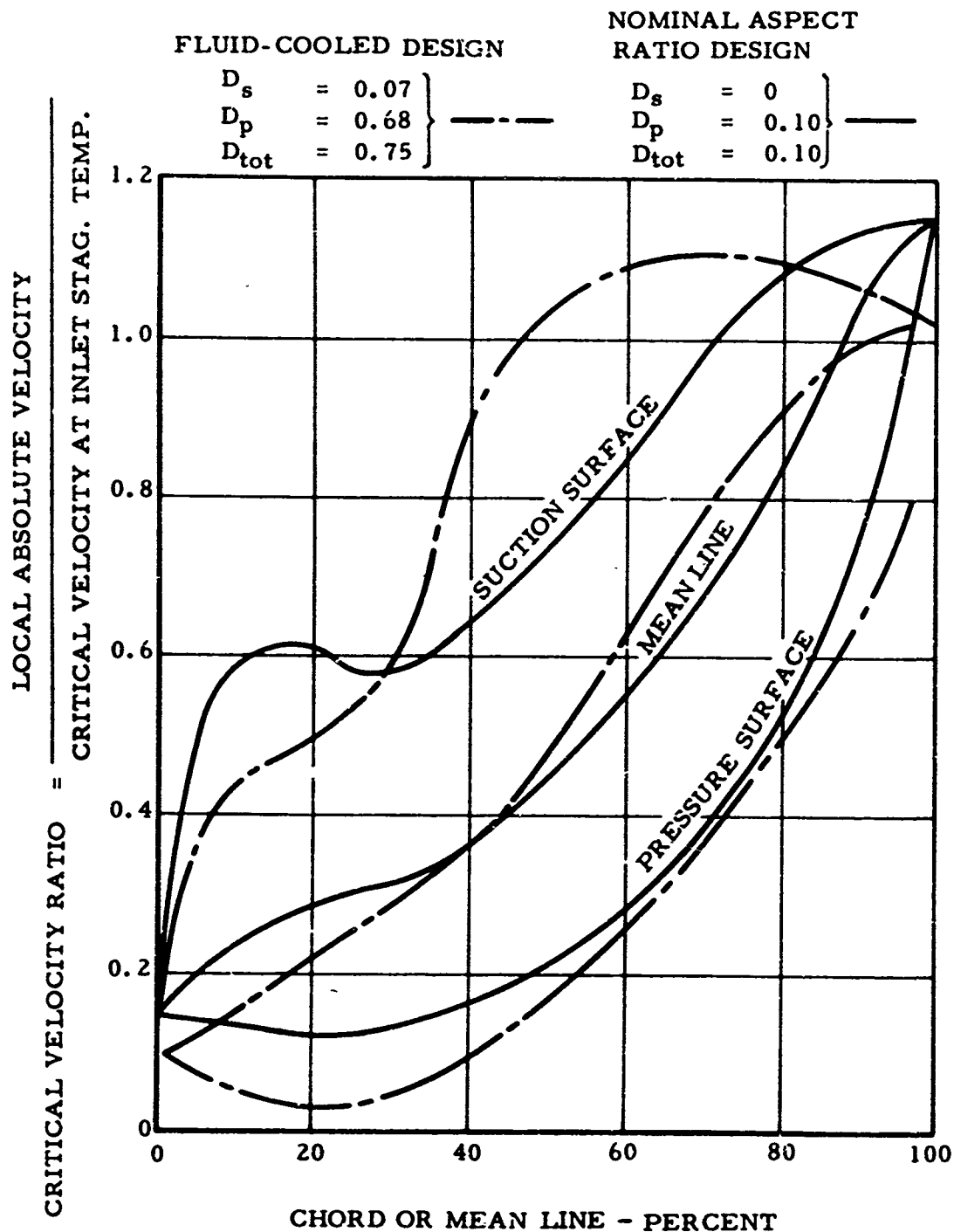


Figure 15. Nozzle Vane Velocity Distribution and Diffusion Factor Comparison; Hub Section, 12.5-Percent Blade Height.

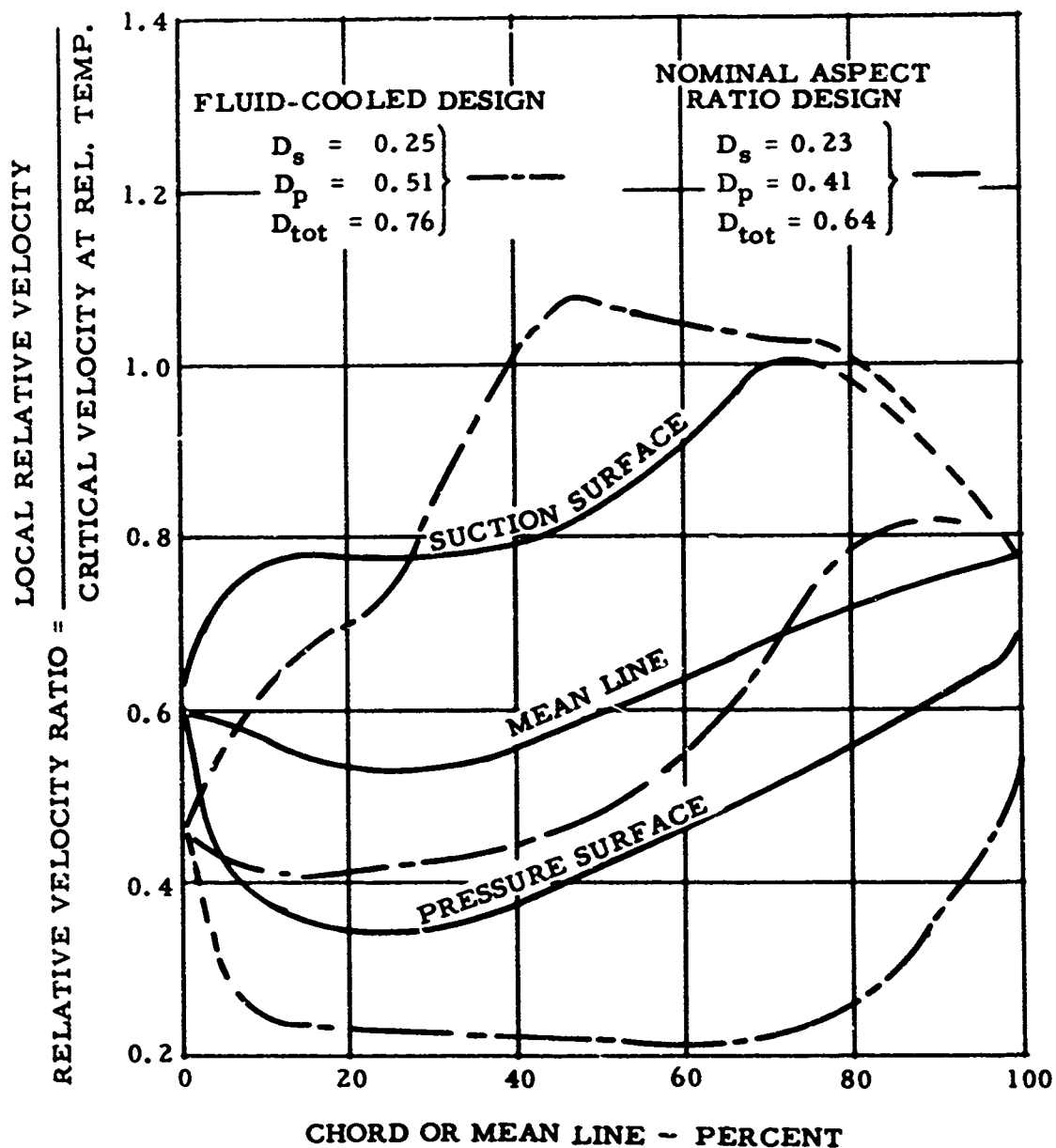


Figure 16. Rotor Blade Velocity Distribution and Diffusion Factor Comparison; Hub Section, 12.5-Percent Blade Height.

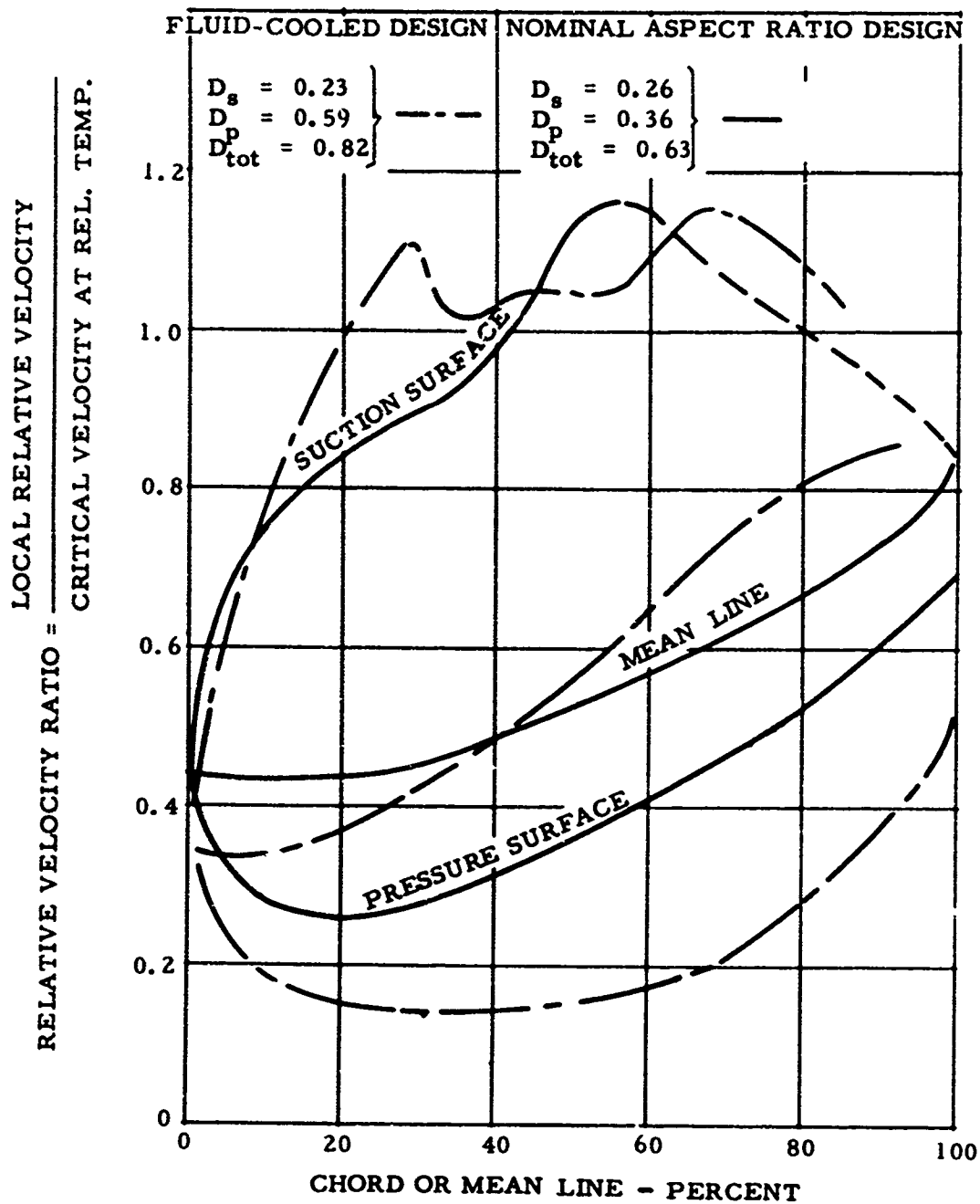


Figure 17. Rotor Blade Velocity Distribution and Diffusion Factor Comparison; Tip Section, 87.5-Percent Blade Height.

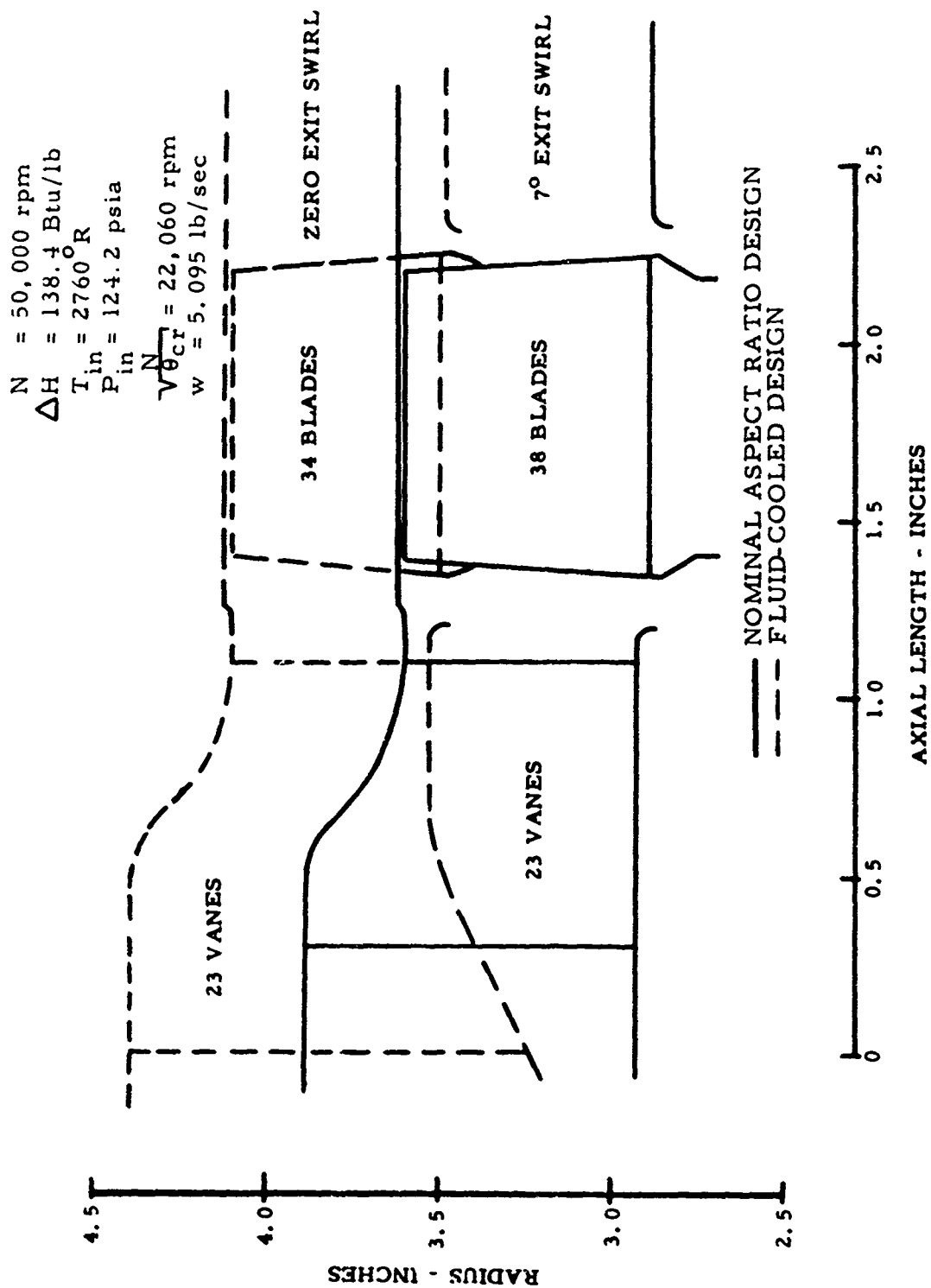


Figure 18. Flowpath Comparison - Fluid-Cooled Turbine Design and Nominal Aspect Ratio Turbine.

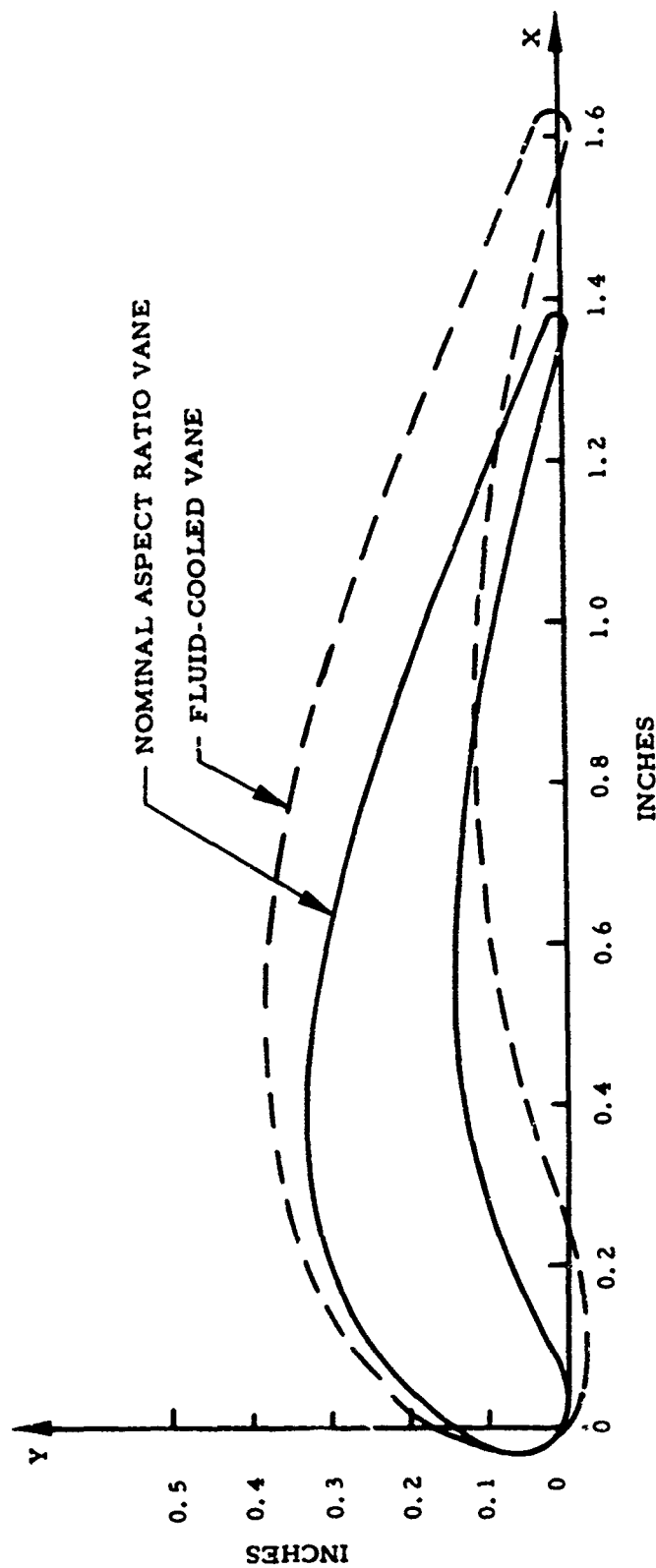


Figure 19. Profile Comparison of Nominal Aspect Ratio Nozzle Vane to Fluid-Cooled Turbine Design Vane - Mean Sections.

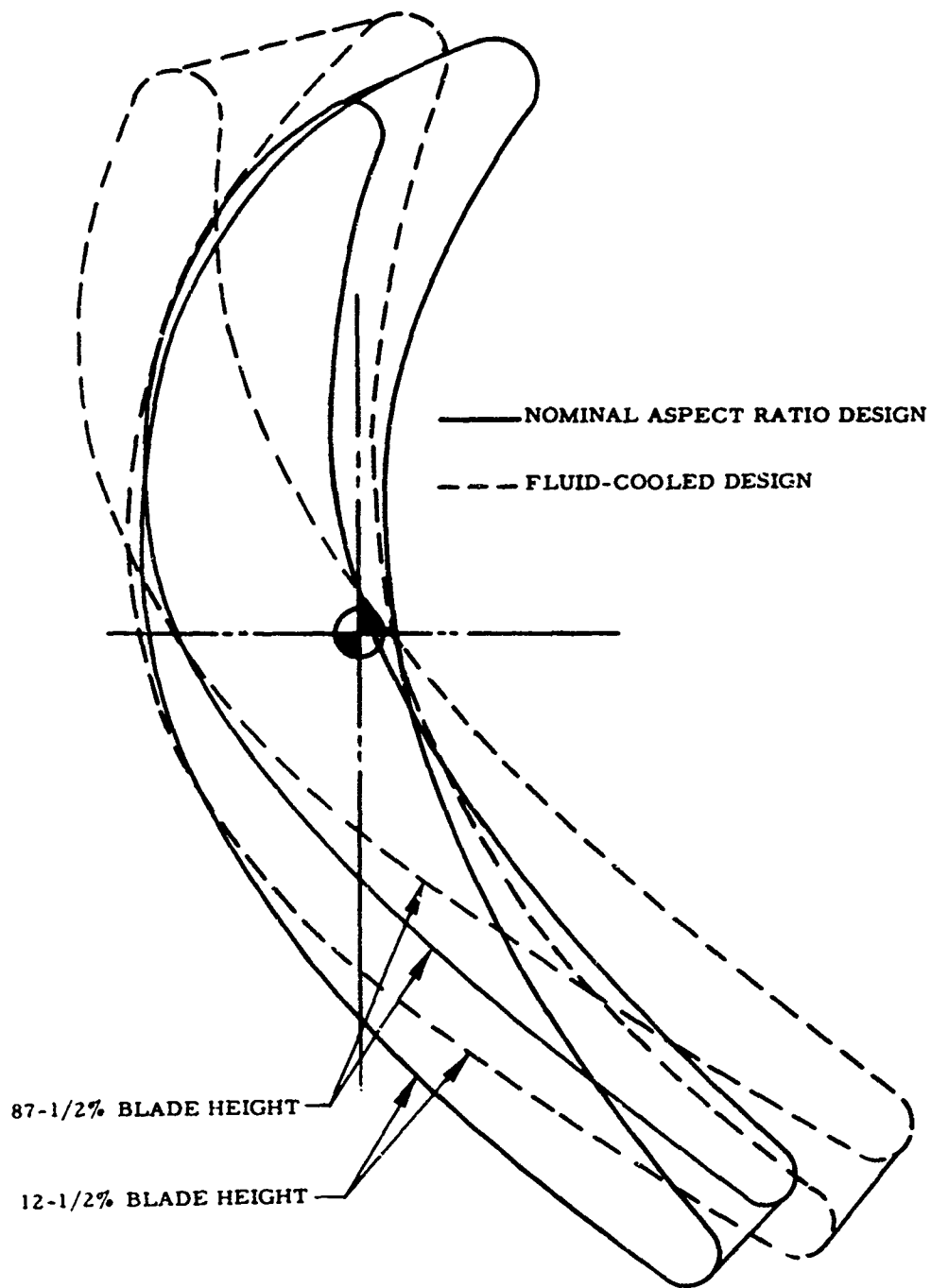


Figure 20. Profile Comparison of Nominal Aspect Ratio Rotor to Fluid-Cooled Rotor.

TABLE III
GEOMETRIC DESIGN PARAMETER COMPARISON OF
NOMINAL ASPECT RATIO TO FLUID-COOLED TURBINE

Parameter	Nominal Aspect Ratio Design	Fluid-Cooled Turbine
Stage Mean Work Coefficient, $\psi = \frac{U_m}{\sqrt{2gJ\Delta H}}$	0.541	0.633
Flow Coefficient, $\psi = \frac{(V_x)}{(U_m)_8}$	0.715	0.566
Hub to Tip Radius Ratio, $\frac{R_h}{R_t}$	0.800	0.849
Rim Speed, ft/sec	1265	1529
Mean Rotor Solidity	1.63	1.2
Number of Nozzle Vanes	23	24
Number of Rotor Blades	38	31
Nozzle Aspect Ratio	0.55	0.52
Rotor Aspect Ratio	0.825	0.671
Rotor Blade Height, in.	0.724	0.624
Nozzle Zwiefel Coefficient, ϕ_n	0.52	0.37
Rotor Zwiefel Coefficient, ϕ_r	0.985	1.063
Nozzle Thickness to Chord Ratio	0.15	0.20
Rotor Thickness to Chord Ratio	0.18	0.17
Nozzle Trailing Edge Thickness, in.	0.025	0.050
Rotor Trailing Edge Thickness, in.	0.0475	0.050

TABLE IV
VELOCITY TRIANGLE AND DIFFUSION PARAMETER COMPARISON
OF NOMINAL ASPECT RATIO TO FLUID-COOLED TURBINE

Parameter	Nominal Aspect Ratio Design			Fluid-Cooled Turbine		
	Hub	Mean	Tip	Hub	Mean	Tip
Absolute Nozzle Exit Critical Velocity Ratio	1.155	1.043	1.012	1.019	0.969	0.927
Rotor Relative Inlet Critical Velocity Ratio	0.686	0.567	0.467	0.464	0.397	0.345
Rotor Relative Exit Critical Velocity Ratio	0.791	0.835	0.878	0.821	0.857	0.891
Rotor Gas Turning Angle	109.1	104.2	97.2	99.3	91.6	81.8
Nozzle Reaction Defined as: Exit Velocity - Inlet Velocity Inlet Velocity	7.00	6.55	6.05	9.75	9.25	8.84
Rotor Reaction Defined as: Exit Relative Velocity - Inlet Relative Velocity Inlet Relative Velocity	0.13	0.32	0.47	0.43	0.54	0.61
Nozzle Suction Surface Diffusion Factor, D_s	0	0.03	0.06	0.07	0	0
Nozzle Pressure Surface Diffusion Factor, D_p	0.10	0.15	0.20	0.68	0.74	0.79
Nozzle Total Surface Diffusion Factor, D_{tot}	0.10	0.18	0.26	0.75	0.74	0.79
Rotor Suction Surface Diffusion Factor, D_s	0.23	0.25	0.26	0.25	0.21	0.23
Rotor Pressure Surface Diffusion Factor, D_p	0.41	0.39	0.36	0.51	0.60	0.59
Rotor Total Surface Diffusion Factor, D_{tot}	0.64	0.63	0.62	0.76	0.81	0.82

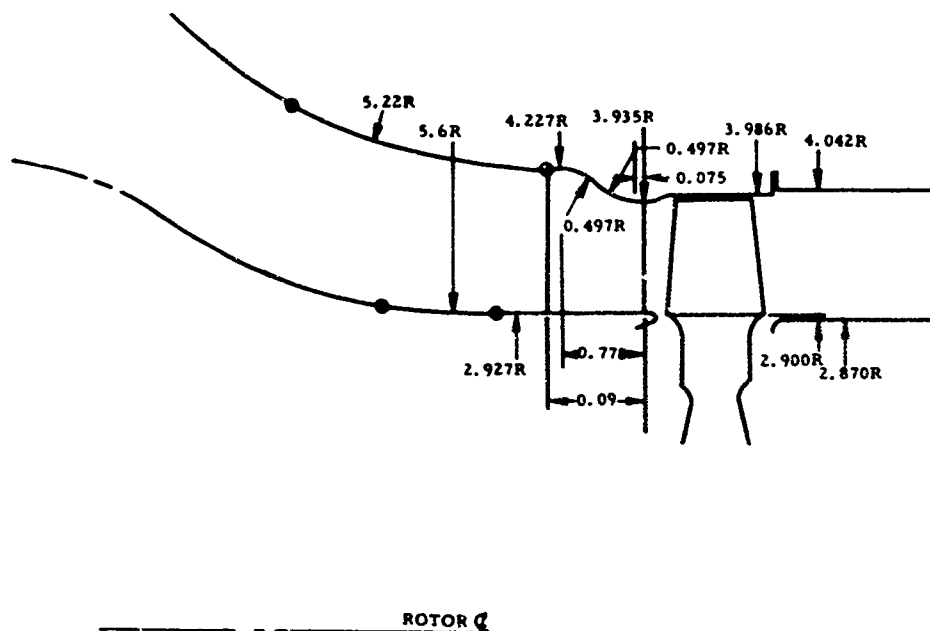


Figure 21. Aspect Ratio Evaluation - 150-Percent Nominal Turbine Flowpath.

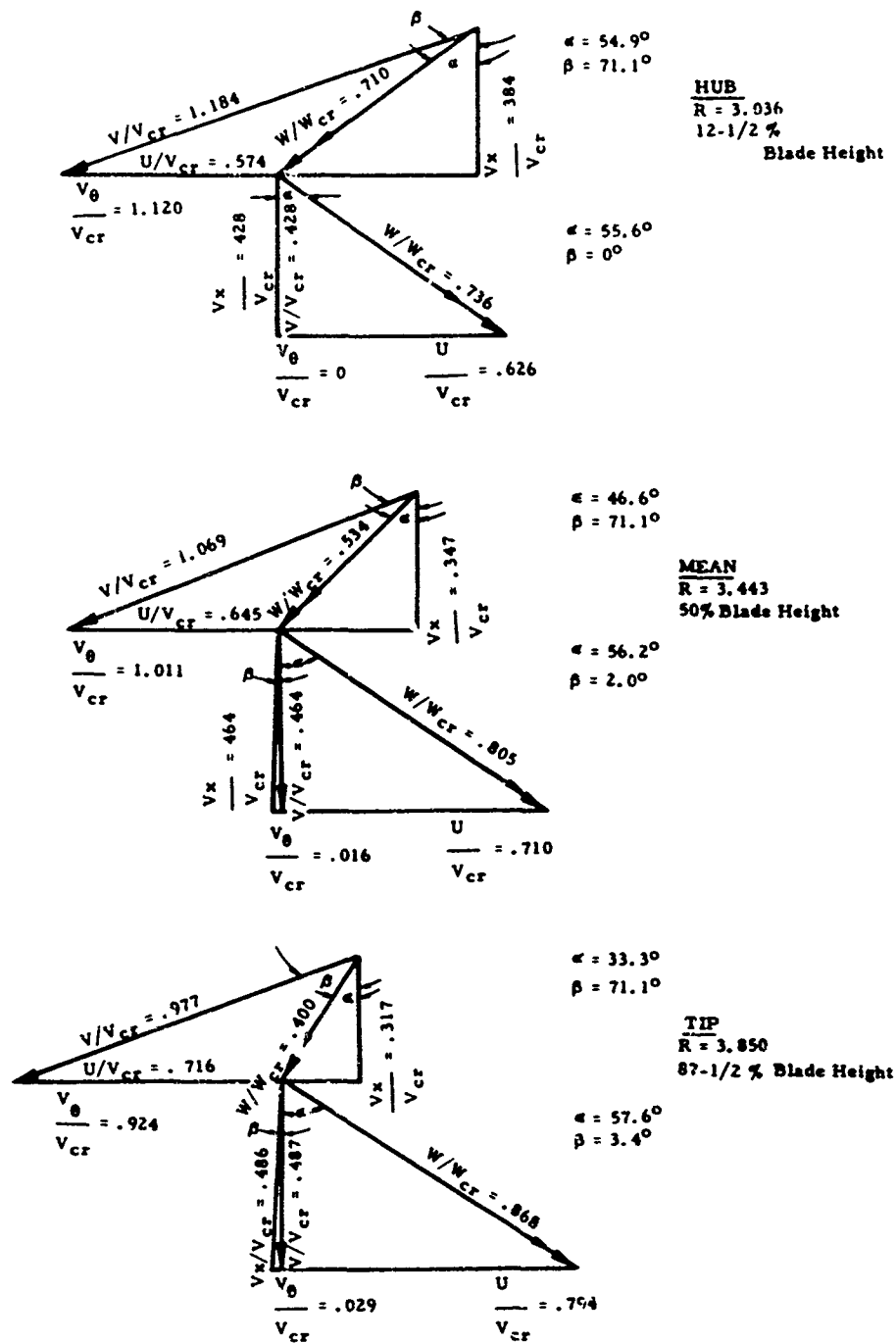


Figure 22. High Aspect Ratio - 150-Percent Nominal Flowpath Velocity Diagrams.

Figure 23. Rotor Blade Velocity Dis- tributions - High Aspect Ratio Design, Hub Section, 8-Per- cent Blade Height.

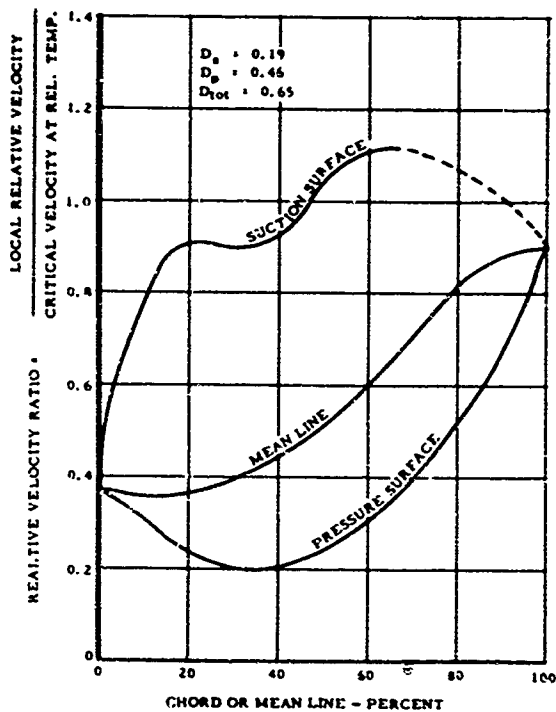
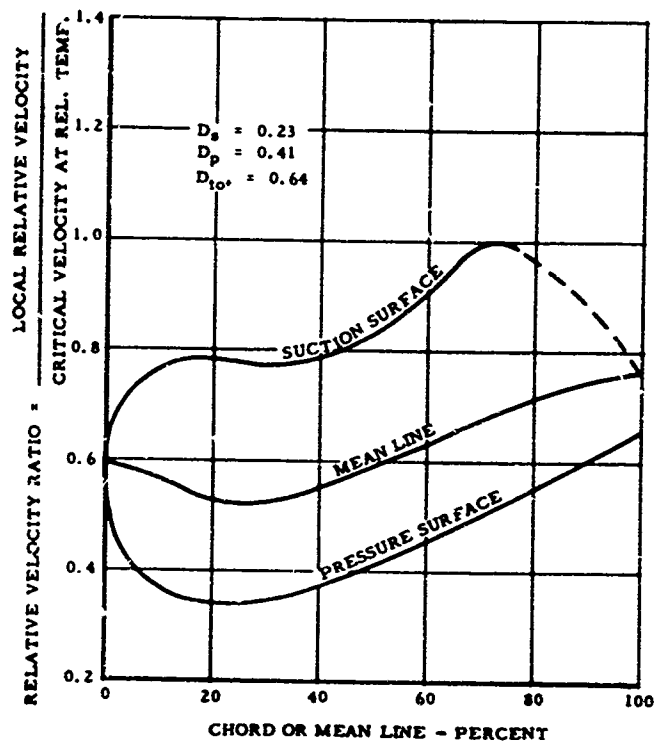


Figure 24. Rotor Blade Velocity Distributions - High Aspect Ratio Design, Tip Section, 100-Percent Blade Height.

TABLE V
BLADE LOSS BREAKDOWN OF THREE ASPECT
RATIO TURBINES

Parameter	High Aspect Ratio Design	Nominal Aspect Ratio Design	Low Aspect Ratio Design
<u>Nozzle Vane</u>			
Profile Loss, Y_p	0.0480	0.0490	0.0472
Trailing Edge Loss, Y_{te}	0.0114	0.0142	0.0149
Incidence Loss, Y_i	0	0	0
Secondary Loss, Y_s	0.0559	0.0806	0.1605
Clearance Loss, Y_{cl}	0	0	0
Total Loss, Y_{tot}	0.1153	0.1438	0.2226
Mean Exit Angle, deg	71.1	70.76	70.0
Mean Camber Angle, deg	71.1	70.76	70.0
Average Vane Height, in.	1.154	0.772	0.387
<u>Rotor Blade</u>			
Profile Loss, Y_p	0.0597	0.0620	0.0762
Trailing Edge Loss, Y_{te}	0.0690	0.0760	0.1045
Incidence Loss, Y_i	0	0	0.0116
Secondary Loss, Y_s	0.1368	0.1994	0.3656
Clearance Loss, Y_{cl}	0.0375	0.0488	0.0900
Total Loss, Y_{tot}	0.3030	0.3862	0.6479
Mean Exit Angle, deg	56.2	55.7	53.7
Mean Camber Angle, deg	102.8	104.2	103.1
Blade Height, in.	1.086	0.724	0.362

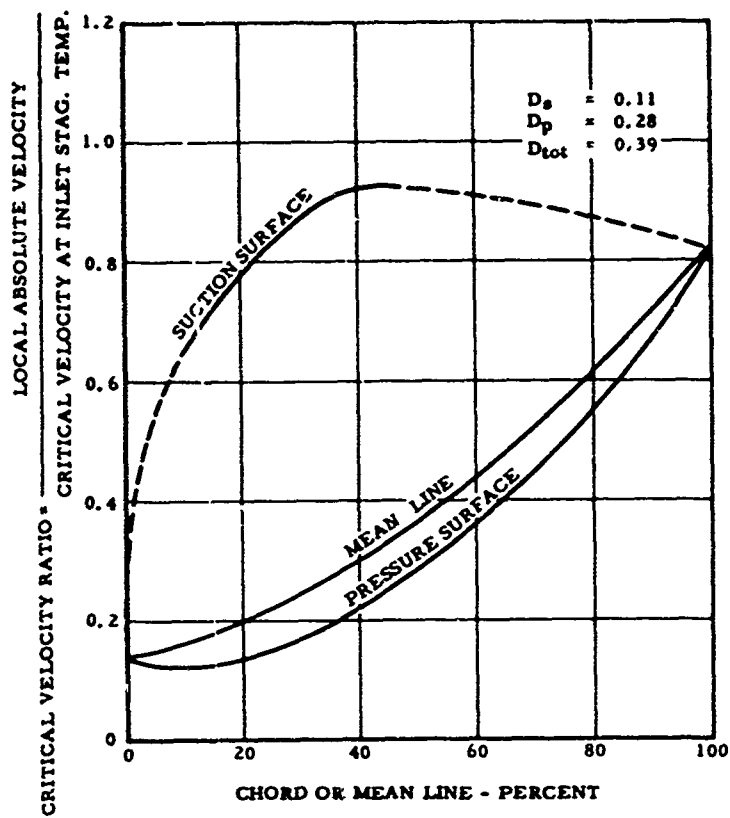


Figure 25. Nozzle Vane Velocity Distributions - High Aspect Ratio Design, Tip Section, 100-Percent Height.

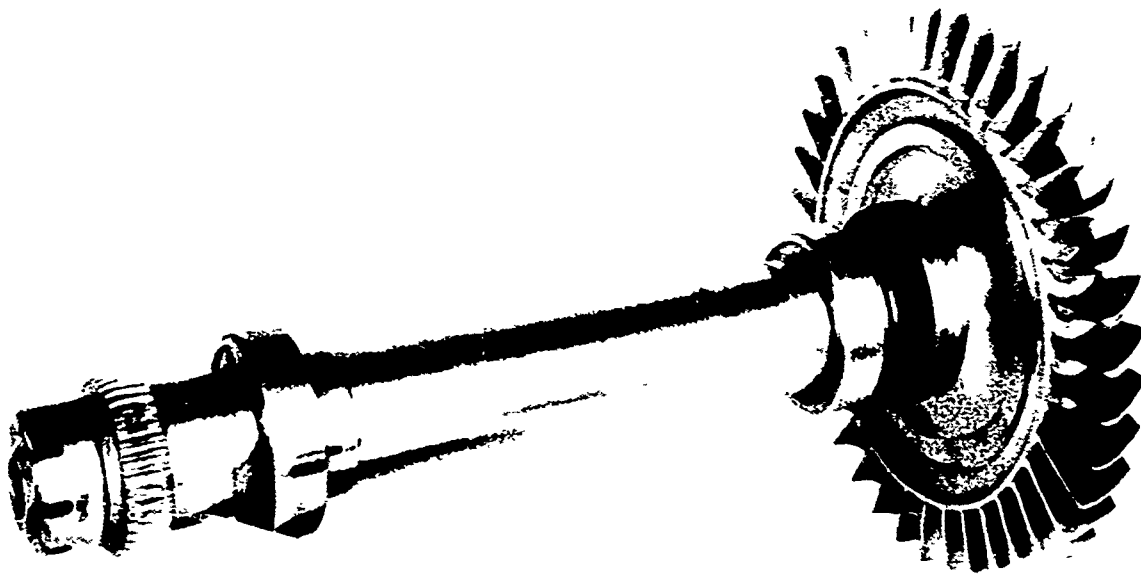


Figure 26. Machined Rotor - High Aspect Ratio Design.

Low Aspect Ratio Design - 50 Percent of Nominal Design

The design work level, $\Delta H/\theta_{cr} = 26.9 \text{ Btu/lb}$, was applied along with design speed and thermodynamic requirements to obtain blade element losses. Iterating on losses, the fixed turbine geometry results in the velocity triangles and the rotor velocity distributions are given in Figures 27 through 29. The nominal design 12.5-percent span nozzle corresponds to the 25-percent span in the low aspect ratio turbine. Since the nominal nozzle diffusion factors at this section were found to be very small, the low aspect ratio nozzle diffusion factors were estimated from Figure 15. The design analysis predicts an efficiency of 74.0 percent with the detailed blade loss breakdown given in Table V.

This design essentially consists of truncating the nominal flow-path by 50 percent. The manner in which the outer shroud contour is profiled in the meridional plane seriously affects the radial distribution of losses for this type of short blading (see References 10 and 11). To preserve similarity of aerodynamics, the shroud was constricted in a manner such that the flow area ratio between any two given points along the mean flowpath was the same as for the nominal design. The resulting meridional flowpath is given in Figure 30.

A photograph of the high, low, and nominal aspect ratio rotor versions is presented as Figure 31.

COLD-FLOW RIG TESTING

Rig Description

Several versions of the turbine were cold-flow tested to substantiate the design and to evaluate the geometrical performance effects. The turbine test stand used for this purpose is pictured in Figures 32 through 34. Laboratory air supply and exhaust systems were used to service the test turbines. The temperature levels of the air are modulated by electric air heaters to prevent icing conditions at the high pressure ratios. Turbine power output is absorbed by a high-speed Industrial Engineering Company C-9504 Hydra-Brake installation, and torque measurements are made with a Baldwin-Lima-Hamilton load cell. Turbine mechanical speed was measured by means of a proximity type impulse pickup tachometer installed on the Hydra-Brake. Airflow was measured by a 3.501-inch-diameter flat plate, sharp-edge orifice installed in a 15.25-inch-diameter facility air supply duct.

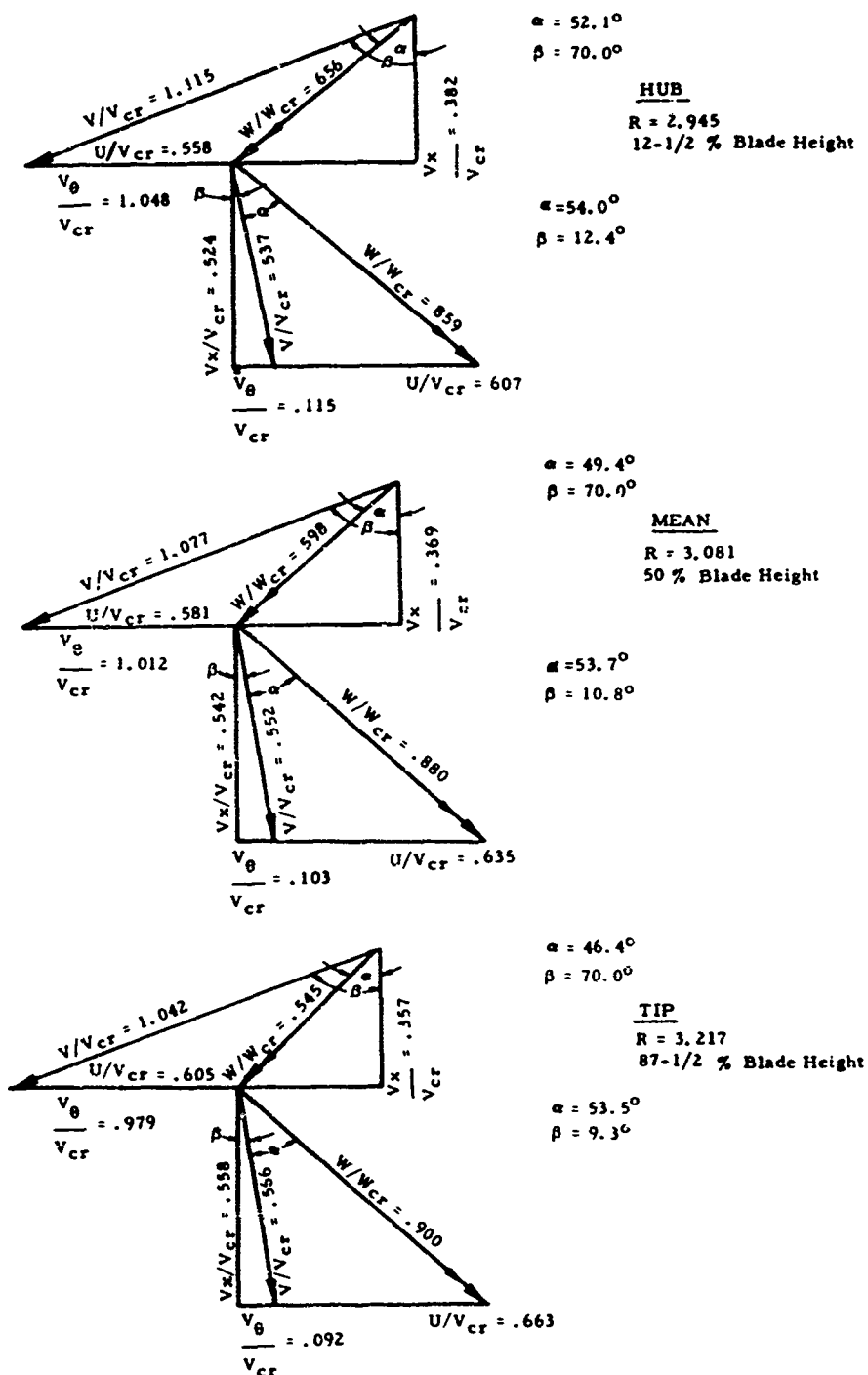


Figure 27. Low Aspect Ratio - 50-Percent Nominal Flowpath Velocity Diagrams.

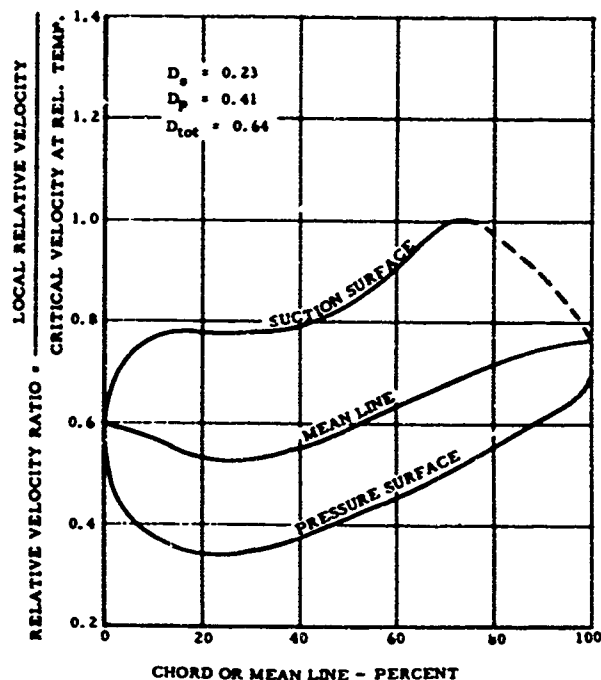
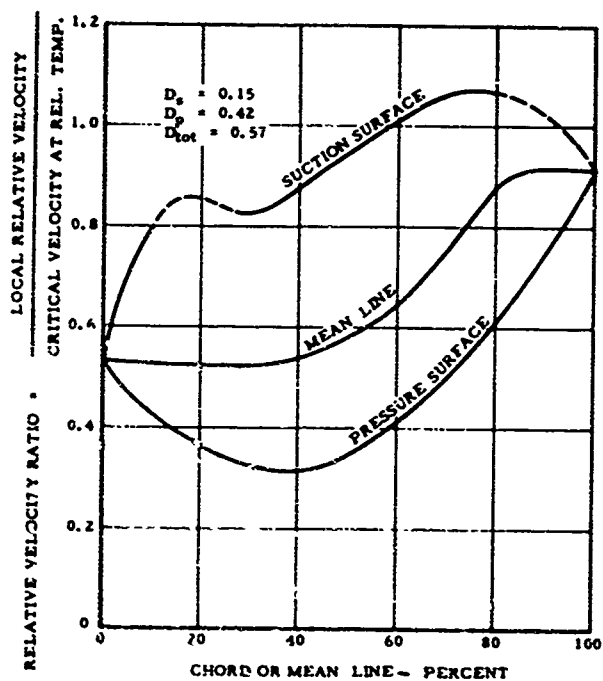


Figure 28. Rotor Blade Velocity Distributions - Low Aspect Ratio Design, Hub Section, 25-Percent Blade Height.

Figure 29. Rotor Blade Velocity Distributions - Low Aspect Ratio Design, Tip Section, 100-Percent Blade Height.



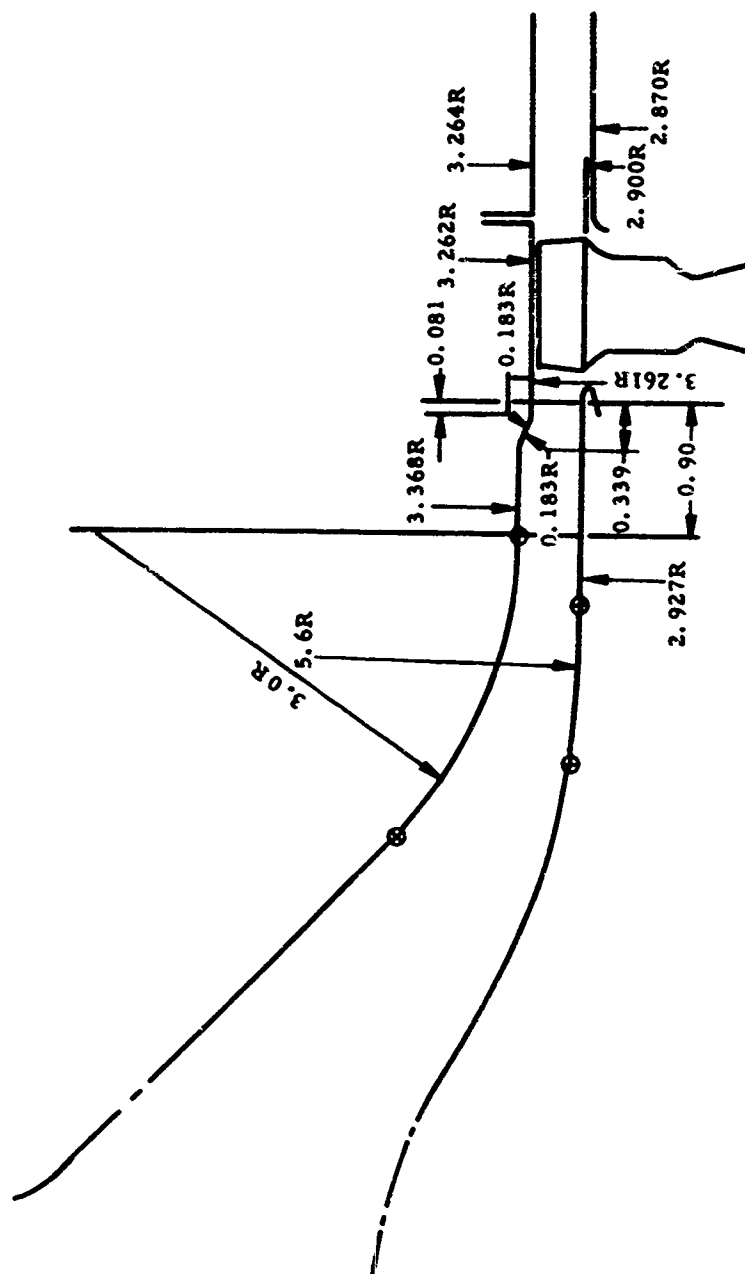


Figure 30. Aspect Ratio Evaluation - 50-Percent Nominal Turbine Flowpath.

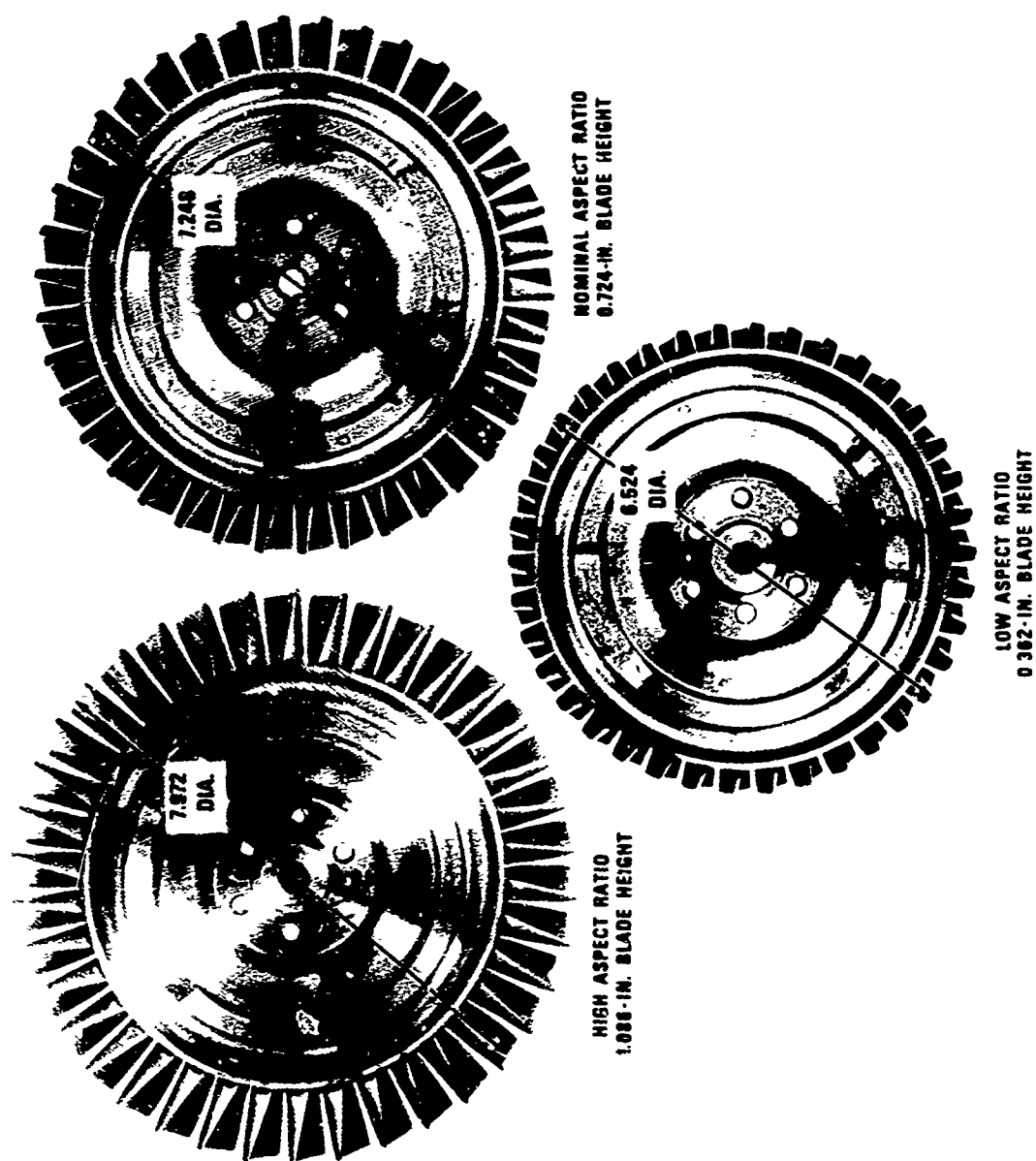


Figure 31. High, Nominal, and Low Aspect Ratio Rotors.



Figure 32. Front View of Turbine Test Stand.

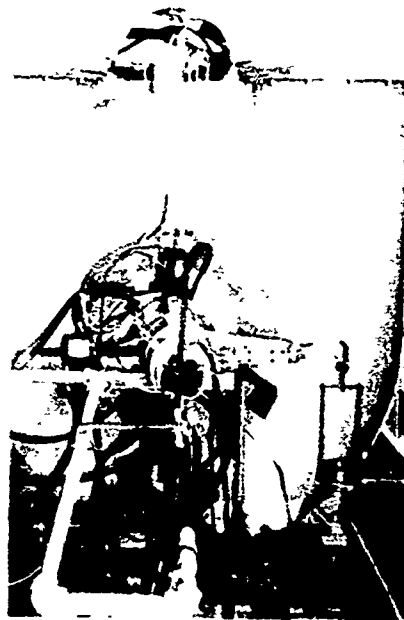


Figure 33. Rear View of Turbine Test Stand.

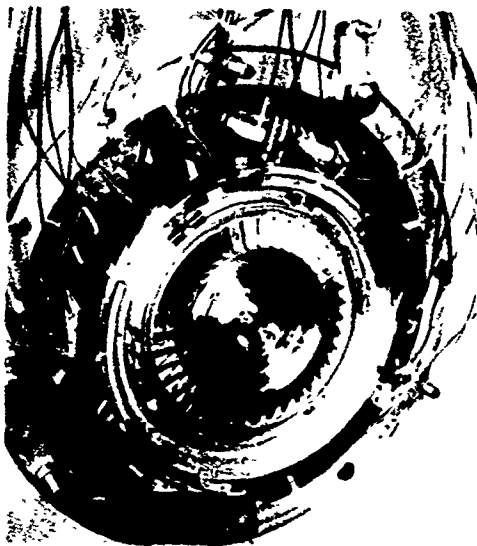


Figure 34. Nozzle and Rotor Assembly in Test Rig.

Test Plan

The objectives of the test program were to investigate, define, and substantiate the effect of low aspect ratio and tip clearance on turbine efficiency. Three basic flowpaths (Figures 12, 21, and 30) were designed and tested (that is, nominal, 150 percent of nominal, and 50 percent of nominal blade height). Tip clearances were varied on each of the configurations. The hardware available for this program consisted essentially of one set of nozzle and rotor blading that was modified by outer annulus changes to produce the three aspect ratio flowpaths. Changes in rotor tip clearances were made by remachining rotor shrouds to larger diameters. The order of testing was, therefore, automatically fixed in a direction of decreasing aspect ratios and increasing tip clearances. A description of geometry, an order of testing, and a schedule for each of the geometries are given in Tables VI and VII.

The measurement of the blade-to-shroud running clearance is a particularly difficult job with the size of machinery used in this investigation. Even the use of elaborate electronic devices can assure an accuracy of ± 0.002 inch. In lieu of the problems and expense associated with measurement of actual running clearances, accurate average cold static values were established for the test program. Thermal expansion and centrifugal growth compensations are readily calculated on the static values, since rig temperatures do not exceed 300°F and centrifugal stresses are quite low.

Instrumentation

Axial and circumferential location of instrumentation common to all test configurations is shown in Figures 35 and 36. Total temperatures at all locations were measured by bare wire premium-grade iron-constantan thermocouples. The probes were tunnel calibrated over a range of Mach numbers for recovery factors. Figure 37 shows the recovery data obtained. The temperature levels and hardware involved make radiation correction factors insignificant. Air preheaters are used to modulate temperature to a maximum of about 300°F to minimize humidity and condensation problems. Radial location of total temperatures and pressures is for centers of equal areas. Requirements for Tests 1 through 6 are:

- Ⓐ* Nozzle inlet total pressure - 4 rakes of 4 probes
Total temperature - 4 rakes of 4 probes
Static taps - 4 on outer wall

* Instrumentation Location ○ (See Figures 35 and 36)

TABLE VI
TEST PLAN FOR TURBINE ASPECT RATIO
AND TIP CLEARANCE EVALUATION

Test No.	Aspect Ratio Flowpath	Rotor Clearance As Function of Annulus Height (percent)	Average Cold Rotor Clearance (inches)	Number of Data Points
1	150 Percent Nominal (Figure 21)	1.5	0.016	20
2	150 Percent Nominal (Figure 21)	5.0	0.056	10
3	Nominal (Figure 12)	1.5	0.011	20
4	Nominal (Figure 12)	3.5	0.026	10
5	Nominal (Figure 12)	5.0	0.0375	10
6	50-Percent Nominal (Figure 30)	1.5	0.055	20

TABLE VII
TEST SCHEDULE

N/ $\sqrt{\theta_{cr}}$		Total-to-Total Pressure Ratio					
24243	--	2.19	2.48	2.85	3.35	Limit Load	Tests 1, 3, and 6
22039	--	↓	↓	↓	↓		
19835	--	↓	↓	↓	↓		
17631	--	↓	↓	↓	↓		
22039	1.9	2.19	2.48	2.85	3.35	Limit Load	Tests 2, 4, and 5

Nozzle and rotor discharge surveys of angle and total pressure taken at all the above points.

P_s , Orifice Upstream, 1
 P_s , Orifice Downstream, 2
 Sharp Edge Orifice Dia. = 3.500 In.
 Pipe Inside Dia. = 15.225

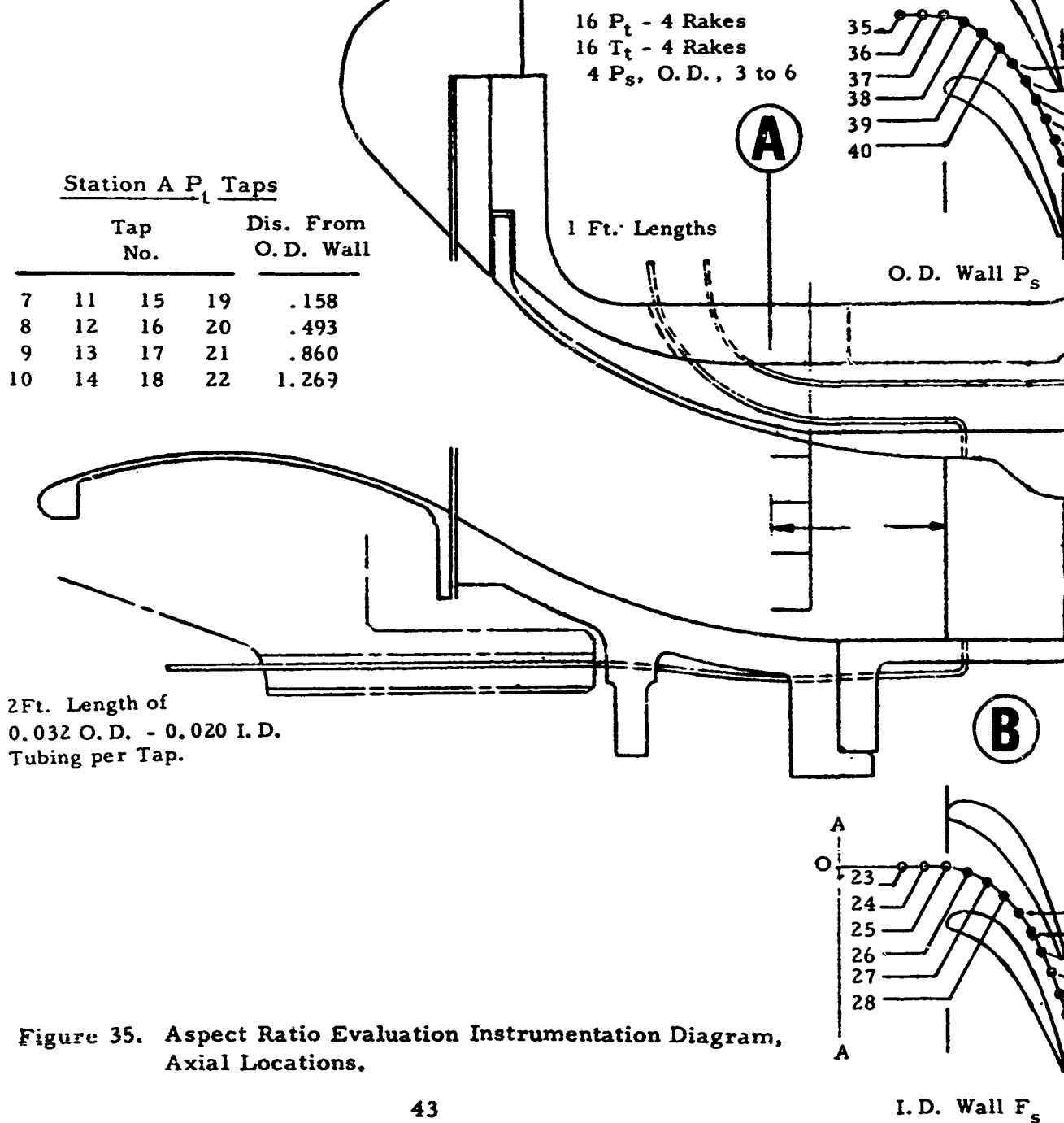


Figure 35. Aspect Ratio Evaluation Instrumentation Diagram,
 Axial Locations.

2 P_t and Angle
Survey Probes

F

35
36
37
38
39
40

41
42
43
44
45
46

4 P_s , I. D., 1B to 4B
4 P_s , O. D., 5B to 8B
2 P_t and Angle
Survey Probes

P_t and T_t rake probes are at equal area centers
and equally spaced circumferentially.
 T_t rakes have bare wire thermocouples.
 P_t rakes have bare tubes with 15° internal taper.

16 P_t = 4 Rakes
16 T_t = 4 Rakes

Station D P_t Taps

Tap No.				Dis. From O. D. Wall
55	59	63	67	.127
56	60	64	68	.395
57	61	65	69	.684
58	62	66	70	1.001

O. D. Wall P_s

6 Tip
Clear. Ind.

C

D

B

E

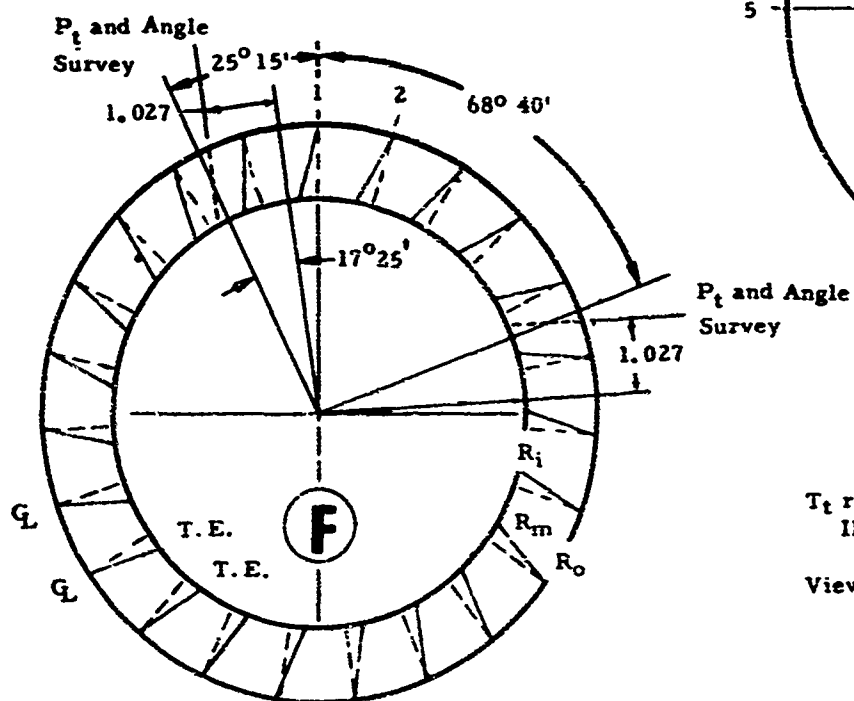
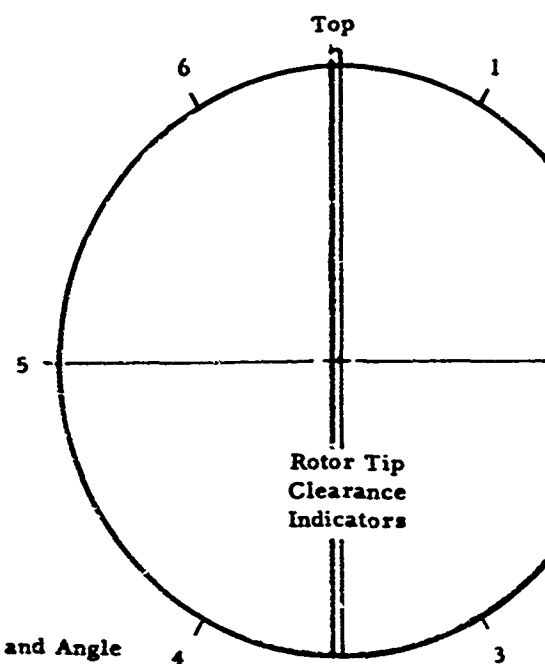
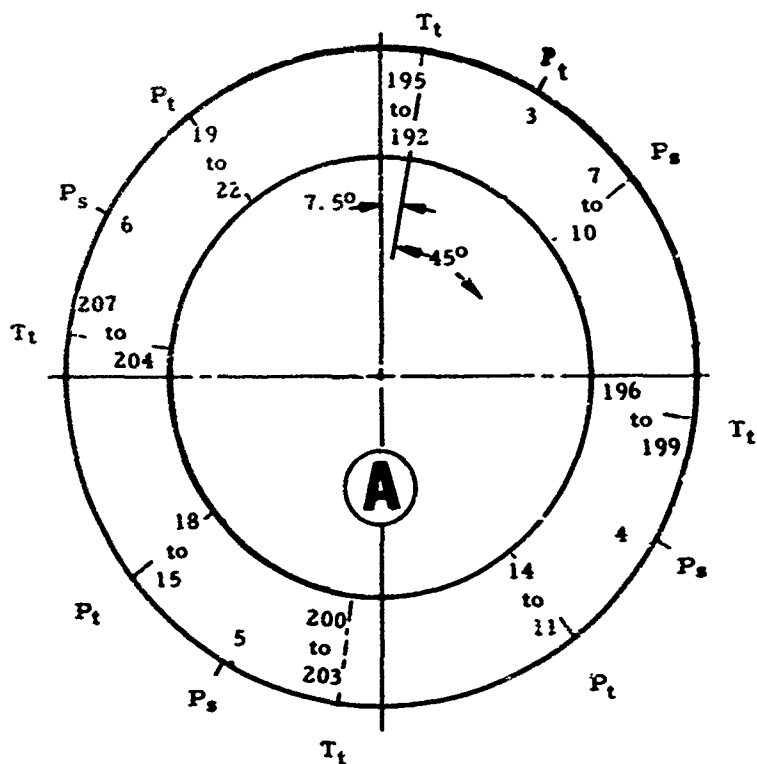
23
24
25
26
27
28

29
30
31
32
33
34

4 P_s , I. D., 47 to 50
4 P_s , O. D., 51 to 54

I. D. Wall F_s

B

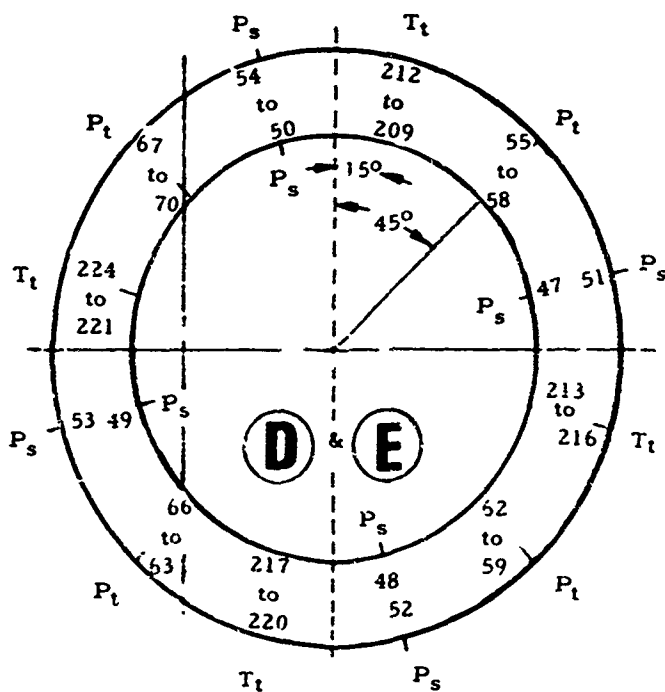


T_t rake probes are identified by data sheet IBM numbers.

Views looking upstream.

Wall static taps between vanes 1 & 2.

Figure 36. Aspect Ratio Evaluation Instrumentation Diagram, Circumferential Locations.



looking upstream.

1

B

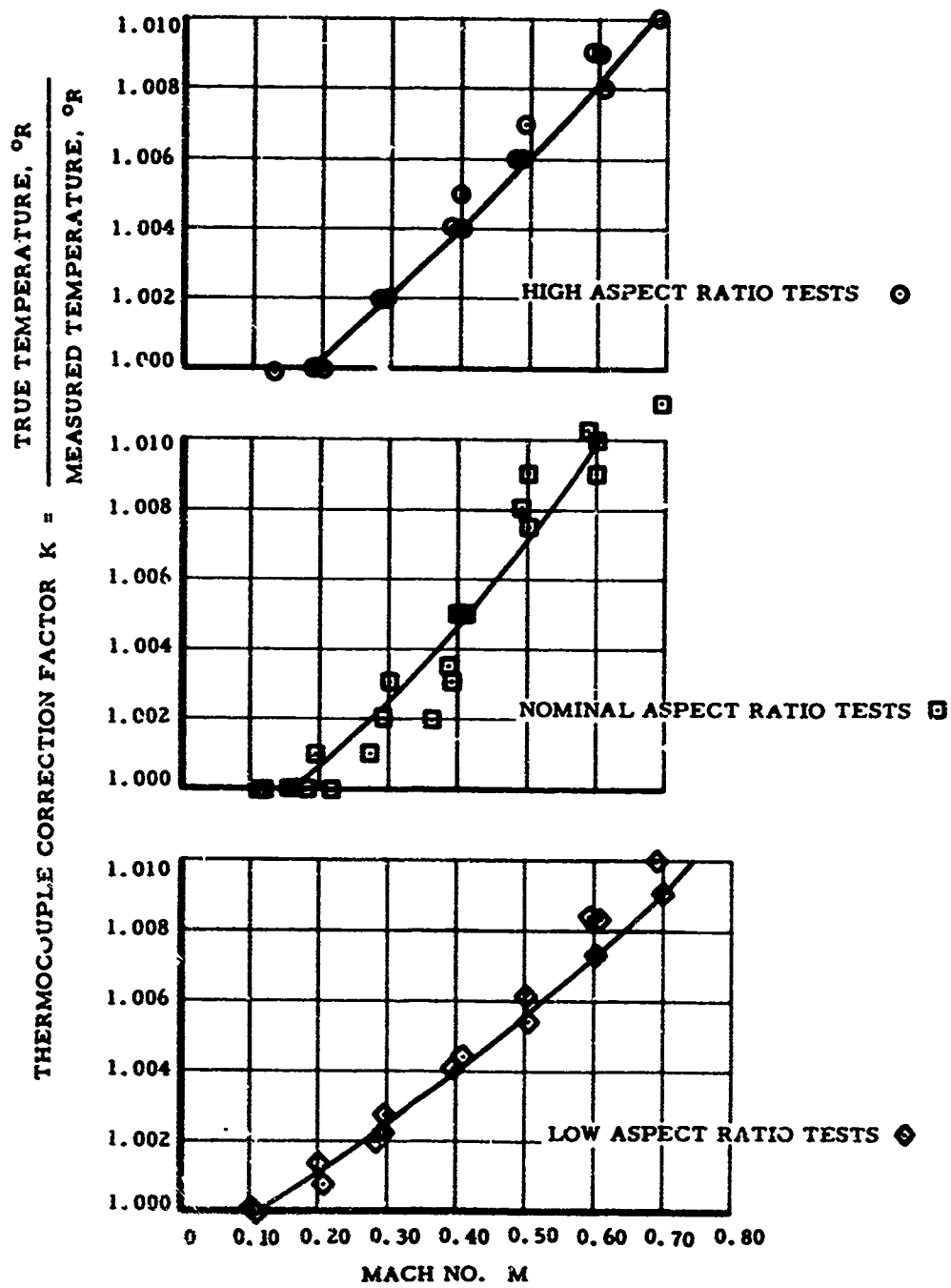


Figure 37. Recovery Calibration of Bare Wire Thermocouples.

- (B) Nozzle wall shroud statics - 12 inner and 12 outer at center of passage.
- (C) Rotor exit surveys of total pressure and angle - 2 combination probes 90° apart.
- (D) Rotor exit total pressure - 4 rakes of 4 probes
Total temperature - 4 rakes of 4 probes
- (E) Static taps - 4 on inner wall and 4 on outer wall at rotor discharge.
- (F) Nozzle exit surveys of total pressure and angle - 2 combination probes 90° apart, center of passage.

Nozzle and rotor total pressure and angle distribution was measured by standard cobra-type probes shown in Figures 38 and 39. The probes consist of a 0.080-inch-diameter support stem with 0.025-inch-diameter angle and total pressure sensing tubing. This instrumentation was also calibrated over a range of Mach numbers in a wind tunnel. Figure 40 presents typical pressure recovery data as a function of Mach number.

Test Results and Discussion

Aspect Ratio Effects. Three complete turbine performance maps were obtained corresponding to high aspect ratio, nominal, and low aspect ratio blading, all with a fixed 1-1/2-percent blade height rotor clearance. Data are presented in terms of referred work, $\Delta H/\theta_{cr}$, speed, $N/\sqrt{\theta_{cr}}$, total-to-total adiabatic efficiency (η), flow, $W_a N \epsilon / 660$, and pressure ratio in Figures 41, 42, and 43.

The flow parameter term is derived from the product of corrected flow $W_a \sqrt{\theta_{cr}} \epsilon / g$ and the referred speed $N/\sqrt{\theta_{cr}}$. Thus, a vertical characteristic for a given referred speed simply means that the turbine is choked at all pressure ratios where $W_a N \epsilon / 660 = \text{constant}$. Inspection of static tap data and total pressures showed that the nozzle, in all cases, was the choked component, thus satisfying design requirements.

Performance is also presented in terms of efficiency versus ratio of mean wheel speed to isentropic velocity ratio in Figures 44, 45, and 46. Peak efficiencies of 84.2, 80.7, and 71.3 were obtained, respectively, for high, nominal, and low aspect ratio blading. Efficiency as

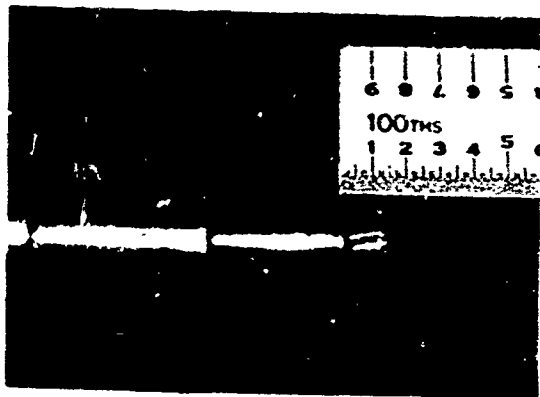


Figure 38. Standard Cobra-Type Probe, Front View.

Figure 39. Standard Cobra-Type Probes, Side View.

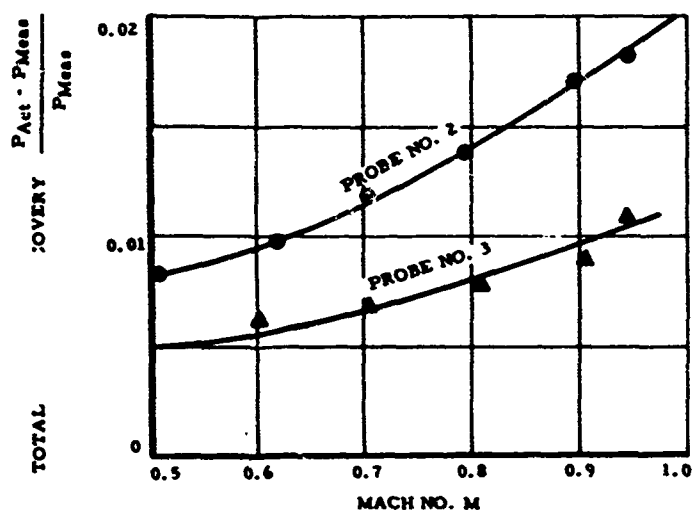
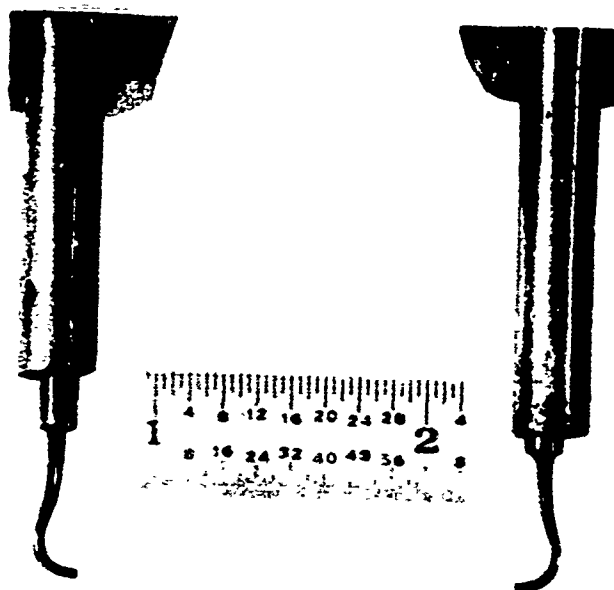
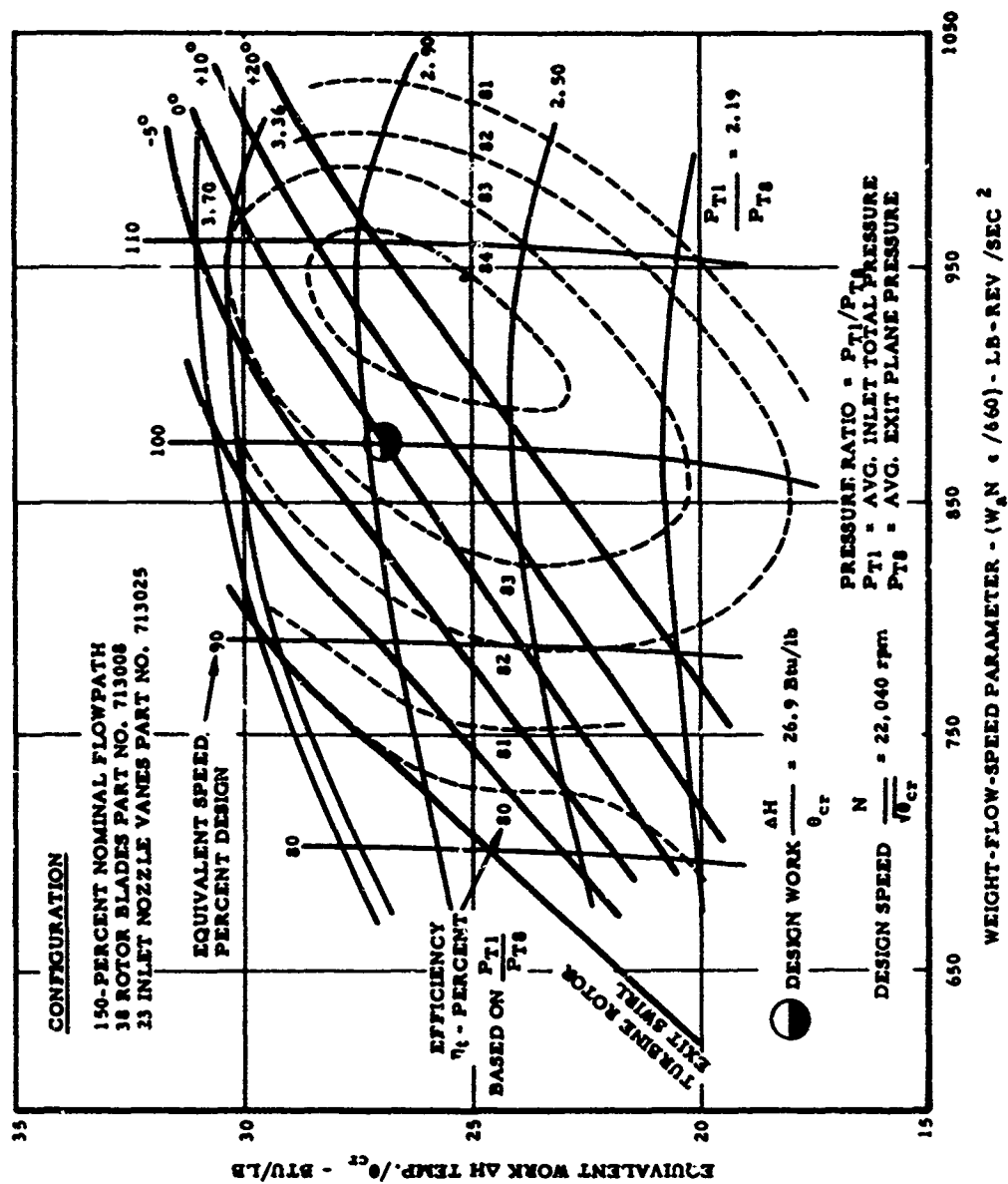


Figure 40. Discharge Survey Cobra Probe Recovery Calibration.



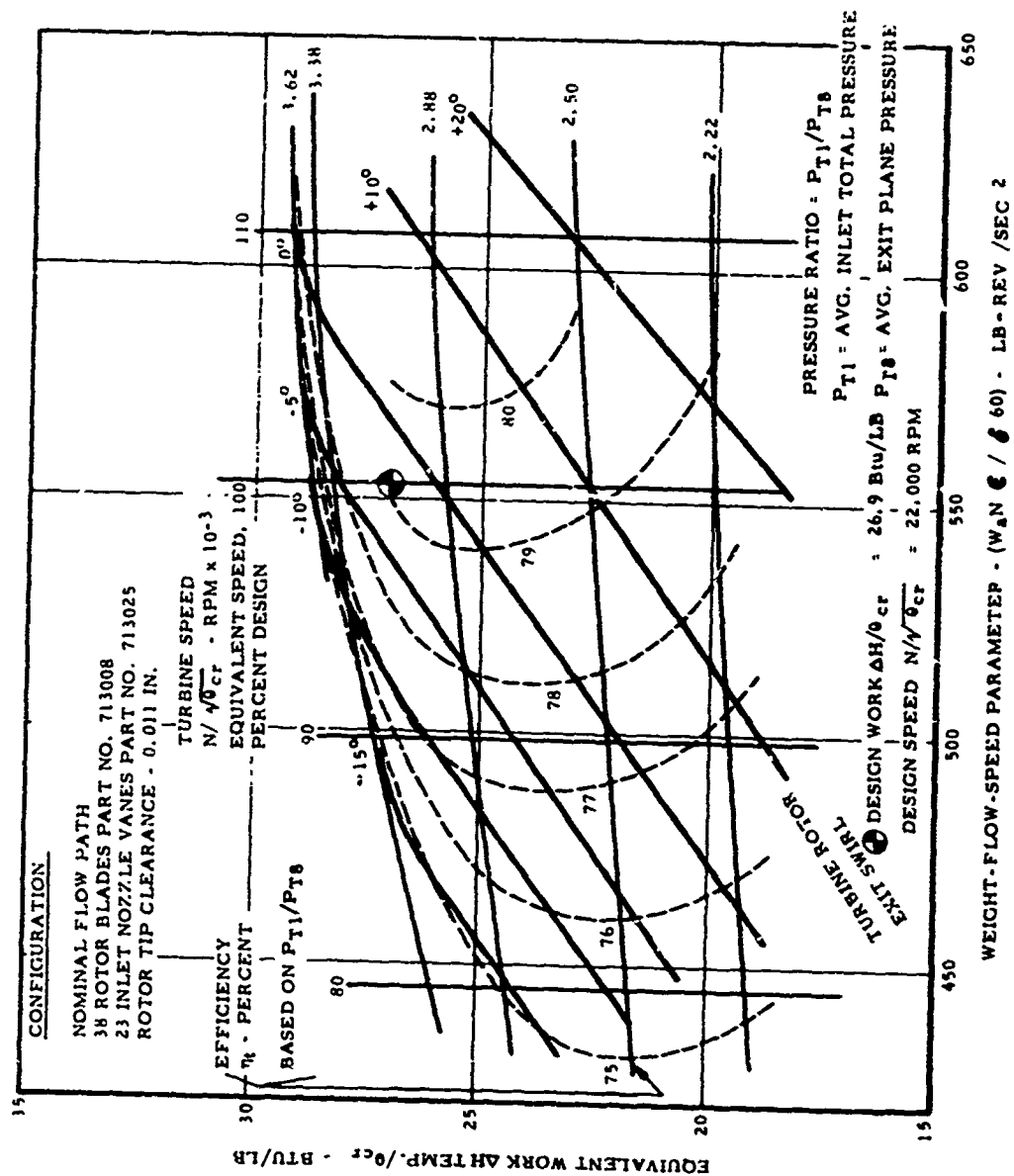


Figure 42. Nominal Aspect Ratio Overall Performance - Clearance at 1.5- Percent Blade Height.

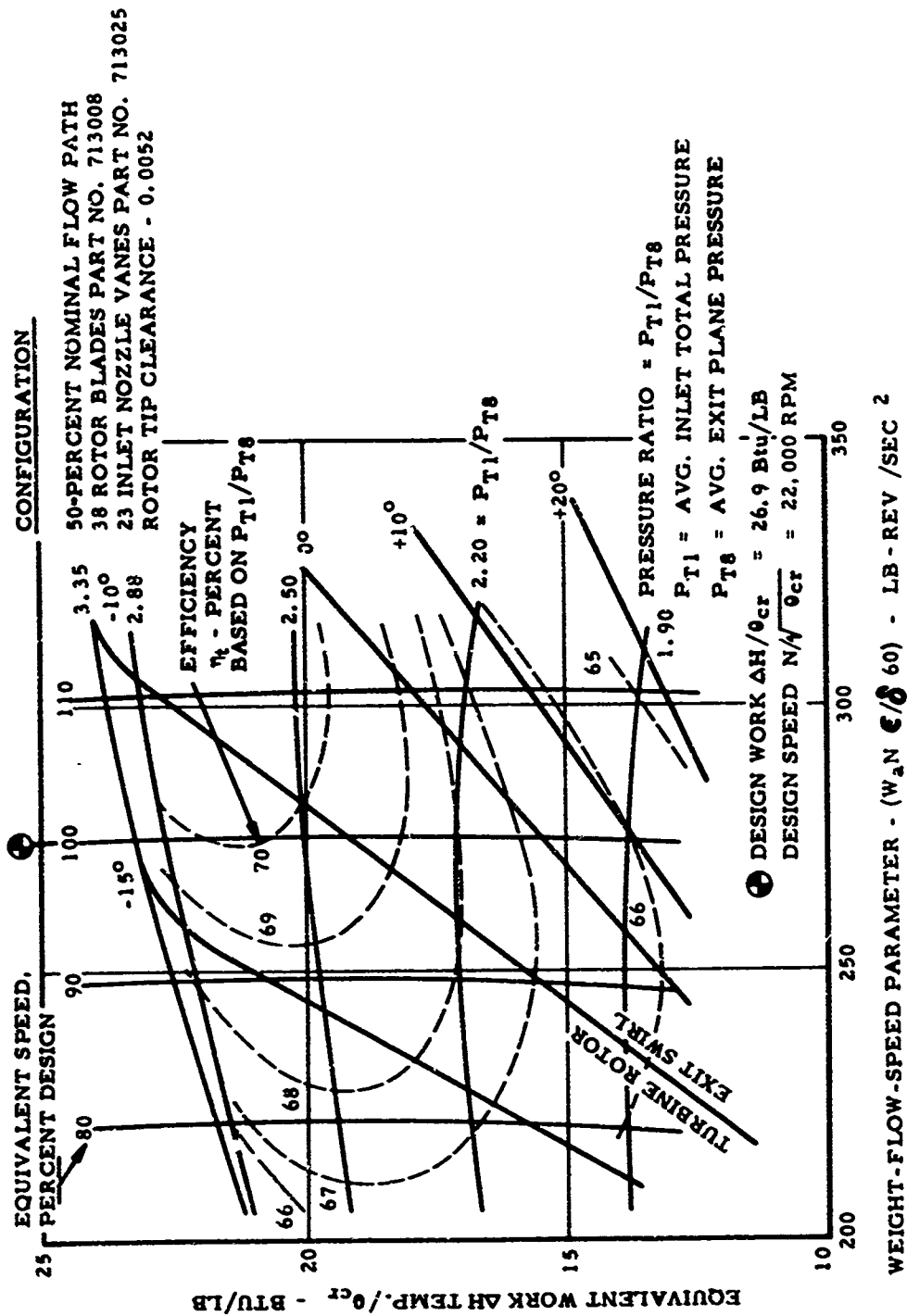


Figure 43. Low Aspect Ratio Overall Performance - Clearance at 1.5-Percent Blade Height.

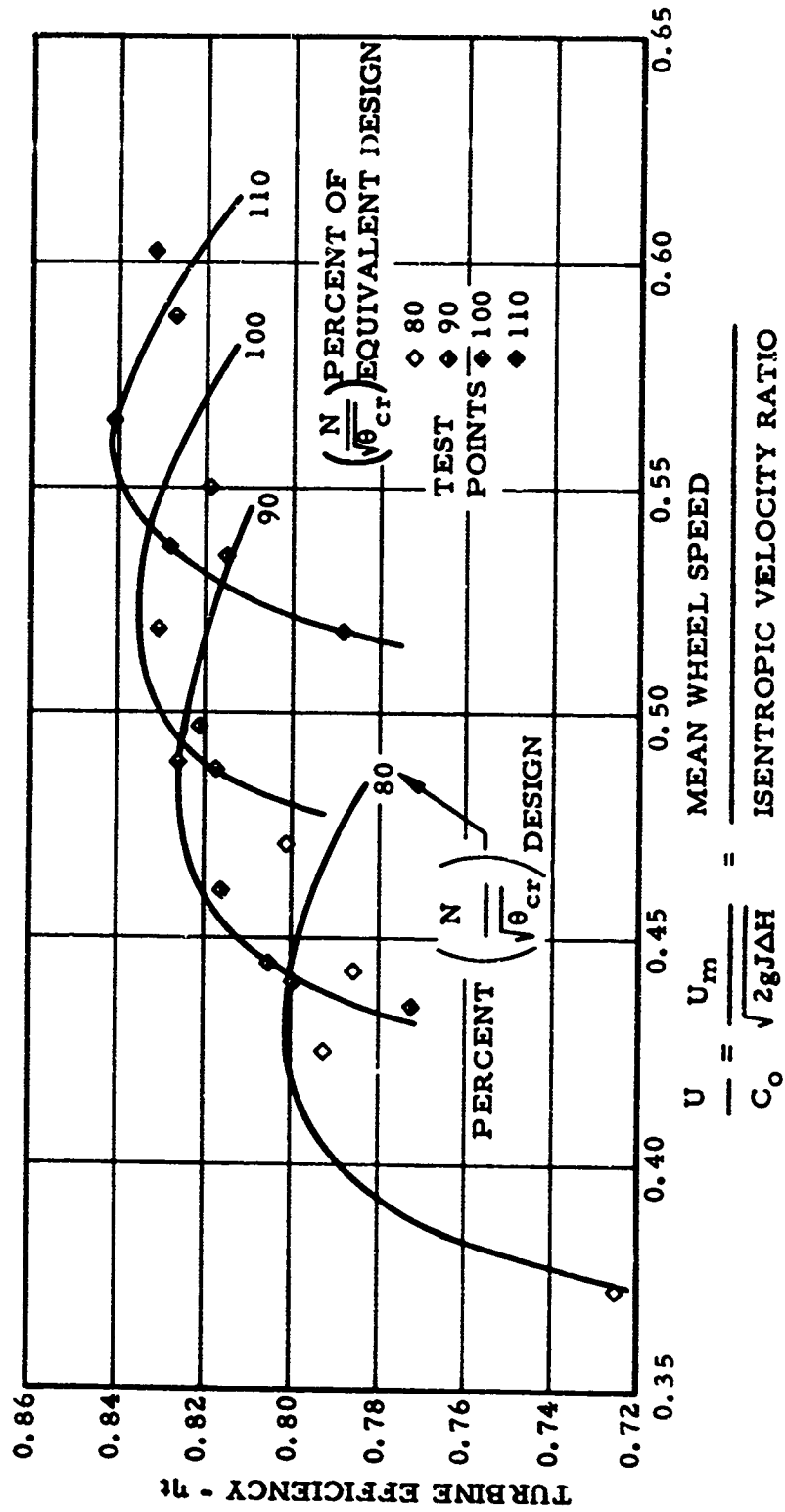


Figure 44. High Aspect Ratio Performance - Efficiency Versus Ratio of Mean Wheel Speed to Isentropic Velocity Ratio.

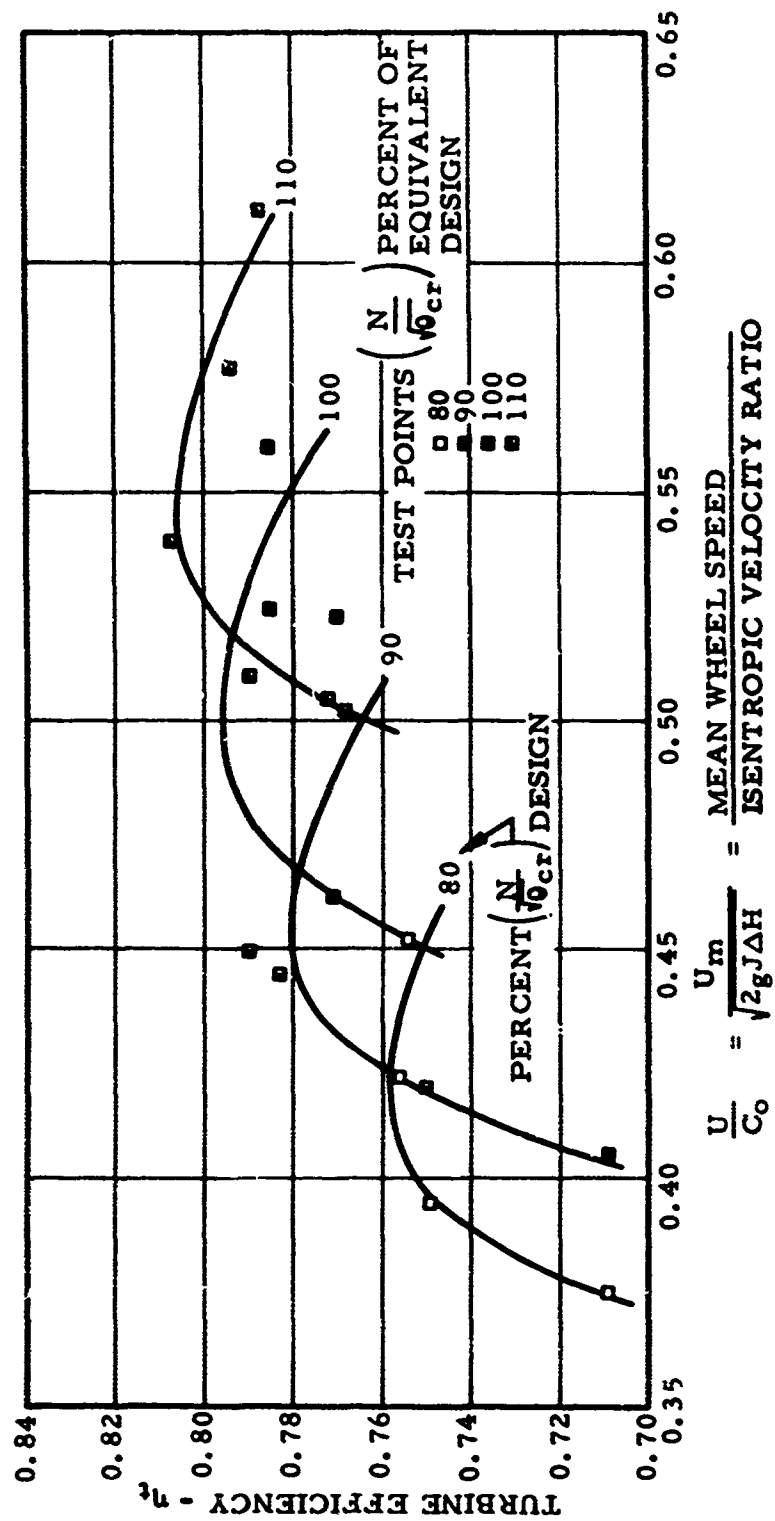


Figure 45. Nominal Aspect Ratio Performance - Efficiency Versus Ratio of Mean Wheel Speed to Isentropic Velocity Ratio.

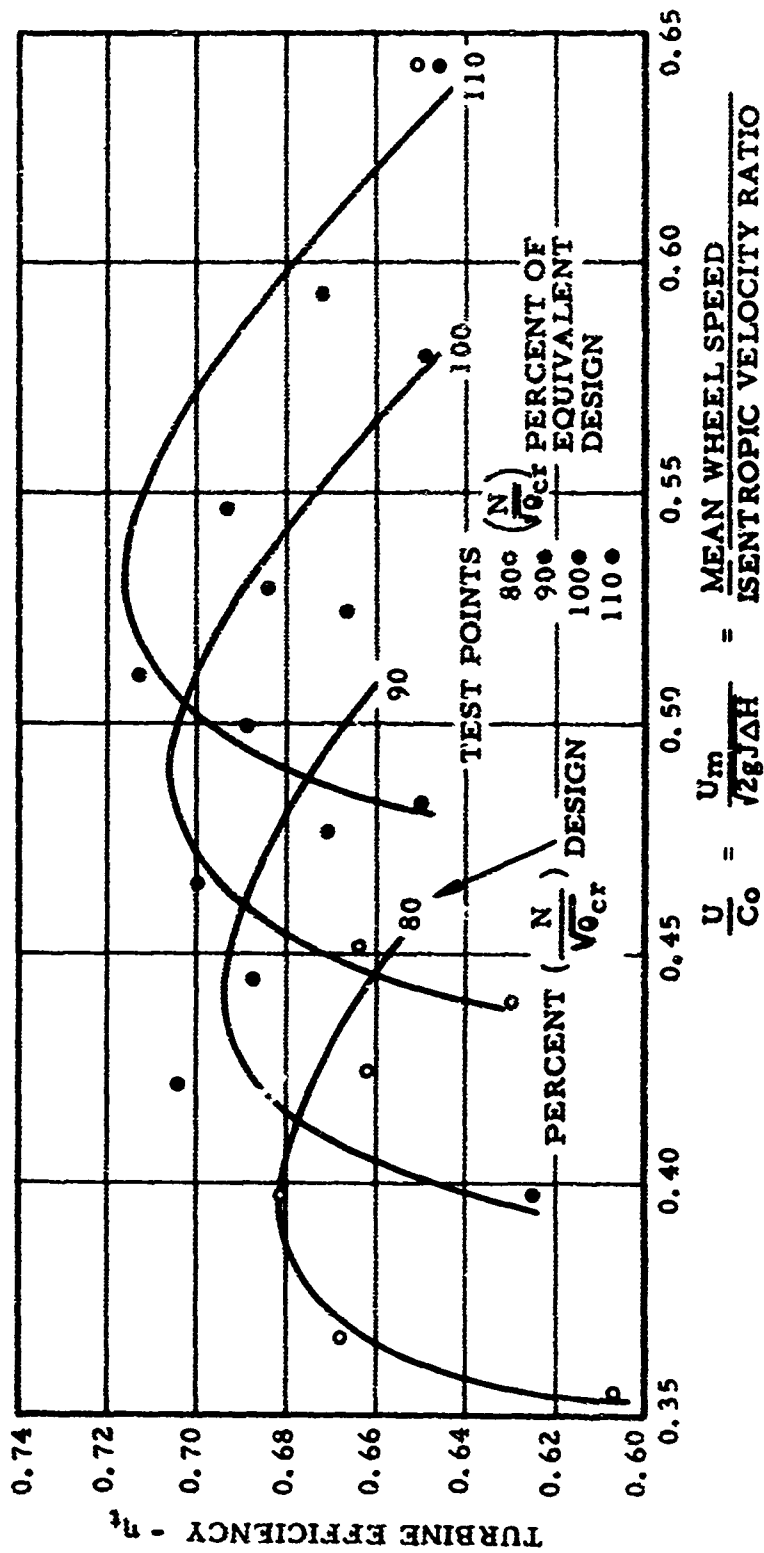


Figure 46. Low Aspect Ratio Performance - Efficiency Versus Ratio of Mean Wheel Speed to Isentropic Velocity Ratio.

a function of aspect ratio and pressure ratio at 100 percent design equivalent speed is shown in Figure 47. Performance over the whole operating range deteriorates rapidly with the decreasing aspect ratio. This degradation is exponential, since 3 percent is lost in going from a rotor blade height of 1.09 inches to 0.72 inch, whereas over 10 percent is lost in a change of blade height from 0.72 inch to 0.36 inch. Torque characteristics are also seriously affected (see Figures 48, 49, 50, and 51). Table VIII summarizes some of the overall effects of span aspect ratio on performance. The lowest blade heights penalized the performance to the extent that the turbine became limit loaded before design work could be achieved.

Reference to the overall performance maps, Figures 41, 42, and 43, also shows that the peak total-to-total performance for all three aspect ratios occurs between 105 and 110 percent design speed. A comparison of efficiency and exit swirl for the three designs at design work of $\Delta H/\phi_{cr} = 26.9$ is given in Table IX.

The nominal turbine was designed for an average exit swirl of -5 degrees (against rotation), which was closely achieved. The overspeed performance, although higher on a total-to-total basis, would require downstream stators and an associated pressure loss. Overspeed performance would be penalized in the cycle, and centrifugal stresses in the blade would be unacceptable.

Predicted efficiency goals for the nominal aspect ratio turbine were not achieved. Loss considerations were based on overall blading geometry and are rigorous within conventional diffusion factor limits. Loss of performance is exponential when total diffusion factors exceed 0.6 (Reference 12), and definition of this loss region is not defined adequately. Since all three aspect ratio turbines were designed for the same average diffusion, all performance comparisons should be rigorous.

Static pressure taps were installed on the inner and outer shrouds of the nozzle to measure wall velocity distributions. Nozzle inlet and exit total pressures were measured with rakes and survey probes. A linear variation of total pressure from inlet to exit was assumed to calculate the local total-to-static pressures. These data were then translated into velocities. Figure 52 gives the nozzle wall velocity distributions for the three span aspect ratios at test conditions nearest the design. Little or no diffusion is evident on either wall, and acceleration uniformly increases up to the nozzle trailing edge. Hub and tip exit velocities for the nominal blading fall close to the design. The low exit velocities on the 50 percent of nominal blading reflect high rotor secondary losses and limit loading of the turbine.

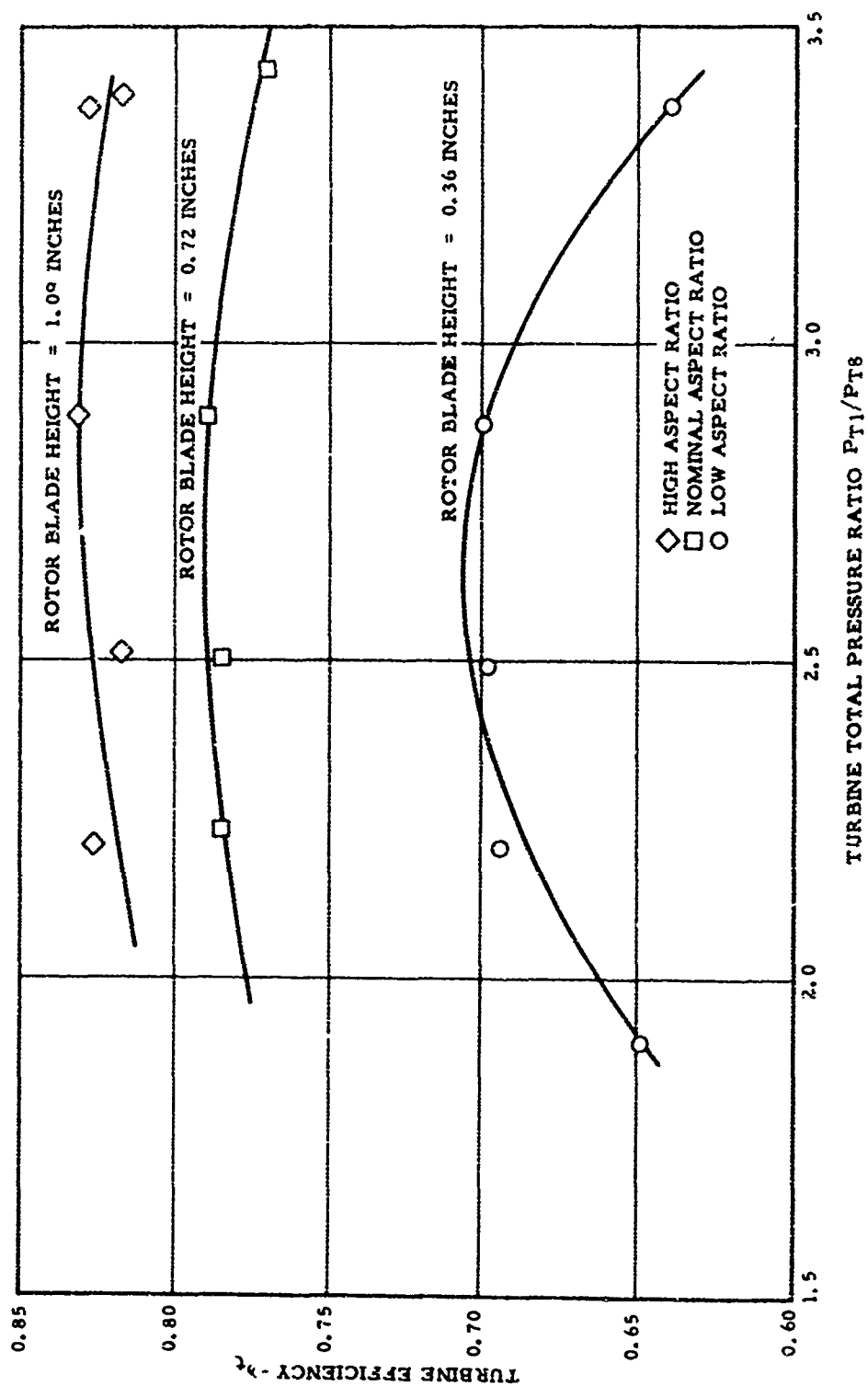


Figure 47. Effect of Aspect Ratio on Efficiency - Clearance at 1.5-Percent Blade Height.

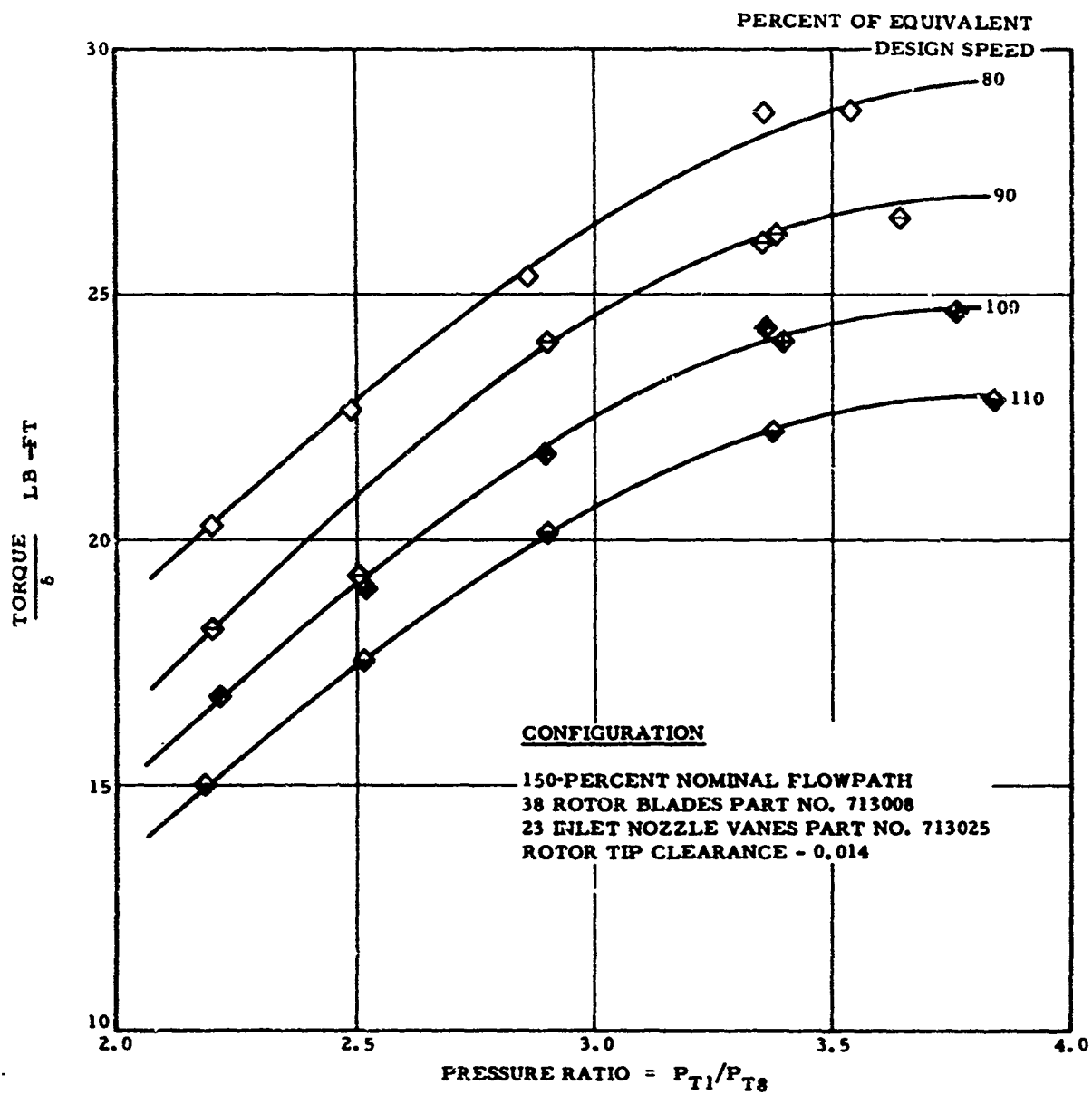


Figure 48. High Aspect Ratio Performance - Torque Characteristics.

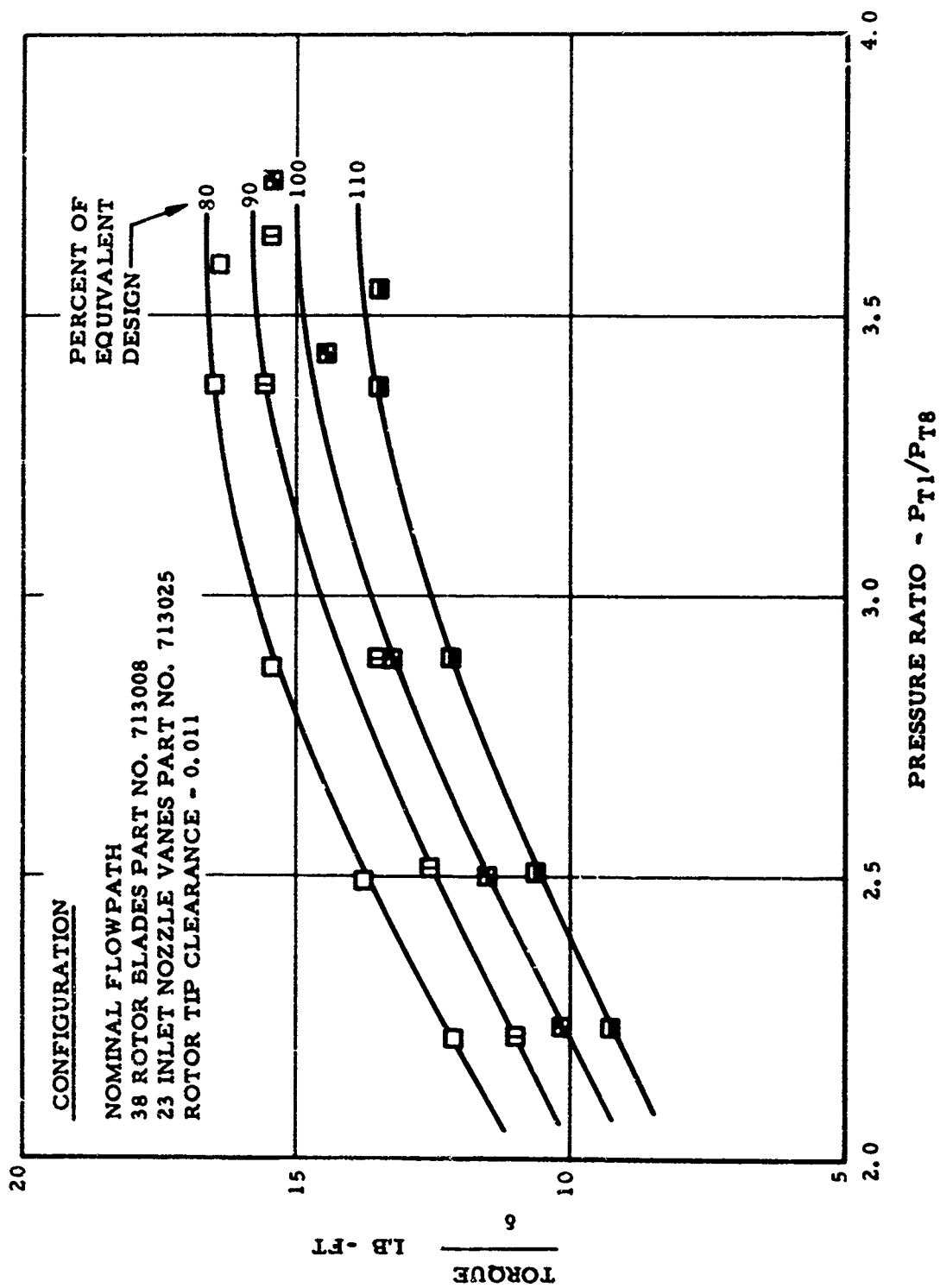


Figure 49. Nominal Aspect Ratio Performance - Torque Characteristics.

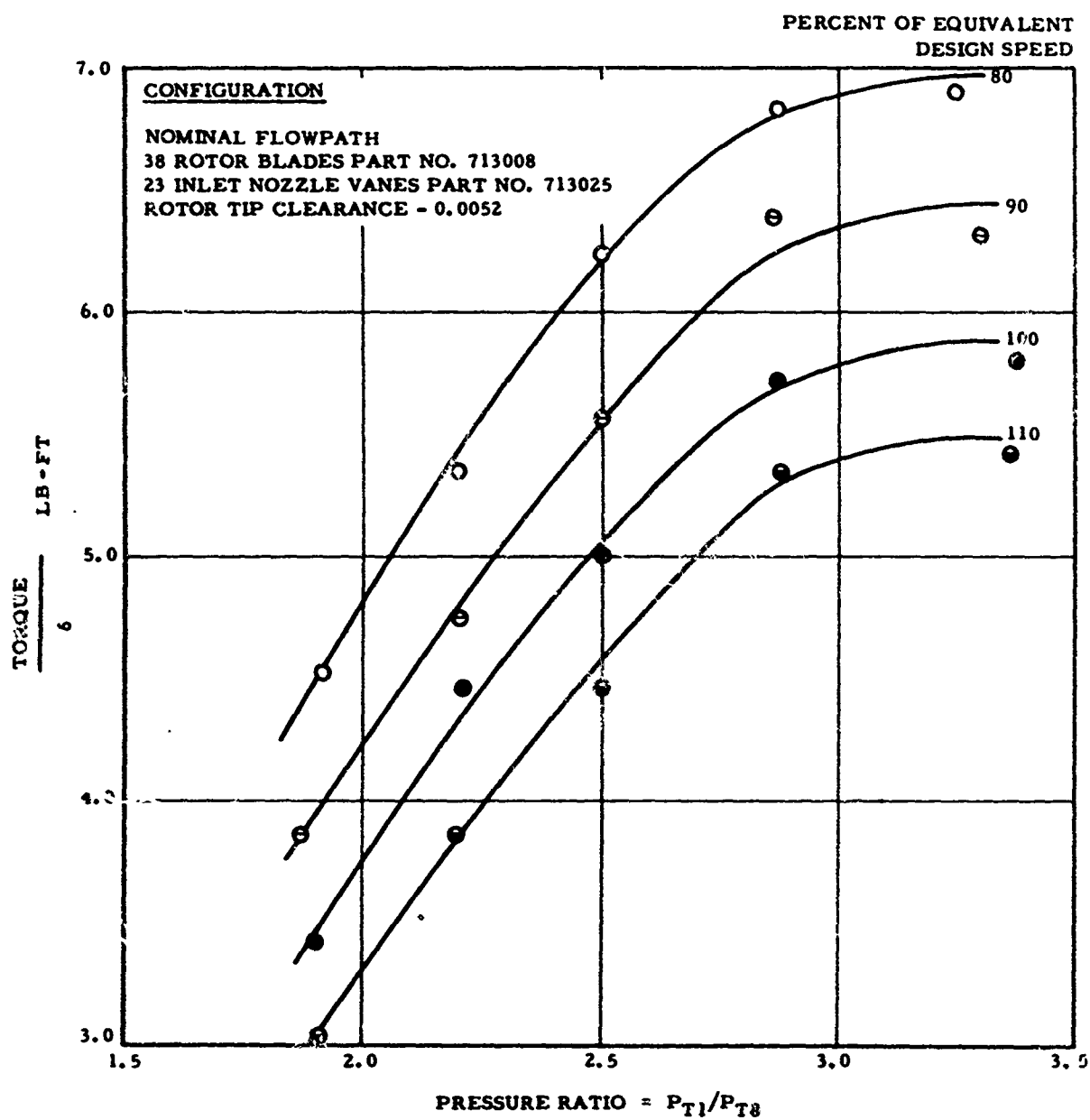


Figure 50. Low Aspect Ratio Performance - Torque Characteristics.

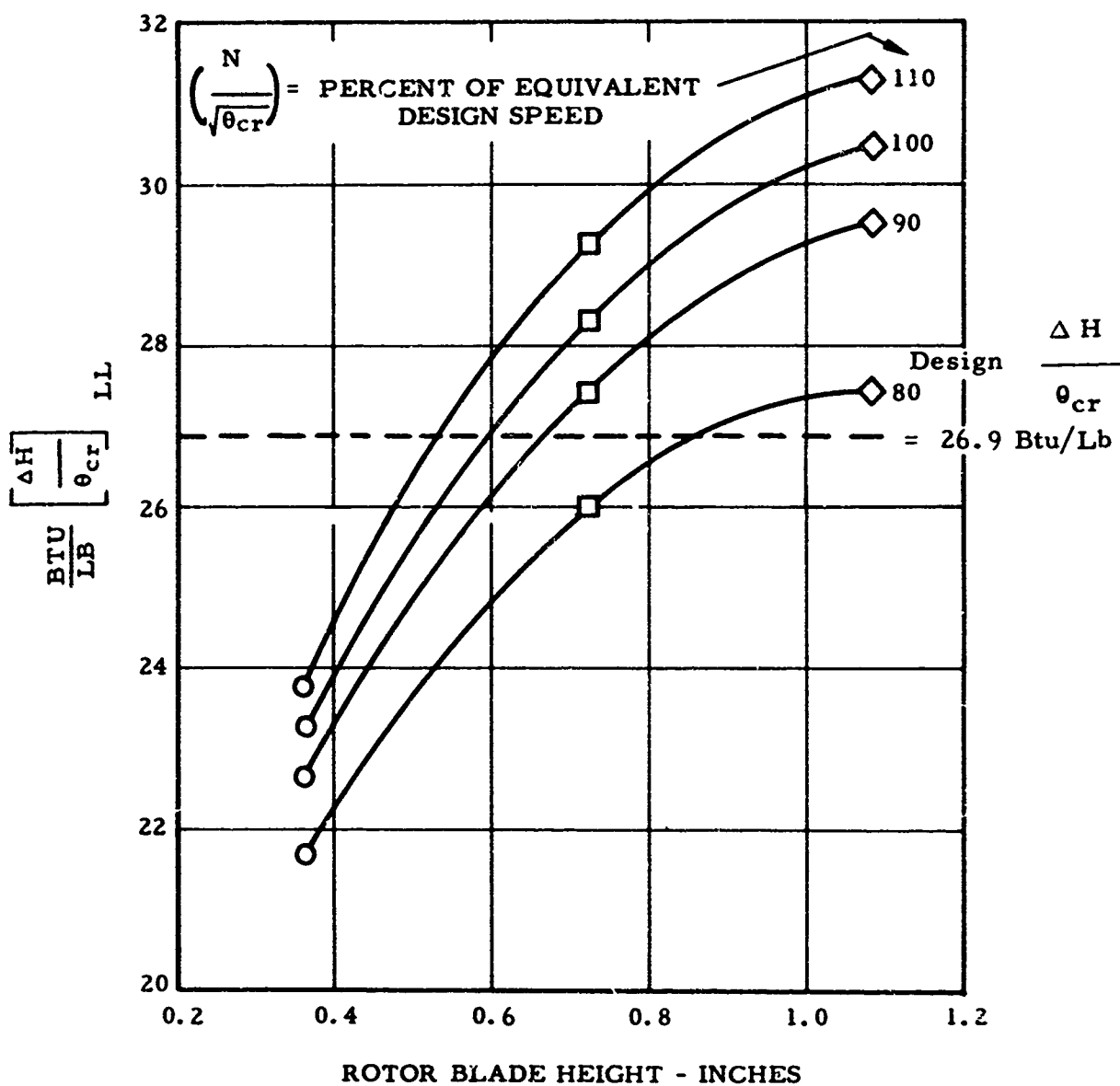


Figure 51. Effect of Aspect Ratio on Limit Load Work Capability - Clearance at 1.5-Percent Blade Height.

TABLE VIII
OVERALL EFFECTS OF SPAN ASPECT RATIO ON PERFORMANCE -
CLEARANCE AT 1.5-PERCENT BLADE HEIGHT

Parameter	Turbine Flowpath Configuration				Change From High to Low Aspect Ratio (Percent)
	High Aspect Ratio (Figure 21)	Nominal Aspect Ratio (Figure 12)	Low Aspect Ratio (Figure 30)	Fluid- Cooled Turbine (Figure 18)	
Rotor Aspect Ratio	1.260	0.825	0.405	0.673	
Average Nozzle Aspect Ratio	0.725	0.482	0.240	0.344	
Referred Work, $\Delta H/\theta_{cr}$, at Design Pressure Ratio and Design Equivalent Speed Btu/Lb	27.02	25.62	22.76	26.44	19.4 Decrease
Total-to-Total Efficiency, η , at Design Pressure Ratio and Design Equivalent Speed	83.1	78.8	70.0	81.3	$\Delta\eta$ 13.1 Decrease
Maximum Corrected Torque Per Pound of Air, T/δ at Design Equivalent Speed Ft-Lb/Lb Air	10.3	9.6	7.8	9.8	24.3 Decrease
Rotor Exit Swirl at Design Pressure Ratio and Design Equivalent Speed, Degrees	-4.0	-5.5	-11.0	0	$\Delta\beta_g = 7^\circ$ Increase
Maximum or Limit Load Referred Work, $\Delta H/\theta_{cr}$, at Design Equiva- lent Speed, Btu/Lb	30.4	28.3	23.25	29.0	23.5 Decrease

TABLE IX
COMPARISON OF PERFORMANCE AND EXIT SWIRL
FOR HIGH, NOMINAL, AND LOW ASPECT RATIO TURBINES
AT TWO SPEEDS

Configuration	100 Percent Design Speed		110 Percent Design Speed	
	η_t	Swirl Degrees	η_t	Swirl Degrees
High Aspect Ratio	83.4	0	84.2	+20
Nominal Aspect Ratio	79.3	-3	80.7	+ 8
Low Aspect Ratio	Limit Load Conditions			

Surveys of total pressure and angle were recorded at discharge from the turbine rotors. Data corresponding to the same test points in Figure 52 are given in Figure 53. Average design discharge whirl values were +2, -5, and -11 degrees for the respective high, nominal, and low turbines. Test data indicate -4.5, -5, and -11 degrees whirl against rotation for these points. Gradients in discharge pressure were fairly uniform, and the whirl design objectives were closely approached.

Nozzle discharge surveys were used to separate losses from the turbine rotor. Tests were conducted on the nozzle assembly alone to avoid the possibility of instrument breakage causing destruction of the turbine wheel. Two-dimensional data were recorded at discharge total-to-static pressure ratios up to 2.5. Since all three turbine flowpaths were designed for choke in nozzle, the removal of the turbine rotor does not affect flow and loss characteristics of the nozzle at the design condition. Data in the form of nozzle efficiency versus exit total-to-static pressure ratio for the nominal and low aspect ratios are presented in Figure 54. Efficiencies are higher than expected for nozzle cascades of nearly 70 degrees of deflection. This information, along with the static tap data, suggests that the meridional wall constriction was successful in minimizing the nozzle secondary losses. Because of the minimum instrumentation used, the cascade test results are qualitative in nature. For a complete analysis, three-dimensional surveys are recommended to separate profile, trailing edge, and secondary losses.

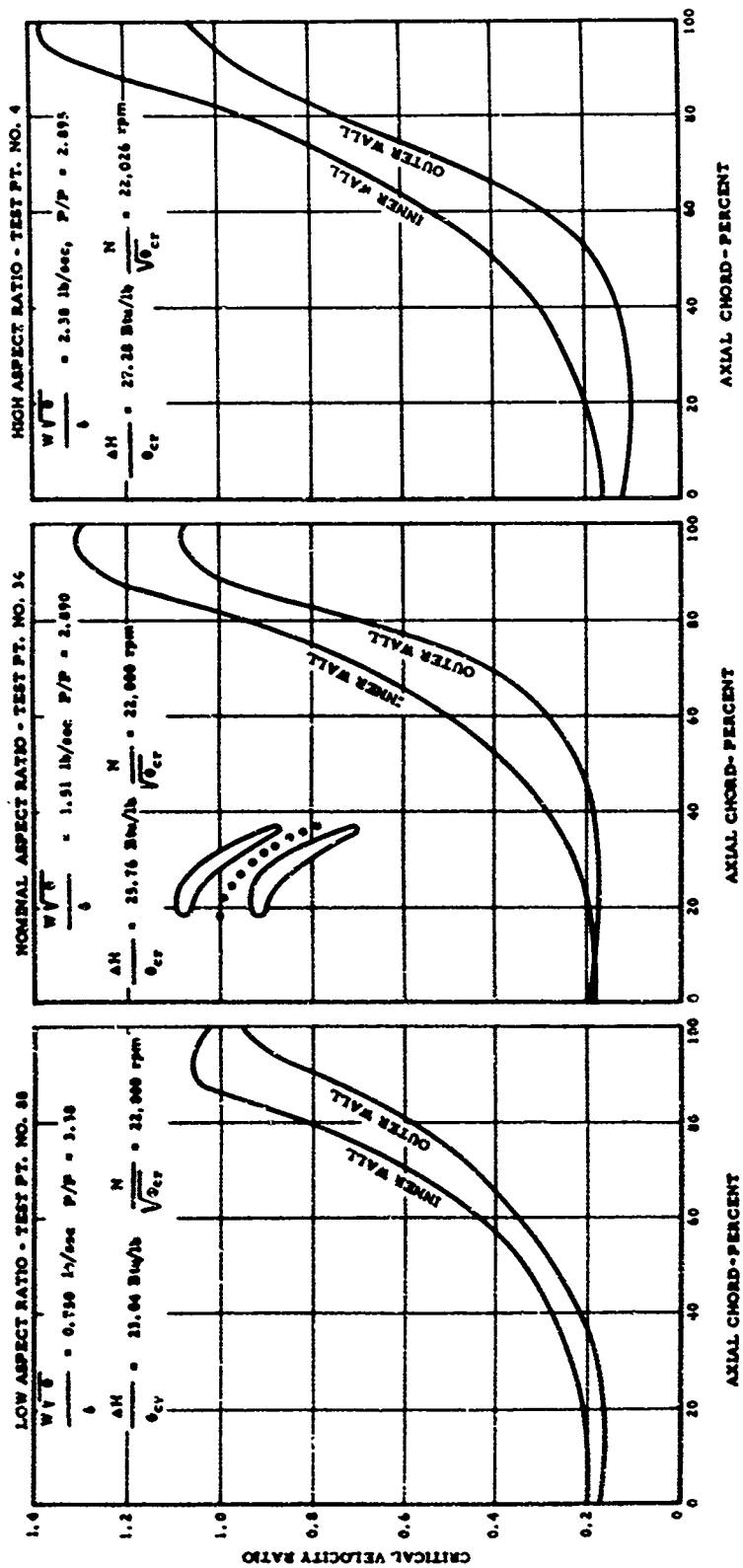


Figure 52. Nozzle Wall Velocity Distributions for Low, Nominal, and High Aspect Ratio Blading.

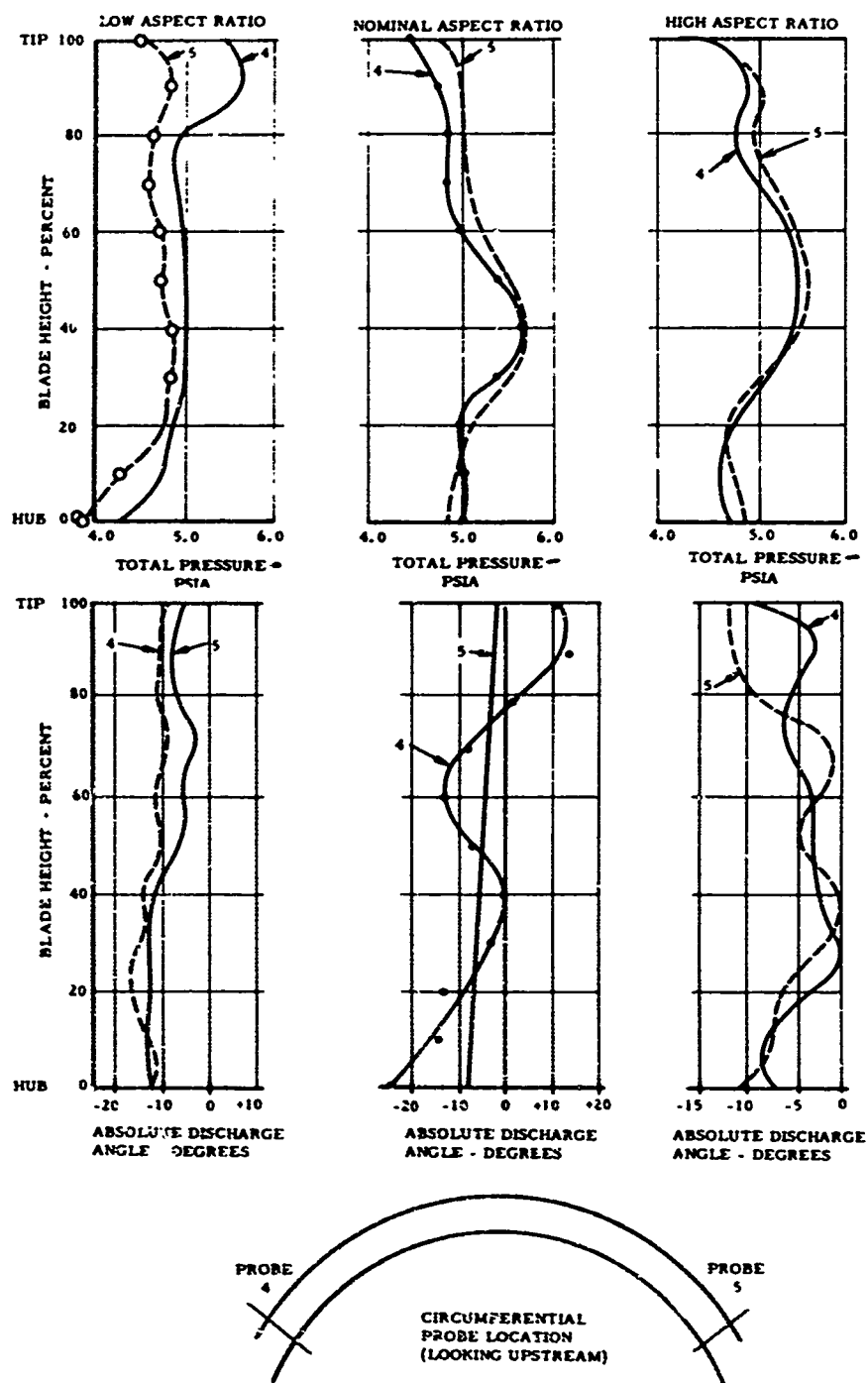


Figure 53. Rotor Discharge Pressure and Angle Survey Data for Low, Nominal, and High Aspect Ratio Turbines.

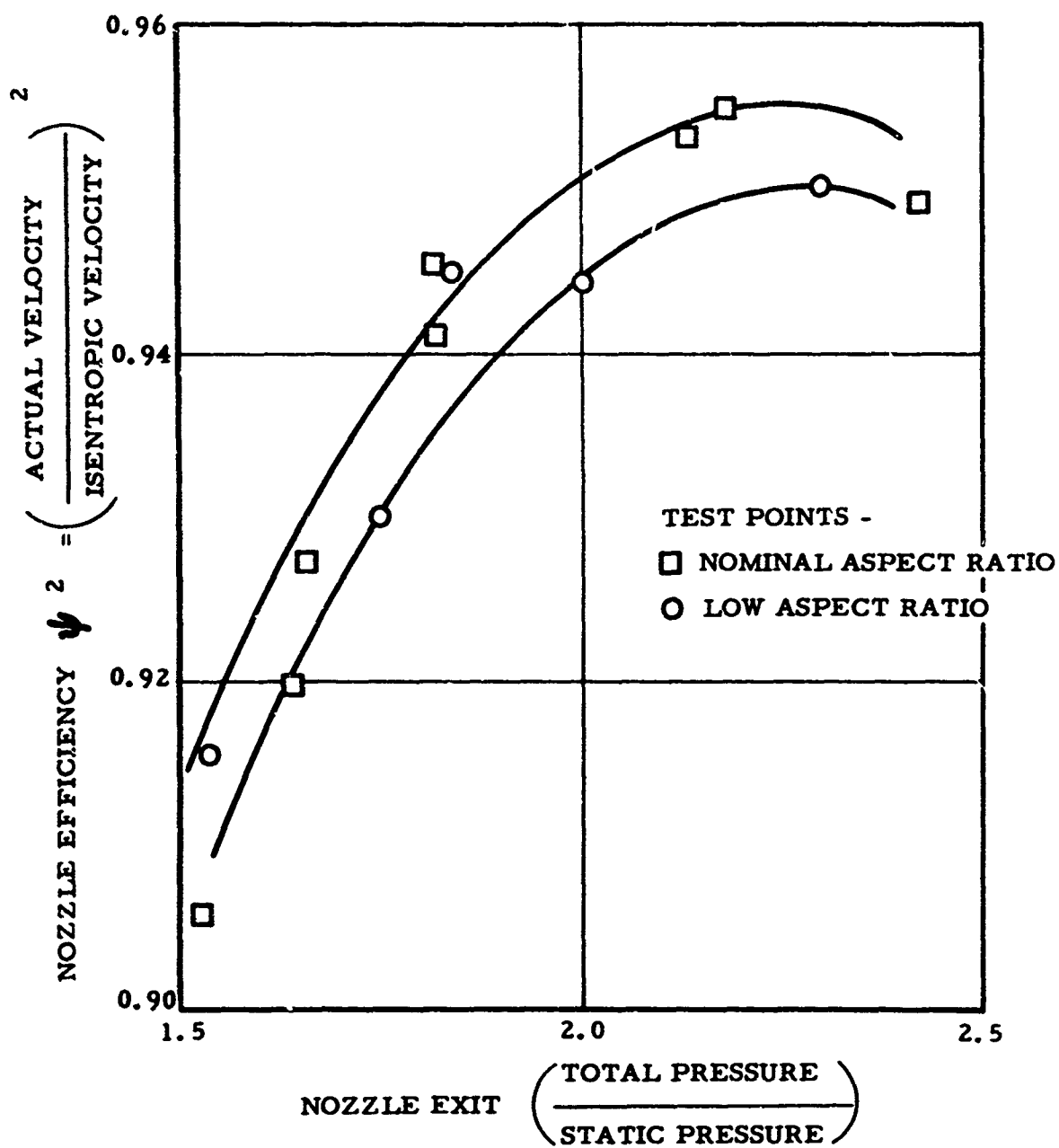


Figure 54. Nozzle Efficiency Versus Exit Total-to-Static Pressure Ratio for Nominal and Low Aspect Ratio Vanes.

Tip Clearance Effects. The effects of tip clearance on nominal performance were evaluated by opening up the rotor shrouds from the nominal 1.5-percent blade height values to 5.0 percent in two increments. The 100-percent equivalent design speed was used as a rating condition, and performance was measured at total-to-total pressure ratios ranging from 1.8 to 3.4. Similarly, the high aspect ratio was evaluated at 1.5 percent and 5 percent blade height clearances. Comparison test data for these tests as a function of efficiency, pressure ratio, and clearance are presented in Figures 55 and 56. A near constant performance degradation was evident over the whole pressure range investigated. Tip clearance effects for the given design work requirements as a function of rotor blade height are presented in Figure 57. Because of secondary losses, a given increase in relative clearance at a very low blade height changes the performance to a lesser extent than the same increase at a higher aspect ratio. This effect is particularly important in the small machinery class, where tight clearances are difficult to achieve and maintain. However, if low secondary loss blading is achieved, the importance of very tight clearances again becomes paramount.

A number of techniques of theoretically predicting clearance effects on performance appear in the literature (References 4, 5, 13, and 14). Most of the classical methods require laborious calculations. A rather simplified technique (Reference 14) is based on the following assumptions:

1. Flow in the tip clearance section is essentially undeflected.
2. Near-zero whirl is produced by the turbine.
3. The nozzle has zero tip clearance.
4. The mean angular momentum changes are representative of the overall stage performance.

With these assumptions, it may be shown that efficiency may be related to rotor tip clearance by the simple expression

$$\frac{\eta_t}{\eta_t(\text{ref})} \approx \frac{A_7 - 2\pi r_{t9}(\Delta h)}{A_7}$$

where:

$$A_7 = \text{Total rotor throat area to tip of blade shroud, in}^2$$

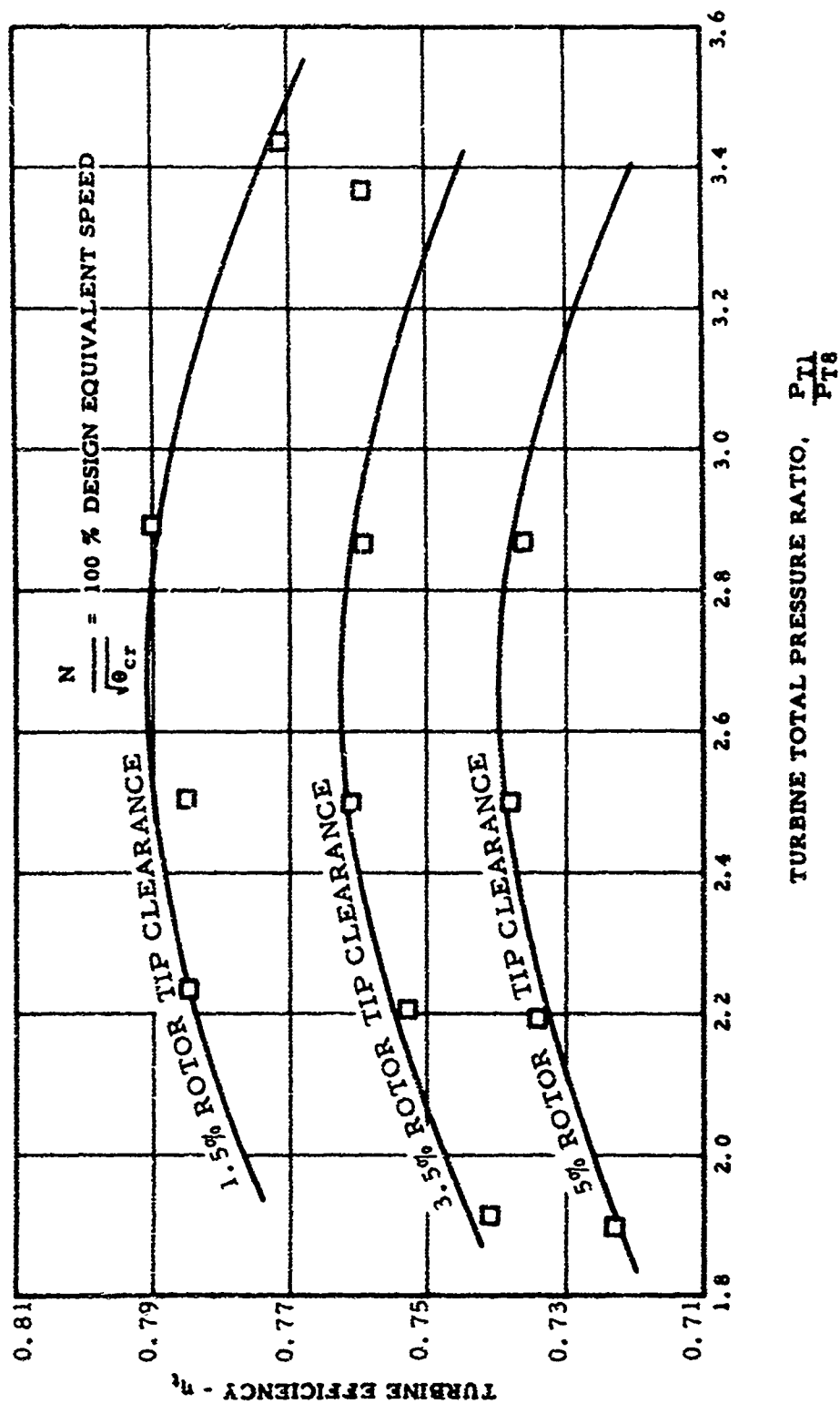


Figure 55. Nominal Aspect Ratio - Rotor Clearance Effect on Performance at Rated Design Equivalent Speed.

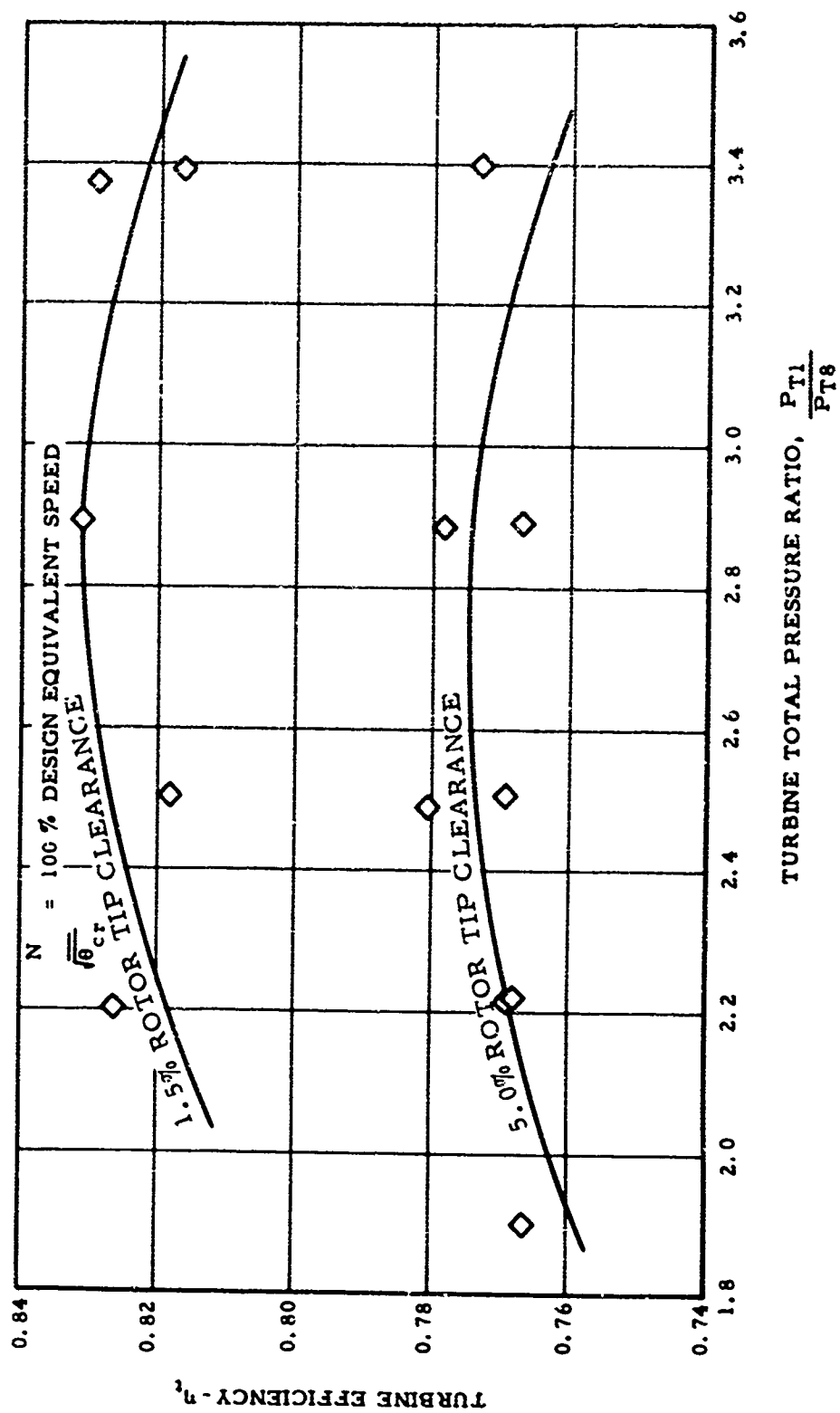


Figure 56. High Aspect Ratio - Rotor Clearance Effects on Performance at Rated Design Equivalent Speed.

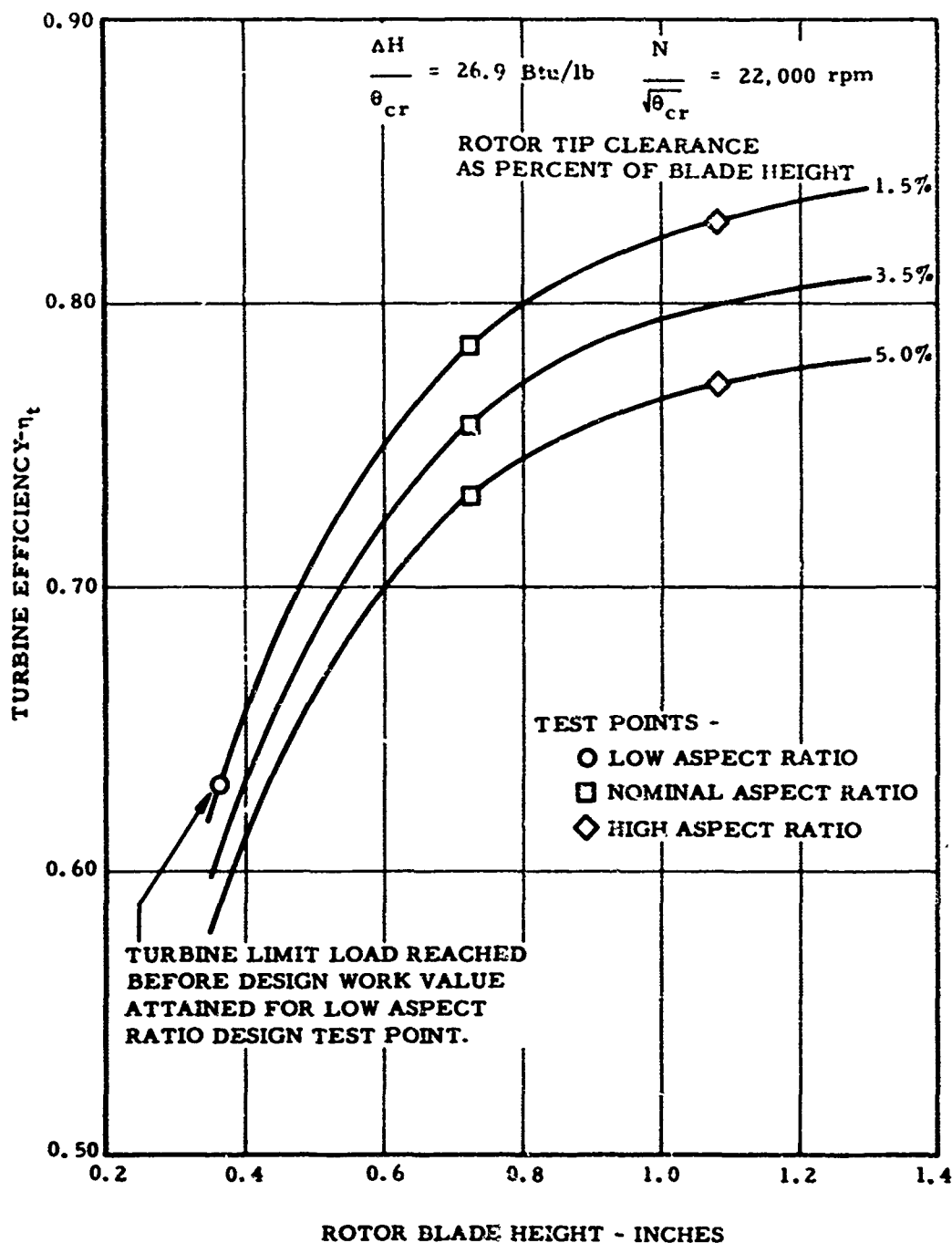


Figure 57. Turbine Efficiency Versus Rotor Blade Height at 1.5, 3.5, and 5.0-Percent Blade Height Clearance.

r_{t9} = Tip radius of rotor, in.

Δh = Tip clearance of rotor, in.

$\eta_{t(\text{ref})}$ = Reference test point total-to-total adiabatic efficiency

η_t = Predicted efficiency, total-to-total adiabatic

This expression was applied to the aspect ratio test data at design equivalent speed and work conditions. A comparison of test data and theoretical prediction is presented in Figure 58. Agreement is well within experimental error and is accurate in lieu of the very approximate assumptions made. To a first quick approximation, efficiency degradation can be closely predicted by the expression above, provided the clearances are not high.

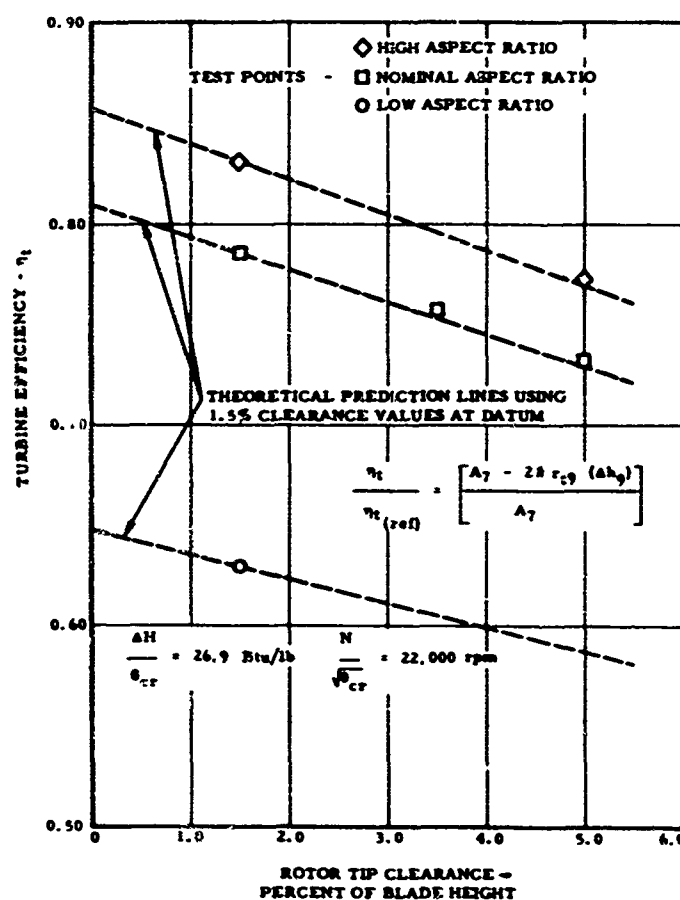


Figure 58. Comparison of Test Data to Theoretical Prediction of Turbine Efficiency as a Function of Clearance and Blade Height.

Mechanical Design

The basic test rig was a modification to the Continental Aviation and Engineering designed rig envelope used for developing the Fluid-Cooled Turbine Blading, Figure 59. One turbine rotor was used for all the aspect ratio tests. The rotor blades were modified by tip machining from 150 to 100 percent to 50 percent normal. One set of 23 turbine inlet nozzle vanes was used in all three flowpath builds. The three flowpaths were formed by changing the outer wall and keeping the inner wall contour constant. A separate rotor shroud was made for each of the six tip-clearance test configurations.

The entire bearing rotor, nozzle, and tip shroud system was suspended from the plenum chamber centerbody. The "O" rings in the outer housing served to damp and seal the internal package and to provide a support independent of the exhaust ducting. This allowed close control of clearances by eliminating the effect of pressure and temperature distortion of the plenum chamber from the aerodynamic package. Rig vibration was minimized by using a reinforced plenum front cover and a lightweight spindle-to-brake coupling.

Two arbors were procured to facilitate balancing and machining of the turbine rotor. The arbor used for machining of the turbine blades allowed rotor concentricities to be maintained. The arbor used for balancing eliminated the need for complete rig teardown. This allowed the rotor to be balanced after each machining operation, independent of the spindle system. Once properly balanced and installed, the spindle was not removed from its bearing system after each series of tests.

The turbine inlet nozzle vane assembly design consisted of a single set of nozzle vanes and three slotted outer shrouds used for flow-path variations with a single inner shroud for mounting. This was done to eliminate machining time and to provide aerodynamic data with a minimum amount of variables. The vanes were held in place to the inner shroud nozzle by screws which were lightly torqued. This allowed proper positioning of the vanes. Once in this position, the vanes were tack welded to the outer shroud. This permitted maintenance of axial and centering alignments of parts during boring of instrumentation holes in the outer shroud. It also facilitated weld removal during nozzle teardown. The nozzle vane gaps at the outer shroud were sealed with Silastic RTV 732.

All tests were conducted with no major hardware breakdowns.

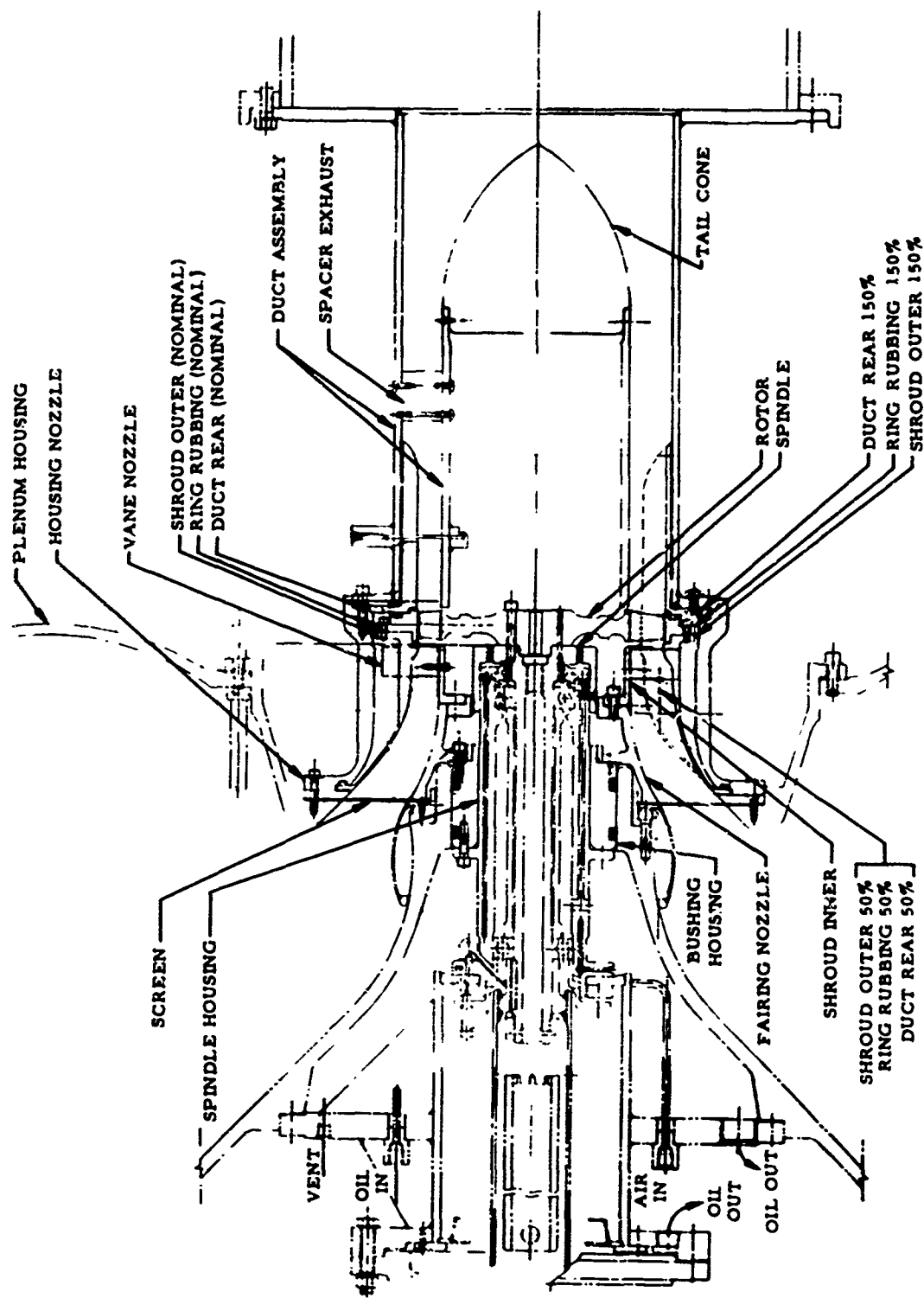


Figure 59. Test Rig - Turbine Aspect Ratio.

Structural Analysis

A structural analysis of the 150-percent aspect ratio design was made. This configuration is the highest stressed rotor. The corrected cold-flow operating condition imposed on the rotor was 30,000 rpm (50,000 rpm uncorrected). The maximum disc bidirectional stress levels determined were:

Tangential	27,000 psi
Radial	33,000 psi
Average Tangential	23,000 psi

These stresses were calculated assuming material density of 0.286 pound per cubic inch. The maximum blade inertial stresses were in the order of 15,000 psi.

CONCLUSIONS

The results of the design and test investigation are summarized as follows:

1. The nominal turbine produced nearly the same performance as the fluid-cooled wheel, designed under the Fluid-Cooled Turbine Contract DA 44-177-AMC-184(T), that is, 79.3 as compared to 81.0 at design work (see Figures 1 and 38). A significant improvement was made with the high aspect ratio blading producing a total-to-total efficiency of 83.3 percent. These performance levels were achieved in spite of a reduction of rim wheel speed of 21 percent over the fluid-cooled turbine design.
2. Performance over the whole operating range deteriorates rapidly with decreasing aspect ratio. Degradation is exponential since three percent, total-to-total efficiency, was lost in going from a rotor aspect ratio of 1.26 to 0.83, whereas over ten percent is lost in a change of aspect ratio from 0.83 to 0.41.
3. The nominal design developed a high limit load capability of $\Delta H/\theta_{cr} = 28.3$ Btu/lb at design equivalent speed. Performance fell with the low aspect ratio blading to the extent that limit load, $\Delta H/\theta_{cr} = 23.25$ Btu/lb, occurred before design, $\Delta H/\theta_{cr} = 26.9$ Btu/lb.
4. A meridional wall constriction on the nozzle was successful in reducing vane secondary losses. A nozzle efficiency of 95 percent was produced with the nominal aspect ratio vane of 0.48.
5. Rotor tip clearance tests were conducted at two values for the high aspect ratio blading, three values for the nominal, and one clearance value for the low aspect ratio turbine. Once a reference efficiency is established, clearance effects may be accurately predicted from a simple theoretical expression (see Figure 58). The combination of test data and the theoretical curve shows that a given increase of relative clearance on the rotor decreases the performance to a lesser extent at very low blade heights than the same increase at higher aspect ratios. A clearance increase from 1.5 to 5.0-percent blade height changed

efficiency four points at the low aspect ratio, as compared to six points at the high aspect ratio.

The test data were gathered on three flow capacity turbines with identical chords, rim speeds, and identical overall diffusion blade loadings. Test flow conditions were the same for all three configurations, and, therefore, all chordal blade Reynolds numbers were preserved. Differences in performance are thus directly attributable to blade span aspect ratio and secondary loss effects.

RECOMMENDATIONS

The cold-flow testing of three different sets of span aspect ratio blading has confirmed the presence of high secondary losses and performance degradation with short vane and blade heights. The program has also demonstrated that loading, defined by $(2gJ\Delta H/U_h^2)$, could be increased 46 percent over the fluid-cooled design with little or no change in performance. Efficiency falloff was less than two percentage points while producing the identical design work, $\Delta H/\theta_{cr} = 26.9$ Btu/lb. This was accomplished by nozzle constriction and tradeoff of decreased wheel speeds for higher span aspect ratio and lower secondary and disc friction losses. Although a smaller, lighter turbine of the same performance was achieved, the baseline efficiency level is still low. Therefore, additional study and test investigations should be conducted for additional improvement.

Test results have confirmed the beneficial effects of meridional constriction on performance of the nozzle. Because of the instrumentation used, it was impossible to separate profile, trailing edge, and secondary losses.

Therefore, it is recommended that the following projects be pursued:

1. Three-dimensional surveys on the nominal configuration should be made to establish loss distribution and regions for performance improvement.
2. Several wall constriction shapes should be tested on the nozzle and rotor to determine an optimum geometry.
3. Alternate channel flow design techniques should be evaluated. In particular, the effect of radial distribution change of reaction caused by tilting nozzle vanes with respect to a radial line normal to the wheel axis should be investigated. This would allow nozzle hub losses and pressure gradients to be reduced. Tilting the nozzle pressure side toward the engine centerline directs the flow to the rotor hubs for improved reaction (References 8 and 11 give indications of performance gains in short blading).

4. Design rotor blading similar to that mentioned in Project 3 above. Here the mechanical practicality of the blade lean or constriction could be determined. Tandem or double row blades, as well as jet flap and vortex generator data coming from NASA's recent high load turbine work could be applied (Reference 15).

REFERENCES

1. White, J.W., Advanced Army Components - Technology Program, SAE Paper No. 650707, Society of Automotive Engineers, New York, New York, October 18-21, 1965.
2. Squire, H.B., and Winter, K.G., "The Secondary Flow in a Cascade of Airfoils in a Non-Uniform Stream," Journal of the Aeronautical Sciences, Vol. 18, 1951, pp. 271-277.
3. Scholz, N., "Ueber den Einfluss der Schaufelhoehe auf die Randverluste in Schaufelgittern," Forschung auf dem Gebiete des Ingenieurwesens, Vol. 20, 1954, pp. 155-156; see also "Secondary Flow Losses in Cascades," Journal of the Aeronautical Sciences, Vol. 21, 1954, pp. 707-708.
4. Ainley, D.G., and Mathieson, An Examination of the Flow and Pressure Losses in Blade Rows of Axial-Flow Turbines, A.R.C. Technical Reports R and M No. 2891, 1955.
5. Schlichting, H., and Das, A., Recent Research on Cascade Flow Problems, ASME, Paper No. 65-FE-A, July 12, 1965.
6. Deich, M.E., and Zaryankin, A.E., Method of Increasing the Efficiency of Turbine Stages With Short Blades, Translation No. 2816, Associated Electrical Industries (Manchester) Limited, T.P./T 2816, 29 April 1960.
7. Zwiefel, O., "The Spacing of Turbomachine Blading Especially With Large Angular Deflection," The Brown Boveri Review, Vol. 32, 12 November 1945.
8. Method of Increasing the Efficiency of Turbine Stages With Short Blades, Translation No. 2816, Associated Electrical Industries (Manchester) Limited, 29 April 1960.
9. Huppert, M.C., and MacGregor, Charles, Comparison Between Predicted and Observed Performance of Gas Turbine Stator Blade Designed for Free Vortex Flow, NACA TN 1810, 1949.
10. A New Method of Profiling the Guide Cascades of Stages With Small Ratios of Diameter to Length, Translation No. 3277, Associated Electrical Industries (Manchester) Limited, 18 July 1963.

11. Effect of the Constructional Factors on the Characteristics of Gas Turbine Stages With a Low Ratio of Mean Diameter/Height, Translation No. 3276, Associated Electrical Industries, Limited, 19 July 1963.
12. Stewart, W. L., Whitney, W. J., and Miser, J. W., Use of Effective Momentum Thickness in Describing Turbine Rotor Blade Losses, NACA Report No. RME 56B29, 14 May 1956.
13. Horlock, J. H., Axial Flow Turbines, Butterworth and Company (Publishers) Limited, 1966.
14. Amann, C. A., Dawson, D. W., and Mason, K. Yu., Consideration in the Design and Development of Turbines for Automotive Gas Turbine Engines, SAE Paper 653C, January 1963.
15. Lueders, H. G., Experimental Investigation of Advanced Concepts to Increase Turbine Blade Loading, NASA CR-735, I Analysis and Design, June 1967.

Unclassified

Security Classification

DOCUMENT CONTROL DATA - R & D		
(Security classification of title, body of abstract and indexing annotation must be entered when the overall report is classified)		
1. ORIGINATING ACTIVITY (Corporate author) Continental Aviation and Engineering Corporation Detroit, Michigan		25. REPORT SECURITY CLASSIFICATION Unclassified
		26. GROUP
3. REPORT TITLE EXPERIMENTAL INVESTIGATION OF LOW ASPECT RATIO AND TIP CLEAR- ANCE ON TURBINE PERFORMANCE AND AERODYNAMIC DESIGN		
4. DESCRIPTIVE NOTES (Type of report and inclusive dates) Summary Report		
5. AUTHOR(S) (First name, middle initial, last name) Roy Marshall Casimir Rogo		
6. REPORT DATE May 1968	7a. TOTAL NO. OF PAGES 97	7b. NO. OF REFS 15
8a. CONTRACT OR GRANT NO. DA 44-177-AMC-447(T) b. PROJECT NO. Task 1M125901A01409 c. d.		9a. ORIGINATOR'S REPORT NUMBER(S) USAAVLABS Technical Report 67-80 9b. OTHER REPORT NO(S) (Any other numbers that may be assigned this report) No. 1043
10. DISTRIBUTION STATEMENT This document has been approved for public release and sale; its distribution is unlimited.		
11. SUPPLEMENTARY NOTES		12. SPONSORING MILITARY ACTIVITY U.S. Army Aviation Materiel Laboratories Fort Eustis, Virginia
13. ABSTRACT >The aerodynamics of any cooled turbine are compromised by mechanical design, fabrication techniques, heat transfer, and cooling restrictions. Additional require- ments of high outputs out of small turbomachinery packages result in limitations on the turbine that are unique to low-airflow, high-pressure-ratio, small-category machines. These practical considerations limit the tip clearance, axial chord lengths, tolerances, and geometry. The resultant blading is usually of low-aspect- ratio type, and characteristically high secondary losses predominate. This report presents the aerothermodynamic design considerations of three turbine flowpaths, which were cold-flow tested to evaluate the performance effects of span aspect ratio and tip clearance on turbine efficiency. Complete maps were generated for the three configurations, and tip clearance effects were evaluated at design speed over a range of pressure ratios. Rotor blade aspect ratios were tested from 0.41 to 1.26, and blade heights varied from 0.36 inch to 1.09 inches. Rotor tip clear- ance was varied from 1.5 to 5.0 percent of the blade span. Results of the investi- gation suggest that predominance of high secondary losses should allow a design with high-aspect-ratio blading and low wheel speeds to produce the same perfor- mance as low-aspect-ratio blading with high rim speeds.		

DD FORM 1473
1 NOV 66

REPLACES DD FORM 1473, 1 JAN 64, WHICH IS
OBSOLETE FOR ARMY USE.

Unclassified

Security Classification

Unclassified
Security Classification

14. KEY WORDS	LINK A		LINK B		LINK C	
	ROLE	WT	ROLE	WT	ROLE	WT
Fluid-cooled turbine Turbine blade aspect ratio Turbine tip clearance effects Short turbine blading Meridional constriction to improve turbine efficiency						

Unclassified
Security Classification

6123-68